Dynamic Methods for Thermodynamic Equilibrium Calculations in Process Simulation and Process Optimization

Dissertation

zur Erlangung des akademischen Grades

Doktoringenieur

(Dr.-Ing.)

von	Dipl.-Ing. Alexander Zinser
geb. am	2. Mai 1984
in	Biberach an der Riß

genehmigt durch die Fakultät für Verfahrens- und Systemtechnik
der Otto-von-Guericke Universität Magdeburg

Promotionskommission:	Prof. Dr.-Ing. habil. Dr. h. c. Lothar Mörl (Vorsitz)
	Prof. Dr.-Ing. habil. Kai Sundmacher (Gutachter)
	Prof. Dr.-Ing. habil. Achim Kienle (Gutachter)
	Dr.-Ing. Jan Schöneberger (Gutachter)

eingereicht am:	3. April 2018
Promotionskolloquium am:	2. November 2018

Abstract

This thesis proposes a novel framework for the application of chemical and phase equilibrium calculations in process simulation and optimization. Therefore, a generalized methodology for the computation of chemical and phase equilibria is presented. This method is physically motivated and simulates the dynamic evolution of a thermodynamic system from an initial point into its final equilibrium state. This approach is exemplified at several examples of different type and complexity and it is compared against the conventional Gibbs energy minimization method.

After that, the proposed method is extended to a method for process simulation by connecting different process units with each other according to the process flowsheet via the mass balances of the streams between the units. This approach allows the simultaneous solution of the process simulation in one step and overcomes the iterative coupling between the unit models and the process model in conventional tearing methods.

After that, the developed method for process simulation is employed for optimization of a methanol synthesis process.

Employing the developed methods allows computationally efficient simulation of complex reactive multiphase systems, as well as the simulation and optimization of chemical processes.

Zusammenfassung

Diese Arbeit entwickelt eine Methodik zur Berechnung chemischer Gleichgewichte und Phasengleichgewichte in Prozesssimulation und Prozessoptimierung. Dazu wird ein allgemeiner Ansatz zur Berechnung von chemischen Gleichgewichten und Phasengleichgewichten hergeleitet. Diese Methode ist physikalisch motiviert und simuliert die dynamische Entwicklung eines thermodynamischen Systems von einem Startpunkt in sein thermodynamisches Gleichgewicht. Diese Vorgehensweise wird anhand verschiedener Beispiele unterschiedlichen Typs und unterschiedlicher Komplexität demonstriert und mit der konventionellen Methode der Minimierung der Gibbs-Energie verglichen.

Danach wird diese Methode erweitert, um in Prozesssimulationen die einzelnen Prozesselemente simultan berechnen zu können. Dies geschieht durch die Verschaltung der einzelnen Elemente entsprechend des Fließbildes durch die Massenbilanzen der Stoffströme zwischen den jeweiligen Prozesseinheiten. Dieser Ansatz erlaubt die simultane Lösung der Prozesssimulation in einem Schritt und umgeht damit die iterative Kopplung zwischen den Modellen der Prozesseinheiten und dem Modell der Prozesssimulation in konventionellen Tearing-Methoden.

Anschließend wird die entwickelte Methode zur Optimierung eines Methanol-Synthese-Prozesses eingesetzt.

Die Anwendung der entwickelten Verfahren erlaubt sowohl eine rechentechnisch effiziente Simulation komplexer reaktiver Mehrphasensysteme, als auch die Simulation und Optimierung verfahrenstechnischer Prozesse.

Contents

Notation

Latin Symbols

A	(absolute) Helmholtz energy	J
$\mathbf{A}$	elemental matrix (Gibbs minimization)	
$\mathbf{A}$	stoichiometric matrix	
a	cohesion pressure (equation of state parameter)	$Pa\,m^6mol^{-2}$
b	covolume (equation of state parameter)	m^3mol^{-1}
a_m, b_m	equation of state parameter of a mixture	$[a], [b]$
A, B	dimensionless equation of state parameter	
a_{ij}, b_{ij}, c_{ij}	binary interaction coefficients between groups i and j (UNIFAC)	
$a_{\alpha\beta}, b_{\alpha\beta}, c_{\alpha\beta}$	binary interaction coefficients between species α and β (UNIQUAC)	
$\mathbf{A}, \mathbf{B}, \mathbf{C}$	matrices of binary interaction coefficients	
$\mathbf{b}$	vector of elemental composition (Gibbs minimization)	
c_0, c_1, c_2	equation of state parameter of the dimensionless CEoS	
c_1, c_2, c_3	Mathias-Copeman parameters	
$\mathbf{C}$	companion matrix	
c_p	ideal gas heat capacity	$J\,mol^{-1}K^{-1}$
$\mathbf{e}_j$	j-th unit vector	
err	error estimation	
f, F	general functions	
f_α	partial fugacity of species α	Pa
F_α	surface contribution of species α (UNIQUAC, UNIFAC)	
F	objective function in optimization	
g	(molar) Gibbs energy	$J\,mol^{-1}$
G	(absolute) Gibbs energy	J
$\Delta_f g$	Gibbs energy of formation	$J\,mol^{-1}$
$\Delta_r g$	Gibbs energy of reaction	$J\,mol^{-1}$
$\Delta_{trs} g$	Gibbs energy of phase transition	$J\,mol^{-1}$
$G_i^{(\alpha)}$	group increment of group i in species α (UNIFAC)	
$\mathbf{G}$	matrix of group increments (UNIFAC)	
h	(molar) enthalpy	$J\,mol^{-1}$
H	(absolute) enthalpy	J
$H(.)$	Heaviside step function	
$\Delta_f h$	enthalpy of formation	$J\,mol^{-1}$
$\Delta_{vap} h$	enthalpy of vaporization	$J\,mol^{-1}$
$\mathbf{I}$	identity matrix	

Latin symbols (cont.)

$\mathscr{I}^{\pi,\pi'}$	set of species on the interface between phases π and π'	
$\mathbf{J}$	Jacobian matrix	
$\mathbf{J}^{\pi,\pi'}$	stoichiometric submatrix describing phase transitions	
K	initial distribution among phases, in set-up of the Dynamic Method	
k_{ij}	binary interaction coefficient between species i and j (equation of state parameter)	
$k_\alpha^{\pi,\pi'}, k_\rho^\pi$	kinetic rate constants	
$K_{\text{eq},\rho}$	equilibrium constant of reaction ρ	
k_{H}	Henry coefficient	
L	liquid fraction	
m	general physical property	$[m]$
M	threshold in numerical error estimation	
n	amount of substance	mol
$\mathbf{n}$	vector of molar composition	mol
n_{t}	total amount of substance	mol
$\dot{n}$	molar stream	mol s^{-1}
$\dot{\mathbf{n}}$	vector of molar streams	mol s^{-1}
p	total number of phases	
p	polarity	
P	pressure	Pa
P^{vap}	vapour pressure	Pa
p_i	process parameter	$[p]$
$\mathbf{p}$	vector of process parameter	$[p]$
$\mathscr{P}$	set of phases	
q_1	equation of state parameter in g^{E} mixing rules	
q_α	relative van-der-Waals surface of species α	
Q_i	group contribution of group i to the relative van-der-Waals surface	
$\dot{Q}$	heat stream	
R	universal gas constant, $R = 8.3144621 \, \text{J}/_{\text{mol K}}$	$\text{J mol}^{-1}\text{K}^{-1}$
$R(.)$	ramp function	
r_α	relative van-der-Waals volume of species α	
R_i	group contribution of group i to the relative van-der-Waals volume	
$r_\alpha^{\pi,\pi'}$	rate expression of species α between phase π and π'	
$\mathbf{r}^{\pi,\pi'}$	vector of rate expressions between phase π and π'	
r_ρ^π	rate expression of reaction ρ in phase π	
$\mathbf{r}^\pi$	vector of rate expressions due to chemical reactions in phase pi	
$\mathbf{r}$	vector of rate expressions	

Latin symbols (cont.)

$\mathscr{R}^{\pi}$	set of chemical reactions in phase π	
s	total number of species	
S	stiffness ratio	
S	solubility	
s	(molar) entropy	$\mathrm{J\,mol^{-1}K^{-1}}$
S	(absolute) entropy	$\mathrm{J\,K^{-1}}$
$\Delta_{\mathrm{f}}s$	entropy of formation	$\mathrm{J\,mol^{-1}K^{-1}}$
$\mathscr{S}$	set of species	
$\mathscr{S}^{\pi}$	set of species in phase π	
T	temperature	K
U	internal energy	J
$\mathscr{U}$	set of process units	
$\Delta u_{\alpha\beta}$	binary interaction coefficient (UNIQUAC)	
v	molar volume	$\mathrm{m^3mol^{-1}}$
V_{α}	volume contribution of species α (UNIQUAC, UNIFAC)	
x_{α}	mole fraction of species α	
$\mathbf{x}$	vector of mole fractions	
X	standard normally distributed random variable	
Z	compressibility factor	

Greek Symbols

α	chain growth probability, in the Flory distribution
α	temperature-dependent α-function of a cubic equation of state
α_i	α-function of species i
γ_α	activity coefficient of species α
$\Gamma_i, \Gamma_i^{(\alpha)}$	group activity coefficients (UNIFAC)
δ, ε	equation of state parameter
δ_{ij}	Kronecker delta
Δ	discriminant
η	isentropic efficiency
κ	heat capacity ratio
$\kappa(\alpha)$	preferred phase of a species α, in set-up of the Dynamic Method
$\kappa(\omega)$	polynomial of the acentric factor (part of α-functions in some cubic equations of state)
λ	eigenvalue
λ	method parameter for the tearing methods
$\nu_{\alpha\rho}$	stoichiometric coefficient of species α in reaction ρ
ξ	extent of reaction, in chapter 3 in chemical equilibrium calculations
ξ	purge ratio, in chapter 4 in process simulations
ρ	structural density of a matrix
τ	time s
$\tau_{\alpha\beta}$	binary interaction coefficient (UNIQUAC)
ϕ_α	fugacity coefficient of species α
Ψ_{ij}	binary interaction coefficient (UNIFAC)
ω	acentric factor
Ω_a, Ω_b	equation of state parameter

Operators and Special Symbols

det   determinant
diag   diagonal matrix
lim   limit
max   maximum
min   minimum
$\emptyset$ empty matrix
$(.)'$ (partial) derivative
$\times$ Cartesian product
$|.|$ cardinality (if the argument is a set)
$|.|$ absolute value (if the argument is a real number)
$||.||_2$ Euclidean norm
$\bigstar$ non-negative entry in a structural Jacobian matrix

Indices

Indices referring to special objects are given in Greek letters, e. g. species α or phases π. General indices are the Latin letters i, j, k, etc. Sometimes, also the general Latin indices are used for the special objects to avoid confusion, e. g. in context with the α-functions in equations of state.

i,j,k,m,n general indices
u index referring to a process unit, $u \in \mathscr{U}$
α, β, δ index referring to a species, $\alpha \in \mathscr{S}$
ε index referring to an element of matter
π, π', π_i index referring to a phase, $\pi \in \mathscr{P}$
ρ index referring to a chemical reaction, $\rho \in \mathscr{R}$

Subscripts

0	initial state
b	boiling point
c	critical property, e. g. critical temperature T_c
cool	cooling duty
costs	utility costs
el	electricity
eq	equilibrium
heat	heating duty
in	inlet
m	melting point
opt	optimum
out	outlet
p	phase transition
prod	product
r	chemical reaction
r	reduced property, e. g. reduced temperature $T_r = T/T_c$
react	reactor
sep	separation

Superscripts

○	standard state
C	combinatorial part
E	excess property
id	ideal gas
L, Li	liquid
R	residual part
T	transposition
V	vapour

Abbreviations

0PVDW	$\underline{0}$ parameter $\underline{v}$an-$\underline{d}$er-$\underline{W}$aals (mixing rule)
1PVDW	$\underline{1}$ parameter $\underline{v}$an-$\underline{d}$er-$\underline{W}$aals (mixing rule)
CEoS	$\underline{C}$ubic $\underline{E}$quation $\underline{o}$f $\underline{S}$tate
DM	$\underline{D}$ynamic $\underline{M}$ethod
EoS	$\underline{E}$quation $\underline{o}$f $\underline{S}$tate
LL, LLE	$\underline{l}$iquid-$\underline{l}$iquid ($\underline{e}$quilibrium)
LLL, LLLE	$\underline{l}$iquid-$\underline{l}$iquid-$\underline{l}$iquid ($\underline{e}$quilibrium)
MeOH	methanol, $\underline{me}$thyl (CH_3-) alcohol(-$\underline{OH}$)
NLP	$\underline{n}$on$\underline{l}$inear $\underline{p}$rogramming (optimization problem)
NRTL	$\underline{n}$on-$\underline{r}$andom $\underline{t}$wo-$\underline{l}$iquid model (activity coefficient model)
ODE	$\underline{o}$rdinary $\underline{d}$ifferential $\underline{e}$quation
PR	$\underline{P}$eng-$\underline{R}$obinson (equation of state)
PRG	$\underline{P}$eng-$\underline{R}$obinson-$\underline{G}$asem (equation of state)
PSRK	$\underline{p}$redictive $\underline{S}$oave-$\underline{R}$edlich-$\underline{K}$wong (equation of state)
RK	$\underline{R}$edlich-$\underline{K}$wong (equation of state)
SDM	$\underline{S}$imultaneous $\underline{D}$ynamic $\underline{M}$ethod
SLE	$\underline{s}$olid-$\underline{l}$iquid $\underline{e}$quilibrium
SRK	$\underline{S}$oave-$\underline{R}$edlich-$\underline{K}$wong (equation of state)
UNIFAC	$\underline{uni}$versal $\underline{q}$uasichemical $\underline{f}$unctional group $\underline{a}$ctivity $\underline{c}$oefficients (activity coefficient model)
UNIQUAC	$\underline{uni}$versal $\underline{q}$uasi$\underline{c}$hemical (activity coefficient model)
VdW	$\underline{v}$an-$\underline{d}$er-$\underline{W}$aals (equation of state)
VL, VLE	$\underline{v}$apour-$\underline{l}$iquid ($\underline{e}$quilibrium)
VLL, VLLE	$\underline{v}$apour-$\underline{l}$iquid-$\underline{l}$iquid ($\underline{e}$quilibrium)

Introduction

In process engineering, simulation and optimization are important tools to predict and improve the efficiencies of chemical processes. In process simulation a large variety of thermodynamic equilibria has to be calculated. Chemical equilibria have to be applied in reactor units and phase equilibria are used to describe separation processes. Examples of phase equilibria are vapour-liquid equilibria in the flash evaporation or liquid-liquid equilibria in a decanter unit. In integrated units such as reactive distillation also the simultaneous calculation of chemical and phase equilibria are vital. The chemical and phase equilibria represent the thermodynamic limit of a process as a reference point for further investigations.

In a process simulation, these unit models are connected with each other according to the mass balances of the molar streams between the particular process units. Additionally, in process optimization the parameters of a process simulation are varied until an objective function reaches its minimum. Typical objective functions are the energy demand or the costs of a process.

On each hierarchy level, process unit, process simulation, and process optimization, a variety of computational methods are available, see also Fig. 1.1. On the unit level a common approach for chemical equilibrium calculations is the Gibbs energy minimization technique (Lwin, 2000; Luckas and Krissmann, 2001). In case of phase equilibria calculations there are also algorithms available that solve the equilibrium condition, the equality of the chemical potentials, directly which is an algebraic set of equations (Poling et al., 2001).

On the level of process simulation a robust approach to solve the mass balances in the process is the class of tearing methods (Ramirez, 1997) or the Wegstein algorithm (Wegstein, 1958). These methods set streams in the process which are *a priori* unknown, such as recycle streams, to a certain value, e. g. to zero. In each iteration, the values for these streams are updated according to the particular rule of the tearing method.
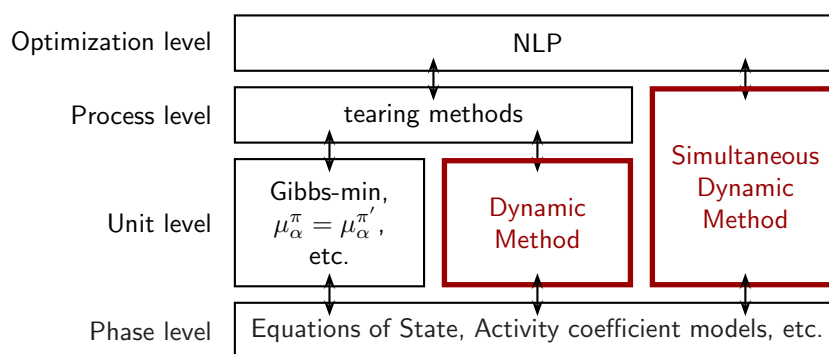
Figure 1.1: Hierarchical structure of methods in flowsheet simulations. The emphasized boxes refer to the methods derived in this thesis.

And finally on the level of process optimization a given objective function, such as the energy demand or the costs of the process, has to be minimized. For this task a large variety of algorithms of different complexity is available. This reaches from the simple and robust downhill simplex method (Nelder and Mead, 1965; Lagarias et al., 1998) up to advanced gradient-based methods, e. g. interior-point methods (Byrd et al., 1999, 2000; Waltz et al., 2006).

All these methods for the different hierarchy levels are iterative approaches that require a subsequent evaluation of the underlying models. This leads to nested iteration cycles when solving process simulations or performing a process optimization which can be very cost intensive in terms of computing power. Hence, its application can be infeasible for time-critical tasks or real-time applications, such as model predictive control of a process.

The aim of this work is to provide a methodological framework that integrates the challenges on each of these hierarchy levels and eliminates the need of time-consuming intermediate iteration cycles. Therefore, a physically motivated approach for solving thermodynamic equilibria is derived. This dynamic method is based on the solution of a set of differential equations that describe the evolution from an non-equilibrium point towards the thermodynamic equilibrium in its steady-state. The approach of relaxation of differential equations into their steady state in chemical engineering dates back to Ketchum (1979). The dynamic evolution of the composition of a system for the computation of chemical equilibria was also proposed by Seidel (1990). In case of phase equilibria, this approach was used by Steyer et al. (2005) and Ye (2014). In the present work, a consistent method is presented which is able to handle thermodynamic equilibria including chemical and phase equilibrium problems, also of mixed type.

After that, this approach is extended from the unit level to the process simulation level in a simultaneous way that avoids any iterative coupling between the two hierarchy levels.

Chapter 2 summarizes the thermodynamic fundamentals for the description of the properties of vapour and liquids which are used within this thesis. Topics are cubic Equations of State and their application for the computation of fugacity coefficients of vapour and liquids, as well as the use of activity coefficient models for predicting the behaviour of liquids. If the reader is familiar with the

prediction of thermodynamic properties using Equations of State and activity coefficient models, this chapter might be skipped when reading this thesis.

Chapter 3 introduces methods for computation of thermodynamic equilibria. First, a brief overview of the conventional Gibbs energy minimization technique is given. After that, the Dynamic Method (DM) is derived and its applicability is demonstrated on several example calculations of different type and complexity. The DM solves the thermodynamic equilibrium conditions by relaxing a system of ordinary differential equations (ODE) from an arbitrary initial state towards the thermodynamic equilibrium. It is able to solve chemical equilibria, phase equilibria, as well as equilibria of mixed type. The presented examples are employed for several studies of properties of the DM, e. g. a comparison of the DM with the Gibbs energy minimization technique or an analysis of the numerical properties of the resulting ODE system. In the case of more than two coexisting phases, an approach for reduction of the mathematical complexity of the resulting ODE system is presented.

Chapter 4 addresses process simulations where models for the particular units are connected with each other according to the flowsheet connectivity. Besides the thermodynamic equilibria in each process unit, the mass balances throughout the process have also to be fulfilled. Therefore, iterative methods for process simulation are introduced and discussed. After that, the Dynamic Method is extended to the Simultaneous Dynamic Method (SDM). The SDM is able to solve the thermodynamic equilibria in each process unit simultaneously and it satisfies the mass balances in the process flowsheet always implicitly. Hence, the SDM does not require any iterative solution procedure and therefore, it is significantly more efficient than conventional approaches.

Chapter 5 touches the area of process optimization. Here, a set of optimal process parameters for a methanol synthesis process is computed with respect to the energy demand of the process. Therefore, a basic optimization algorithm is employed in order to solve the process simulation according to the SDM.

Chapter 6 summarizes this work, discusses the results and gives an outlook to possible further improvements of the proposed methods.

Thermodynamic Fundamentals

For the description of the state of a thermodynamic system, the relationship

$$F(T,P,v) = 0 \qquad (2.1)$$

between temperature T, pressure P, and volume v if the equation of state (EoS). With the knowledge of the equation of state and, additionally, the ideal gas heat capacity c_P^{id}, all other thermodynamic properties can be calculated (Gmehling et al., 2012, p. 5).

2.1 Ideal Gas Law

The most simple equation of state is the ideal gas law,

$$Pv = RT \,, \qquad (2.2)$$

which was formulated by Clapeyron in 1834 who connected the results of Boyle ($Pv = $ const.), Charles and Gay-Lussac ($v/T = $ const.). For a more detailed history of the development of equations of state, see also Walas (1985, p. 3). According to Mohr et al. (2012), the currently acknowledged value of the universal gas constant R is given by

$$R = 8.3144621 \,\mathrm{J\,mol^{-1}K^{-1}} \,. \qquad (2.3)$$

The ideal gas law assumes, that

- the molecules have no particular volume, and

- no intermolecular forces occur in the system.

Therefore, it is applicable to gas-phase systems that are far away from the vapour pressure curve, i. e. for $v \to \infty$. In general it can be applied to substances that do not condense at the considered process conditions in terms of temperature and pressure.

2.2   Cubic Equations of State

The PvT-relationship (2.1) is commonly is formulated as a pressure-explicitly

$$P = f(T, v) \tag{2.4}$$

which also holds for the class of the cubic equations of state (CEoS), e. g. for the van-der-Waals equation of state. Starting with the ideal gas law, van der Waals (1873) added an expression for the particular volume of a molecule, b, as well as an expression for the attraction between the particles, a, which leads to the equation

$$\left(P + \frac{a}{v^2}\right)(v - b) = RT \tag{2.5}$$

or, in terms of a pressure-explicit formulation,

$$P = \frac{RT}{v - b} - \frac{a}{v^2}. \tag{2.6}$$

The van-der-Waals (VdW) equation of state and all further developed cubic equations of state, such as the

- Redlich-Kwong (RK) equation of state (Redlich and Kwong, 1949), the

- Soave-Redlich-Kwong (SRK) equation of state (Soave, 1972), the

- Peng-Robinson (PR) equation of state (Peng and Robinson, 1976), and the

- Peng-Robinson-Gasem (PRG) equation of state (Gasem et al., 2001)

are able to predict the vapour as well as the liquid phase of a substance. Modern tools for process simulation often use models like the Soave-Redlich-Kwong, the Peng-Robinson equation of state, or extensions of them, such as the predictive Soave-Redlich-Kwong EoS (see also section 2.8) or the volume-translated Peng-Robinson EoS (Ahlers and Gmehling, 2001). A general cubic equation of state can be written generally as

$$P = \frac{RT}{v - b} - \frac{a\alpha(T)}{(v + \delta b)(v + \varepsilon b)} \tag{2.7}$$

Table 2.1: Some cubic equations of state, their corresponding (δ, ε)-parameters and their α-functions in terms of the reduced temperature $T_r = T/T_c$.

CEoS	δ, ε	$\alpha(T_r)$	$\kappa(\omega)$
VdW	0, 0	1	—
RK	0, 1	$1/\sqrt{T_r}$	—
SRK	0, 1	$\left[1 + \kappa(\omega)\left(1 - \sqrt{T_r}\right)\right]^2$	$0.48 + 1.574\omega - 0.176\omega^2$
PR	$1 \pm \sqrt{2}$	$\left[1 + \kappa(\omega)\left(1 - \sqrt{T_r}\right)\right]^2$	$0.37464 + 1.54226\omega - 0.26992\omega^2$
PRG	$1 \pm \sqrt{2}$	$\exp\left[\left(2 + 0.836 T_r\right)\left(1 - T_r^{\kappa(\omega)}\right)\right]$	$0.134 + 0.508\omega - 0.0467\omega^2$

which leads to the above mentioned equations of state for special values of δ and ε and a specific alpha-function $\alpha(T)$. A survey of different cubic equations of state, the corresponding (δ, ε)-parameters and their α-functions are given in Tab. 2.1. The α-functions are designed, that they become unity at the critical temperature, i.e. $\alpha(T = T_c) = 1$, or, in terms of the reduced temperature $T_r = T/T_c$

$$\alpha(T_r = 1) = 1. \tag{2.8}$$

Additionally, a thermodynamic consistent α-function has to satisfy the following conditions

$$\alpha(T) \geq 0, \qquad \text{and } \alpha(T) \text{ continuous} \tag{2.9a}$$

$$\frac{\mathrm{d}\alpha}{\mathrm{d}T} \leq 0, \qquad \text{and } \frac{\mathrm{d}\alpha}{\mathrm{d}T} \text{ continuous} \tag{2.9b}$$

$$\frac{\mathrm{d}^2\alpha}{\mathrm{d}T^2} \geq 0, \qquad \text{and } \frac{\mathrm{d}^2\alpha}{\mathrm{d}T^2} \text{ continuous} \tag{2.9c}$$

$$\frac{\mathrm{d}^3\alpha}{\mathrm{d}T^3} \leq 0, \tag{2.9d}$$

see also Le Guennec et al. (2016) for a derivation of these conditions. The EoS-specific parameters a and b may be obtained from the conditions at the critical point

$$\left.\frac{\partial P}{\partial v}\right|_{T_c, P_c} = 0, \quad \text{and} \tag{2.10a}$$

$$\left.\frac{\partial^2 P}{\partial v^2}\right|_{T_c, P_c} = 0. \tag{2.10b}$$

With these conditions, the parameters a and b can be written as a function of the critical properties T_c and P_c of a substance

$$a = \Omega_a \frac{R^2 T_c^2}{P_c}, \quad \text{and} \tag{2.11a}$$

$$b = \Omega_b \frac{R T_c}{P_c}, \tag{2.11b}$$

Table 2.2: Exact values of the coefficients Ω_a and Ω_b for some equations of state.

EoS	δ, ε	(Ω_a, Ω_b)
VdW	0, 0	$\Omega_a = \dfrac{27}{64} \approx 0.42188$, and $\Omega_b = \dfrac{1}{8} = 0.0125$
RK/SRK	0, 1	$\Omega_a = \left[1 + \sqrt[3]{2} + \sqrt[3]{2^2}\right]/9 \approx 0.42748$, and $\Omega_b = \left[\sqrt[3]{2} - 1\right]/3 \approx 0.08664$
PR/PRG	$1 \pm \sqrt{2}$	$\Omega_a = [(405 - 276\sqrt{2})K^2 + (36 + 111\sqrt{2})K - 118]/1024 \approx 0.45724$, and $\Omega_b = [(15 - 12\sqrt{2})K^2 + (12 - 3\sqrt{2})K - 2]/64 \approx 0.07780$ with $K = \sqrt[3]{8 + 6\sqrt{2}}$

where the coefficients Ω_a and Ω_b only depend on the CEoS parameters δ and ε. A summary of these coefficients is given in Tab. 2.2. The parameters of the van-der-Waals EoS is derived in Walas (1985, p. 15), the derivation of the parameters of an equation of state of the Redlich-Kwong type is given in Gmehling et al. (2012, p. 44), and for an equation of state of the Peng-Robinson type can be found in the appendix, see section A.1.

The VdW and the RK EoS use only the critical data of a compound as information. The other equations of state, such as SRK, PR, and PRG use the acentric factor ω as additional information in their α-function, see Tab. 2.1. The acentric factor is defined by

$$\omega = -\log_{10} \left.\frac{P^{\mathrm{vap}}}{P_{\mathrm{c}}}\right|_{T_{\mathrm{r}}=0.7} - 1 \tag{2.12}$$

which is a measure for the vapour pressure P^{vap} at a reduced temperature of $T_{\mathrm{r}} = 0.7$. For many spheric molecules, e. g. methane or argon, the acentric factor is close to zero, $\omega \to 0$.

With the definition of the acentric factor, it is clear, that equations of state, which include this parameter will lead to a better prediction of the vapour pressure curve. Therefore, those equations of state are also better to predict vapour-liquid equilibria.

2.3 Mixing Rules

The thermodynamic relationships, that are given in the previous section hold only for pure species, as the EoS parameters a and b are functions of the critical point of a unique substance. In the case of mixtures of different species, new parameters a_{m} and b_{m} for the mixture are required.

2.3.1 Empirical Mixing Rules

An empirical approach to obtain the mixture parameter a_m and b_m from the pure substance parameter a_i and b_i is the van-der-Waals mixing rule with a single binary interaction parameter (1PVDW, 1 parameter van-der-Waals mixing rule)

$$a_m = \sum_i \sum_j x_i x_j \sqrt{(a\alpha)_i (a\alpha)_j} \left(1 - k_{ij}\right), \qquad b_m = \sum_i x_i b_i. \qquad (2.13)$$

with the binary interaction parameter k_{ij}. Here, $(a\alpha)_i = a_i \alpha_i(T)$ refers to the pure-compound parameter a_i for species i and the corresponding α-function. In general, binary interaction parameter are obtained by fitting them against vapour-liquid data. Some binary interaction parameter values are given in Walas (1985, p. 54) for the Soave-Redlich-Kwong equation of state and in Walas (1985, p. 58) for the Peng-Robinson equation of state. Note, that specific values of the binary interaction parameter k_{ij} are only valid for a defined equation of state, i.e. $k_{ij}\big|_{\text{SRK}} \neq k_{ij}\big|_{PR}$. By setting the binary interaction coefficients of the 1PVDW model to zero, $k_{ij} = 0$, we get a mixing rule without any interaction parameter (0PVDW)

$$a_m = \sum_i \sum_j x_i x_j \sqrt{(a\alpha)_i (a\alpha)_j}, \qquad b_m = \sum_i x_i b_i. \qquad (2.14)$$

Note, that the 0PVDW model is in most cases not able to predict vapour-liquid equilibria correctly. The boiling-point diagram for the system (1) water—(2) methanol (MeOH) at $P = 101325\,\text{Pa}$ is shown in Fig. 2.1. Here, the dew point curve as well as the bubble point curve is shown using three different methods. The dots refer to experimental values according to Kurihara et al. (1993), the dashed curve is the prediction of the SRK equation of state with the 0PVDW mixing rule. We can see, that this prediction is weak. The solid line shows the prediction of the SRK EoS using the 1PVDW model, were the binary interaction coefficient $k_{12} = -0.0666$ is fitted against the experimental values.

Additionally, we can see, that the EoS models overestimate the boiling points, i.e. $T_{b,\text{H2O}} = 375\,\text{K}$ instead of the correct value of $T_{b,\text{H2O}} = 373\,\text{K}$. This is due to the fact, that the EoS model predicts the boiling point, based on two points of the vapour pressure curve, namely the critical point (T_c, P_c) and the acentric factor ω. A better approximation of the vapour pressure curve, i.e. the boiling point, is possible using modified α-functions as suggested by Mathias and Copeman (1983)

$$\alpha(T_r) = \begin{cases} \left[1 + c_1\left(1 - \sqrt{T_r}\right) + c_2\left(1 - \sqrt{T_r}\right)^2 + c_3\left(1 - \sqrt{T_r}\right)^3\right]^2 & : T_r < 1 \\ \left[1 + c_1\left(1 - \sqrt{T_r}\right)\right]^2 & : T_r \geq 1 \end{cases} \qquad (2.15)$$

where the parameters (c_1, c_2, c_3) are adjusted to the pure compound vapour pressure data, see also Gmehling et al. (2012, p. 53). Note, that Eq. (2.15) reduces for the case $(c_1, c_2, c_3) = (\kappa(\omega), 0, 0)$ to the conventional α-functions of the SRK and PR equation of state.
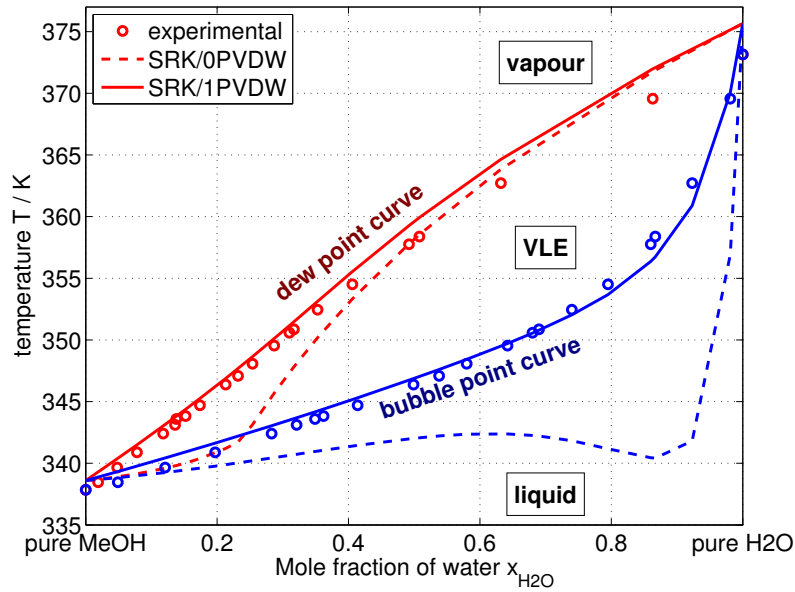
Figure 2.1: Bubble point and dew point curves of the binary system (1) water—(2) MeOH. Experimental data according to Kurihara et al. (1993).

2.3.2 g^{E} **Mixing Rules**

For a general property m, the corresponding excess property

$$m^{\mathrm{E}} = m - m^{\mathrm{id}} \tag{2.16}$$

describes the distance between the real state property m and the ideal mixture property m^{id}, see also Gmehling et al. (2012, p. 157). The class of the so-called g^{E} mixing rules use the excess Gibbs energy g^{E} of a mixture as an additional information, which can be obtained from an activity coefficient model. The excess Gibbs energy can be expressed as function of the activity coefficients γ_i as follows

$$g^{\mathrm{E}} = RT \sum_i x_i \ln \gamma_i . \tag{2.17}$$

Here, the activity coefficients are obtained from a suitable activity coefficient model, such as UNIQUAC or UNIFAC. These activity coefficient models are introduced in section 2.7. The first of the g^{E} mixing rules was introduced by Huron and Vidal (1979) and is given by

$$\frac{a_{\mathrm{m}}}{b_{\mathrm{m}}} = \sum_i \frac{x_i (a\alpha)_i}{b_i} + \frac{g^{\mathrm{E}}}{q_1}, \qquad b_{\mathrm{m}} = \sum_i x_i b_i \qquad \text{with } q_1 = \begin{cases} -0.693 & : \text{SRK EoS} \\ -0.623 & : \text{PR EoS} \end{cases} . \tag{2.18}$$

Another commonly used mixing rule is the PSRK mixing rule by Holderbaum and Gmehling (1991), which was introduced in the context of the development of the predictive Soave-Redlich-

Kwong (PSRK) equation of state. The PSRK mixing rule is given by

$$\frac{a_{\mathrm{m}}}{b_{\mathrm{m}}} = \sum_i \frac{x_i(a\alpha)_i}{b_i} + \frac{1}{q_1}\left[g^{\mathrm{E}} + RT\sum_i x_i \ln\frac{b_{\mathrm{m}}}{b_i}\right], \quad b_{\mathrm{m}} = \sum_i x_i b_i, \quad q_1 = -0.64663 : \mathrm{SRK\ EoS}.$$

(2.19)

The full PSRK equation of state is summarized in section 2.8. A more comprehensive summary of g^{E} mixing rules is given for example by Gmehling et al. (2012, p. 170) or Poling et al. (2001, p. 5.16).

2.4   Solution of a Cubic Equation of State

For the solution of the general cubic equation of state, Eq. (2.7), the equation of state is reformulated using the compressibility factor

$$Z = \frac{Pv}{RT}$$

(2.20)

which leads to

$$Z = \frac{v}{v-b} - \frac{va}{RT(v+\delta b)(v+\varepsilon b)}.$$

(2.21)

We define the dimensionless equation of state parameters A and B

$$A = \frac{aP}{(RT)^2} \qquad\qquad B = \frac{bP}{RT}$$

(2.22)

where a and b refer to the parameters a_{m} and b_{m} of the considered mixture. Now, Eq. (2.21) is reformulated as a cubic polynomial

$$0 = Z^3 + \left[(\delta+\varepsilon-1)B-1\right]Z^2 + \left[(\delta\varepsilon-\delta-\varepsilon)B^2 - (\delta+\varepsilon)B+A\right]Z + \left[\delta\varepsilon\left(B^3+B^2\right)-AB\right]$$

(2.23)

which simplifies for different equations of state to

$$0 = Z^3 - [B+1]Z^2 + AZ - AB \qquad\qquad : \mathrm{VdW} \tag{2.24a}$$

$$0 = Z^3 - Z^2 + \left[A-B-B^2\right]Z - AB \qquad\qquad : \mathrm{RK/SRK} \tag{2.24b}$$

$$0 = Z^3 + [B-1]Z^2 + \left[A-2B-3B^2\right]Z - B^3 - B^2 - AB \qquad : \mathrm{PR/PRG} \tag{2.24c}$$

There are several ways to solve cubic polynomials of the form

$$0 = Z^3 + c_2 Z^2 + c_1 Z + c_0.$$

(2.25)
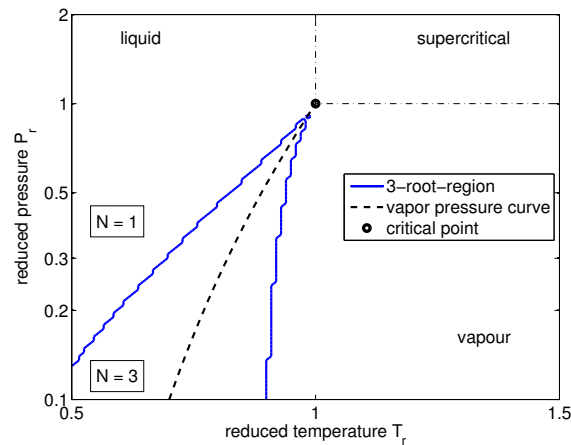
Figure 2.2: Number of real solutions of the Soave-Redlich-Kwong EoS as function of reduced temperature T_r and reduced pressure P_r. In the 3-root-region around the vapour pressure curve, the CEoS has three real solutions ($N = 3$), outside of this region the CEoS has only one real solution ($N = 1$).

One possibility is to compute the eigenvalues λ of the companion matrix

$$\mathbf{C} = \begin{bmatrix} 0 & 0 & -c_0 \\ 1 & 0 & -c_1 \\ 0 & 1 & -c_2 \end{bmatrix} \tag{2.26}$$

via $\det(\mathbf{C} - \lambda\mathbf{I}) = 0$, which is the approach that is also used by Matlabs `roots`-function. Another, more efficient way is an analytical solution of the cubic polynomial using Cardano's formula, see also appendix B.1.

The number of real solutions of the SRK equation of state for a hypothetical species with an acentric factor of $\omega = 0$ is given in Fig. 2.2. Species with an acentric factor close to zero are methane ($\omega = 0.011$) or argon ($\omega = -0.002$), see also Poling et al. (2001). The number of real solutions is plotted as function of reduced temperature $T_r = T/T_c$ and reduced pressure $P_r = P/P_c$ on a range of $1/2 \leq T_r \leq 3/2$ and $1/10 \leq P_r \leq 2$. Additionally, the vapour pressure P^{vap} of this hypothetical species was estimated using the method of Lee and Kesler (1975) and is also shown in the diagram. The Lee-Kesler method gives an approximation of the vapour pressure curve based on the acentric factor of a species, see also appendix A.3.

For a pure compound, the liquid and the vapour phase coexist only on the vapour pressure curve. As we can see in Fig. 2.2, an equation of state has a 3-root-region as well as a 1-root-region. Inside the 3-root-region, the smallest compressibility factor refers to the liquid phase (Z close to zero), the largest compressibility factor refers to the gaseous phase (Z close to one) and the solution in between has no physical meaning. Therefore one has to select the correct phase in this region. One possibility is to compare the current point in terms of temperature T and pressure P against the vapour pressure curve $P^{\mathrm{vap}}(T)$.

The value of the compressibility factor Z for the same system is shown in Fig. 2.3. It can be seen

(a) $Z = Z(T_r, P_r)$

(b) $Z = Z(T_r, P_r^{vap}(T_r))$
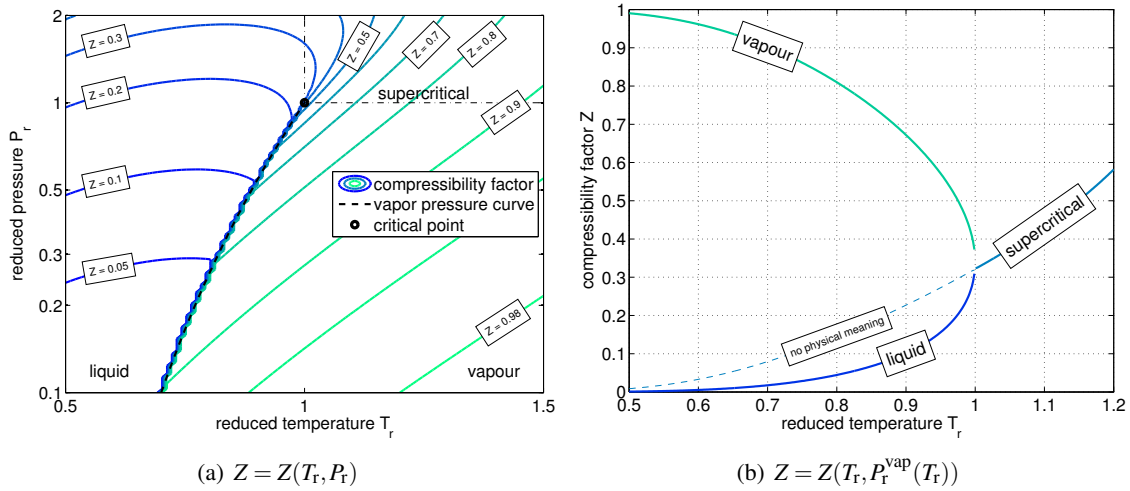
Figure 2.3: (a) Compressibility factor as function of reduced temperature T_r and reduced pressure P_r using the SRK equation of state. (b) Compressibility factors on the vapour pressure curve and beyond.

that there is a discontinuity on the vapour pressure curve, especially at low temperatures/pressures, as well as a smooth transition in the supercritical region.

2.5 Thermodynamic Potentials

Besides of the thermal state of a thermodynamic system which is defined by an equation of state $F(P,T,v) = 0$, also the caloric information in terms of the ideal gas heat capacity $c_p(T)$ as a function of the temperature is required. Applying the fundamental thermodynamic relations and the ideal gas law, Eq. (2.2), one gets the ideal gas enthalpy of formation

$$\Delta_f h^{id}(T) = \Delta_f h^\circ + \int_{T^\circ}^T c_p(\tilde{T}) \, d\tilde{T} \,, \tag{2.27}$$

as well as the ideal gas entropy of a species

$$s^{id}(T,P) = s^\circ + \int_{T^\circ}^T \frac{c_p(\tilde{T})}{\tilde{T}} \, d\tilde{T} - R \ln \frac{P}{P^\circ} \,. \tag{2.28}$$

Here, $\Delta_f h^{id}$ refers to the ideal gas standard enthalpy of formation, and s° refers to the ideal gas standard entropy. The values for standard temperature T° and standard pressure P° that are recommended by the International Union of Pure and Applied Chemistry (1982) are given by

$$T^\circ = 298.15\,\text{K} \quad \text{and} \quad P^\circ = 100\,\text{kPa}\,. \tag{2.29}$$

Applying the fundamental thermodynamic relation

$$g = h - Ts \,, \tag{2.30}$$

one gets also an expression for the ideal gas Gibbs energy of formation

$$\Delta_{\mathrm{f}}g^{\mathrm{id}}(T,P) = \Delta_{\mathrm{f}}h^{\mathrm{id}}(T) - T\Delta_{\mathrm{f}}s^{\mathrm{id}}(T,P) =$$

$$\Delta_{\mathrm{f}}h^\circ + \int_{T^\circ}^{T} c_{\mathrm{p}}(\tilde{T})\,\mathrm{d}\tilde{T} - T\left[\Delta_{\mathrm{f}}s^\circ + \int_{T^\circ}^{T} \frac{c_{\mathrm{p}}(\tilde{T})}{\tilde{T}}\,\mathrm{d}\tilde{T} - R\ln\frac{P}{P^\circ}\right]. \quad (2.31)$$

With the ideal gas standard entropy of formation

$$\Delta_{\mathrm{f}}s^\circ = \frac{\Delta_{\mathrm{f}}h^\circ - \Delta_{\mathrm{f}}g^\circ}{T^\circ}, \quad (2.32)$$

this leads to the expression

$$\Delta_{\mathrm{f}}g^{\mathrm{id}}(T,P) = \Delta_{\mathrm{f}}h^\circ\left(1 - \frac{T}{T^\circ}\right) + \Delta_{\mathrm{f}}g^\circ\frac{T}{T^\circ} + \int_{T^\circ}^{T} c_{\mathrm{p}}(\tilde{T})\,\mathrm{d}\tilde{T} - T\int_{T^\circ}^{T} \frac{c_{\mathrm{p}}(\tilde{T})}{\tilde{T}}\,\mathrm{d}\tilde{T} + RT\ln\frac{P}{P^\circ}, \quad (2.33)$$

see also Poling et al. (2001, p. 3.3) and Gmehling et al. (2012, p. 358). Note that the properties $\Delta_{\mathrm{f}}h^\circ$, $\Delta_{\mathrm{f}}g^\circ$, and $\Delta_{\mathrm{f}}s^\circ$ are related to the chemical elements in their standard state, while s° is related to absolute zero, i. e. $s^\circ(T=0) = 0$. Since the most textbooks for thermodynamic data lists the triplet $(\Delta_{\mathrm{f}}h^\circ, \Delta_{\mathrm{f}}g^\circ, s^\circ)$, and not the standard entropy of formation, a formulation for the Gibbs energy of formation, Eq. (2.33), is used that does not require an information about the entropy. Note also, that the triplets $(\Delta_{\mathrm{f}}h^\circ, \Delta_{\mathrm{f}}g^\circ, s^\circ)$ do not fulfil the fundamental equation Eq. (2.30) due to the different reference points.

With this equations, we are now able to compute the ideal gas properties for pure substances if we know the

- standard ideal gas enthalpy of formation $\Delta_{\mathrm{f}}h^\circ$, the

- standard ideal gas Gibbs energy of formation $\Delta_{\mathrm{f}}g^\circ$, the

- standard entropy s°, and the

- ideal gas heat capacity as a function of temperature $c_{\mathrm{p}}(T)$.

Some databases which provide these thermodynamic properties are Yaws (1999), Yaws (2008), Haynes and Lide (2010), and Linstrom and Mallard (2015). Note that the representations of the heat capacities vary in the literature. Common representations are polynomials in the temperature or the Shomate equation which is a polynomial with an additional reciprocal $1/T^2$-term. Another correlation, which is derived from statistical mechanics was proposed by Aly and Lee (1981) and incorporates some hyperbolic functions. An overview of the different correlations for the heat capacity and a comparison of their accuracy is given in the appendix, see section A.2. The caloric data that is used in this thesis is summarized in appendix A.6.

Additionally, with a defined representation for the ideal gas heat capacity, the integrals $\int c_{\mathrm{p}}\,\mathrm{d}\tilde{T}$ and $\int c_{\mathrm{p}}/\tilde{T}\,\mathrm{d}\tilde{T}$ which occur in the representations of the enthalpy of formation, the entropy, as well as the Gibbs energy of formation can be replaced by their corresponding algebraic expressions.

2.6 Departure Functions and Fugacity Coefficients

In the last section, the thermodynamic potentials for ideal gases m^{id} were defined. In order to describe the real thermodynamic potentials, a residual part m^{R} has to be added

$$m = m^{\text{id}} + m^{\text{R}}. \tag{2.34}$$

These departure functions $\left(m - m^{\text{id}}\right)$ can be derived from fundamental thermodynamic relationships, see e. g. Gmehling et al. (2012).

If we assume a pressure-explicit equation of state in its dimensionless formulation $Z = F(v, T)$, such as Eq. (2.21), the departure functions of the thermodynamic potentials enthalpy and Gibbs energy are given as follows

$$\frac{h - h^{\text{id}}}{RT} = Z - 1 - \int_{v}^{\infty} T \frac{\partial Z}{\partial T} \frac{\text{d}\tilde{v}}{\tilde{v}}, \tag{2.35a}$$

$$\frac{g - g^{\text{id}}}{RT} = Z - 1 - \ln Z - \int_{v}^{\infty} (1 - Z) \frac{\text{d}\tilde{v}}{\tilde{v}}. \tag{2.35b}$$

By applying the general cubic equation of state in its dimensionless formulation, Eq. (2.21), and evaluating the improper integrals, one obtains the following algebraic expressions for these departure functions:

$$\frac{h - h^{\text{id}}}{RT} = Z - 1 - \frac{A}{(\varepsilon - \delta) B} \left[1 - \frac{T}{\alpha} \frac{\text{d}\alpha}{\text{d}T} \right] \ln \frac{Z + \varepsilon B}{Z + \delta B}, \tag{2.36a}$$

$$\frac{g - g^{\text{id}}}{RT} = Z - 1 - \ln[Z - B] - \frac{A}{(\varepsilon - \delta) B} \ln \frac{Z + \varepsilon B}{Z + \delta B}. \tag{2.36b}$$

With a given set of EoS parameters (δ, ε), this leads to the departure functions of specific equation of state. Note, that these expressions are not defined for the case $\delta = \varepsilon$, which is the case when using the van-der-Waals equation of state with $\delta = \varepsilon = 0$. In this case the particular departure function can be obtained by applying the limit

$$\lim_{\varepsilon \to \delta} \frac{A}{(\varepsilon - \delta) B} \ln \frac{Z + \varepsilon B}{Z + \delta B} = \frac{A}{Z + \delta B}. \tag{2.37}$$

Similar to the departure functions, the partial fugacity coefficient ϕ_k of the species k can be expressed by

$$\ln \phi_k = \int_{v}^{\infty} \left[\frac{\partial Z}{\partial n_k} - 1 \right] \frac{\text{d}\tilde{v}}{\tilde{v}} - \ln Z. \tag{2.38}$$

This can also be written as the following algebraic expression for the general cubic equation of

state (2.21)

$$
\ln \phi_k = \frac{(nb)'}{b} (Z-1) - \ln [Z-B] - \frac{A}{(\varepsilon-\delta) B} \left[\frac{(n^2 a)'}{na} - \frac{(nb)'}{b} \right] \ln \frac{Z+\varepsilon B}{Z+\delta B} \tag{2.39}
$$

where

$$
(.)' = \frac{\partial}{\partial n_k} (.) \tag{2.40}
$$

refers to the partial derivative of the mixing rule with respect to the partial molar composition. For the 1PVDW mixing rule, these derivations are given by

$$
\frac{(n^2 a)'}{na} = \frac{2}{a} \sum_i x_i \sqrt{(a\alpha)_i (a\alpha)_k} (1-k_{ik}) , \text{ and} \qquad \frac{(nb)'}{b} = \frac{b_k}{b} . \tag{2.41}
$$

In case of the PSRK mixing rule, these derivatives yield to

$$
\frac{(n^2 a)'}{na} = \frac{bRT}{aq_1} \left[\ln \gamma_k - \ln \frac{b_k}{b} + \frac{b_k}{b} - 1 \right] + \frac{a_k b}{a b_k} + \frac{b_k}{b} , \text{ and} \qquad \frac{(nb)'}{b} = \frac{b_k}{b} . \tag{2.42}
$$

The departure functions of the enthalpy $\Delta h/RT$ and the Gibbs energy $\Delta g/RT$ are shown in Fig. 2.4. Both departure functions are shown as functions of the reduced temperature T_r and the reduced pressure P_r in Fig. 2.4(a) for the enthalpy and in Fig. 2.4(c) for the Gibbs energy, respectively. The enthalpy departure at the vapour pressure as a function of the reduced temperature, i.e. $\Delta h \left(T_r, P_r^{\text{vap}}(T_r) \right) /RT$, is shown in Fig. 2.4(b). Here, the difference between the liquid phase enthalpy departure and the vapour phase enthalpy departure is equal to the enthalpy of vaporization

$$
\frac{\Delta h^{\text{L}}}{RT} - \frac{\Delta h^{\text{V}}}{RT} = \frac{\Delta_{\text{vap}} h}{RT} . \tag{2.43}
$$

The Gibbs energy departure at the vapour pressure is shown in Fig. 2.4(d) w.r.t. the reduced temperature. Since the change in the Gibbs energy at a phase transition is zero, the departure functions for the liquid and the vapour phases are equal. Note, that the SRK equation of state does not know the exact vapour pressure curve, but only the critical point and the vapour pressure at $T_r = 0.7$ which corresponds to the definition of the acentric factor ω. This can also be seen in Fig. 2.4(d) since the distance between vapour and liquid phase Gibbs energy departure is only zero at $T_r = 0.7$ and $T_r = 1$ while at other reduced temperatures a minor deviation can be observed. As already mentioned in section 2.3.1, a better approximation of the vapour pressure curve from an cubic equation of state can be obtained by using the modified α-function by Mathias and Copeman (1983).
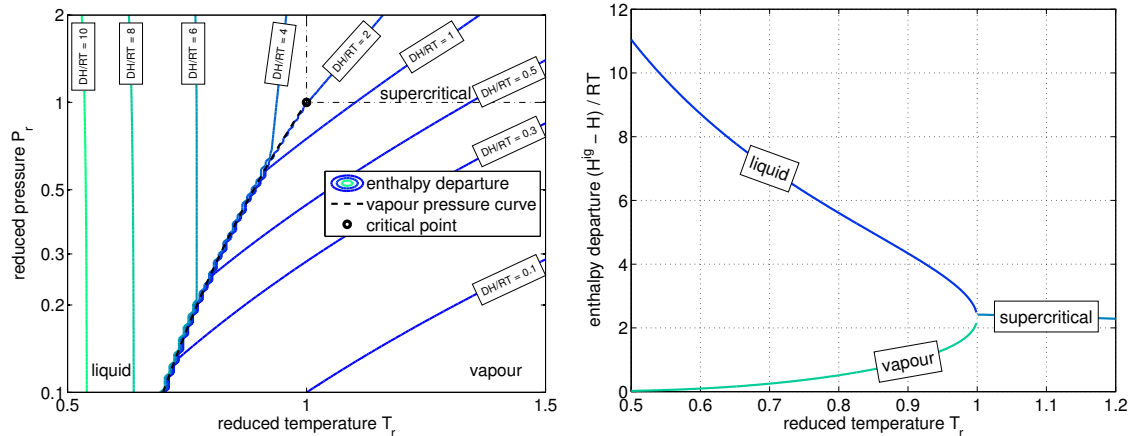
(a) Enthalpy departure as a function of temperature and pressure.

(b) Enthalpy departure on the vapour pressure curve.
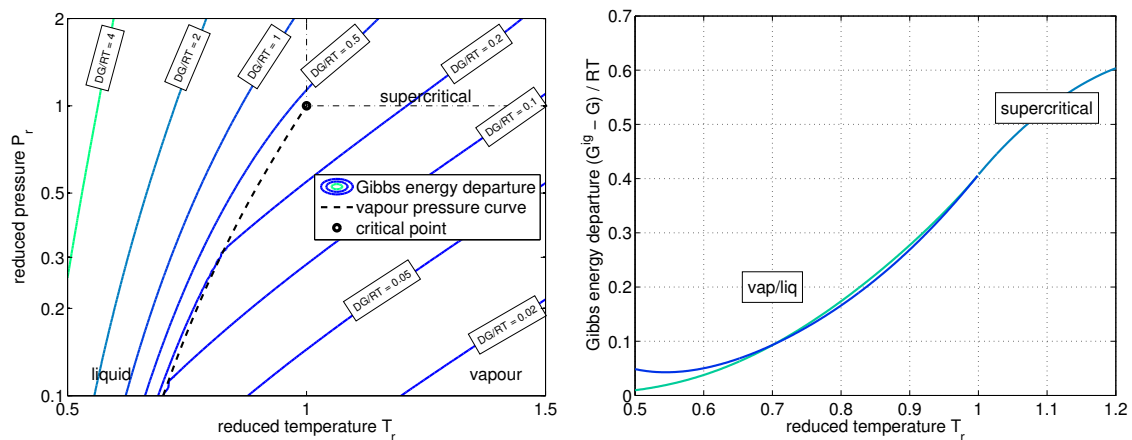
(c) Gibbs energy departure as a function of temperature and pressure.

(d) Gibbs energy departure on the vapour pressure curve.

Figure 2.4: Departure functions for a species with acentric factor $\omega = 0$ using the SRK equation of state. (a) Enthalpy departure $\Delta h/RT$ as a function of the reduced temperature T_r and the reduced pressure P_r. (b) Enthalpy departure on the vapour pressure curve and beyond. (c) Gibbs energy departure $\Delta g/RT$ as a function of temperature and pressure. (d) Gibbs energy departure on the vapour pressure curve and beyond.

2.7 Activity Coefficient Models

The Gibbs excess energy g^E is an excess property which the basis for activity coefficient models. For the definition of an excess property of a general property m, as well as for the Gibbs excess energy in particular, see section 2.3.2. The Gibbs excess energy is used by the so-called g^E-mixing rules in order to predict the properties of mixtures using equations of state. It is expressed in terms of the activity coefficients as follows

$$g^E = RT \sum_\alpha x_\alpha \ln \gamma_\alpha . \tag{2.44}$$

Applying the Gibbs-Duhem equation, the activity coefficient γ_α can be expressed in terms of the Gibbs excess energy by

$$RT \ln \gamma_\alpha = \frac{\partial \left(n_t g^E \right)}{\partial n_\alpha} , \tag{2.45}$$

where $n_t = \sum_\alpha n_\alpha$ refers to the total molar amount in the system. For a derivation of this relationship, see for example Poling et al. (2001, p. 8.13). Common activity coefficient models are the UNIQUAC model or the NRTL model. An extension of the UNIQUAC model towards a group contribution activity coefficient model is the UNIFAC model. Both, the UNIQUAC and the UNIFAC models are introduced in the following sections 2.7.1 and 2.7.2, respectively.

2.7.1 UNIQUAC Method

The UNIQUAC (universal quasichemical) model (Abrams and Prausnitz, 1975) assumes that the activity coefficients consists of a combinatorial part and a residual part, e. g.

$$\ln \gamma_\alpha = \ln \gamma_\alpha^C + \ln \gamma_\alpha^R . \tag{2.46}$$

The combinatorial part accounts for the size and the shape of the molecules and depends only on pure substance parameters. It is given by

$$\ln \gamma_\alpha^C = 1 - V_\alpha + \ln V_\alpha - 5 q_\alpha \left(1 - \frac{V_\alpha}{F_\alpha} + \ln \frac{V_\alpha}{F_\alpha} \right) \tag{2.47a}$$

Table 2.3: Some values for the relative van-der-Waals volume r_α and the relative van-der-Waals surface q_α according to Horstmann et al. (2005).

species α	H_2	H_2O	CO	CO_2	CH_4	CH_3OH
r_α	0.416	0.92	0.711	1.3	1.1292	1.4311
q_α	0.571	1.4	0.828	0.982	1.124	1.432

with

$$V_\alpha = \frac{r_\alpha}{\sum_\beta x_\beta r_\beta} \, , \text{ and} \qquad\qquad (2.47b)$$

$$F_\alpha = \frac{q_\alpha}{\sum_\beta x_\beta q_\beta} \, . \qquad\qquad (2.47c)$$

The pure-compound parameters are the relative van-der-Waals volume r_α and the relative van-der-Waals surface q_α. Some values for these parameters are displayed in Tab. 2.3. The residual part describes the interactions between the distinct molecules and is given by

$$\ln\gamma_\alpha^R = q_\alpha \left(1 - \ln\frac{\sum_\beta x_\beta q_\beta \tau_{\beta\alpha}}{\sum_\beta x_\beta q_\beta} - \sum_\beta \frac{x_\beta q_\beta \tau_{\alpha\beta}}{\sum_\delta x_\delta q_\delta \tau_{\delta\beta}} \right) \qquad\qquad (2.48a)$$

with

$$\tau_{\alpha\beta} = \exp\left(\frac{-\Delta u_{\alpha\beta}}{T} \right) , \qquad\qquad \text{and } \tau_{\alpha\alpha} = 1 \, . \qquad (2.48b)$$

Here, $\Delta u_{\alpha\beta}$ is the binary interaction parameter of the compounds α and β. Some extensions of the original UNIQUAC model introduce a temperature-dependent interaction coefficient using the polynomial

$$\Delta u_{\alpha\beta} = a_{\alpha\beta} + b_{\alpha\beta}T + c_{\alpha\beta}T^2 \qquad\qquad (2.49)$$

or even more complex temperature-dependent expressions, see also Gmehling et al. (2012, p. 214). In general, the binary interaction coefficients $\tau_{\alpha\beta}$ are obtained from the measured vapour-liquid equilibrium data or liquid-liquid equilibrium data by non-linear regression. Additionally, it is possible to predict these binary interaction coefficients using quantum-chemical methods. For instance, the software COSMOtherm which is based on COSMO-RS (Klamt, 1995) is able to predict the binary UNIQUAC parameters. Fig. 2.5 shows the temperature-dependent binary interaction parameters $\tau_{\alpha\beta}(T)$ for the senary system H_2, H_2O, CO, CO_2, CH_4 and CH_3OH on the temperature-range $298 \leq T/\text{K} \leq 398$ which are computed using the COSMOtherm software. The ordinates of this figure are scaled to the interval $0 \leq \tau_{\alpha\beta} \leq 2$.

2.7.2 UNIFAC Method

The UNIFAC (universal quasichemical funcitonal group activity coefficients) model (Fredenslund et al., 1975, 1977) is a group contribution method for estimation of activity coefficients which is derived from the UNIQUAC model. While the parameters for the UNIQUAC model are obtained from experimental data by parameter fitting, the UNIFAC model predicts these parameters without experimental data by the use of molecular group contributions.
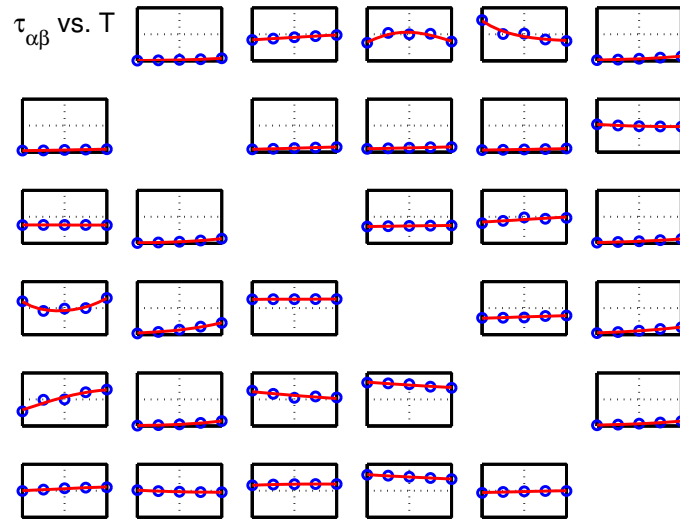
Figure 2.5: The UNIQUAC interaction parameters $\tau_{\alpha\beta}(T)$ for the senary system H_2, H_2O, CO, CO_2, CH_4 and CH_3OH as function of the temperature T. The rows and columns refer to the species α and β, respectively. Since $\tau_{\alpha\alpha} = 1$, the diagonal elements are trivial and not displayed here. For each graph the temperature is plotted on the abscissas on the interval $298 \leq T/K \leq 398$, while the interaction coefficients on the ordinates are normalized to the interval $0 \leq \tau_{\alpha\beta} \leq 2$. The blue dots refer to to predictions by the COSMOtherm software and the red lines are polynomials fitted against these data points.

The UNIFAC model consists also of a combinatorial part and a residual part

$$\ln \gamma_\alpha = \ln \gamma_\alpha^C + \ln \gamma_\alpha^R \tag{2.50}$$

where the structure of the combinatorial part is identical to that one of the UNIQUAC model

$$\ln \gamma_\alpha^C = 1 - V_\alpha + \ln V_\alpha - 5 q_\alpha \left(1 - \frac{V_\alpha}{F_\alpha} + \ln \frac{V_\alpha}{F_\alpha} \right) \tag{2.51a}$$

with

$$V_\alpha = \frac{r_\alpha}{\sum_\beta x_\beta r_\beta}, \text{ and} \tag{2.51b}$$

$$F_\alpha = \frac{q_\alpha}{\sum_\beta x_\beta q_\beta}. \tag{2.51c}$$

In the context of the UNIFAC model the relative van-der-Waals volume r_α and the relative van-der-Waals surface q_α are estimated by group contributions

$$r_\alpha = \sum_i G_i^{(\alpha)} R_i, \text{ and} \tag{2.52a}$$

$$q_\alpha = \sum_i G_i^{(\alpha)} Q_i, \tag{2.52b}$$

where $G_i^{(\alpha)}$ refers to the number of groups i in the molecule α. Here, R_i refers to the contribution

of the group i to the relative van-der-Waals volume r_α, and Q_i refers to the contribution of the group i to the relative van-der-Waals surface q_α. The residual part $\ln \gamma_\alpha^R$ of the UNIFAC model is temperature-dependent and describes the binary interactions between the species.

$$\ln \gamma_\alpha^R = \sum_i G_i^{(\alpha)} \left(\ln \Gamma_i - \ln \Gamma_i^{(\alpha)} \right) \tag{2.53}$$

It consists of the group activity coefficients Γ_i for a group i, and $\Gamma_i^{(\alpha)}$ for a species α, respectively. The mixture term is given by

$$\ln \Gamma_i = Q_i \left[1 - \ln \left[\sum_m \Theta_m \Psi_{mi} \right] - \sum_m \frac{\Theta_m \Psi_{im}}{\sum_n \Theta_n \Psi_{nm}} \right] \tag{2.54a}$$

with

$$\Theta_i = \frac{Q_i X_i}{\sum_j Q_j X_j}, \tag{2.54b}$$

$$X_i = \frac{\sum_\alpha G_i^{(\alpha)} x_\alpha}{\sum_j \sum_\alpha G_j^{(\alpha)} x_\alpha}, \tag{2.54c}$$

and the binary interaction

$$\Psi_{ij} = \exp \left[-\frac{a_{ij} + b_{ij} T + c_{ij} T^2}{T} \right]. \tag{2.54d}$$

Here, the coefficients a_{ij}, b_{ij}, and c_{ij} describe the temperature-dependent binary interactions between the groups i and j. The pure component group activity coefficient is given by

$$\ln \Gamma_i^{(\alpha)} = Q_i \left[1 - \ln \left[\sum_m \Theta_m^{(\alpha)} \Psi_{mi} \right] - \sum_m \frac{\Theta_m^{(\alpha)} \Psi_{im}}{\sum_n \Theta_n^{(\alpha)} \Psi_{nm}} \right] \tag{2.55a}$$

with

$$\Theta_m^{(\alpha)} = \frac{Q_m X_m^{(\alpha)}}{\sum_n Q_n X_n^{(\alpha)}}, \text{ and} \tag{2.55b}$$

$$X_m^{(\alpha)} = \frac{G_m^{(\alpha)}}{\sum_n G_n^{(\alpha)}}. \tag{2.55c}$$

A summary of the group contribution of the pure-compound parameters Q_i and R_i, as well as the binary interaction parameters are given by Horstmann et al. (2005).

2.7.2.1 Example

In order to illustrate how the UNIFAC model works, it is applied here to the ternary system n-heptane–aniline–water. This ternary system is also used as a test problem for computing LLL equilibria in section 3.3.4. The three species can be constructed from the five UNIFAC groups

Table 2.4: Relevant UNIFAC groups for the system *n*-heptane–aniline–water and the corresponding group increments for the relative van-der-Waals volume R_i and the relative van-der-Waals surface Q_i according to Horstmann et al. (2005).

main group		sub group		R_i	Q_i
1	CH_2	1	CH_3	0.9011	0.848
		2	CH_2	0.6744	0.54
3	ACH	9	ACH	0.5313	0.4
7	H_2O	16	H_2O	0.92	1.4
17	$ACNH_2$	36	$ACNH_2$	1.06	0.816

given in Tab. 2.4. For a detailed illustration of these UNIFAC groups, see also Fig. 2.6. There are two types of UNIFAC groups. The

main groups are relevant for the group contributions of the binary interactions, and the

sub groups define the group contributions for the pure-compound data, i. e. the relative van-der-Waals volume and surface, respectively.

Therefore, the matrix with the group increments is given by

$$\mathbf{G} = \left[G_i^{(\alpha)} \right]_{\alpha i} = \begin{bmatrix} 2 & 5 & 0 & 0 & 0 \\ 0 & 0 & 5 & 0 & 1 \\ 0 & 0 & 0 & 1 & 0 \end{bmatrix} \tag{2.56}$$

where each column refers to a UNIFAC subgroup as defined in Tab. 2.4 and the rows refer to the species *n*-heptane, aniline, and water, respectively. The matrix containing the binary interaction coefficients a_{ij} is given by

$$\mathbf{A} = \left[a_{ij} \right]_{ij} = \begin{bmatrix} 0 & 0 & 61.13 & 1318 & 920.7 \\ 0 & 0 & 61.13 & 1318 & 920.7 \\ -11.12 & -11.12 & 0 & 903.8 & 648.2 \\ 300 & 300 & 362.3 & 0 & 243.2 \\ 1139 & 1139 & 247.5 & -341.6 & 0 \end{bmatrix} \tag{2.57}$$
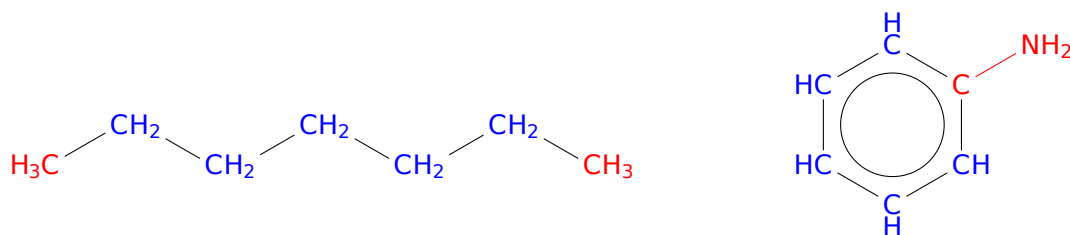
Figure 2.6: The UNIFAC group increments of *n*-heptane are 2 CH_3, 5 CH_2 (left) and the group increments of aniline are 5 ACH, 1 $ACNH_2$ (right). The AC in the identifiers of the aniline refer to an aromatic carbon atom. The third species of the system, water, has its own group.

while the binary interaction coefficients b_{ij} and c_{ij} are all zero for the given system,

$$\mathbf{B} = [b_{ij}]_{ij} = \mathbf{0}, \qquad\qquad \mathbf{C} = [c_{ij}]_{ij} = \mathbf{0}. \qquad (2.58)$$

Due to the fact that the first two sub groups in this system refer to the same main group, the first two rows as well as the first two columns of the matrices $\mathbf{A}$, $\mathbf{B}$, and $\mathbf{C}$ are identical. A summary of all UNIFAC parameters for functional groups, the pure-compound parameters as well as the binary interaction parameters, is given by Horstmann et al. (2005).

2.7.2.2 Implementation

The UNIFAC equations can be implemented in MATLAB very efficiently by vectorization of the original equations. An implementation of the UNIFAC model for the system *n*-heptane–aniline– water is given in the following listing. This code can be adapted to an arbitrary system by modifying the parameters in the first part of the code (lines 6–17).

Listing 2.1: Implementation of the UNIFAC model of the ternary system *n*-heptane–aniline–water.

```matlab
 1  function lnGamma = UNIFAC(x,T)
 2  % LNGAMMA = UNIFAC(X,T)   Implementation of the UNIFAC model. Returns a
 3  %    vector of logarithmic activity coefficients LNGAMMA. Input arguments
 4  %    are a vector of mole fractions X and the temperature T in K.
 5
 6  % === definition of the system parameter ================================= %
 7  R = [ 0.9011 0.6744 0.5313  0.92   1.06  ]';
 8  Q = [ 0.848  0.54   0.4     1.4    0.816 ]';
 9  G = [ 2       5       0       0     0
10        0       0       5       0     1
11        0       0       0       1     0    ];
12  A = [ 0       0     61.13  1318   920.7
13        0       0     61.13  1318   920.7
14      -11.12 -11.12   0      903.8  648.2
15       300    300    362.3    0     243.2
16      1139    1139   247.5  -341.6   0    ];
17  [B,C] = deal(zeros(5));
18
19  % === combinatorial part ================================================= %
20  r    = G * R;
21  q    = G * Q;
22  V    = r / (x' * r);
23  VoF  = (x' * q) * V ./ q;
24  lnGammaC = 1 - V + log(V) - 5*q .* (1 - VoF + log(VoF));
25
26  % === residual part ====================================================== %
```

```
27  [nC,nG] = size(G);
28  oC = ones(nC,1);
29  oG = ones(1,nG);
30
31  PSI = exp(-A/T - B - C*T);          % interaction coefficients --- %
32
33  X     = G' * x / sum(G' * x);       % mixture term -------------- %
34  THETA = Q.* X / (Q' * X);
35  tmp0  = PSI' * THETA;
36  lnGm  = Q .* (1 - log(tmp0) - PSI*(THETA./tmp0));
37
38  X     = G ./ (sum(G,2) * oG);       % pure components term ------- %
39  tmp0  = oC * Q';
40  THETA = tmp0 .* X ./ (X * Q * oG);
41  tmp1  = THETA * PSI;
42  lnGp  = tmp0 .* (1 - log(tmp1) - (THETA ./ tmp1) * PSI');
43
44  lnGammaR = sum(G .* (oC * lnGm' - lnGp), 2);
45
46  lnGamma  = lnGammaC + lnGammaR;
```

2.8 Predictive Soave-Redlich-Kwong Equation of State

The so-called predictive Soave-Redlich-Kwong (PSRK) equation of state is a group contribution equation of state (Holderbaum and Gmehling, 1991; Holderbaum, 1991) which is based on the Soave-Redlich-Kwong EoS (Soave, 1972)

$$P = \frac{RT}{v-b} - \frac{a\alpha(T)}{v(v-b)}. \tag{2.59}$$

It applies the α-function of Mathias and Copeman (1983)

$$\alpha(T_r) = \begin{cases} \left[1 + c_1 \left(1 - \sqrt{T_r} \right) + c_2 \left(1 - \sqrt{T_r} \right)^2 + c_3 \left(1 - \sqrt{T_r} \right)^3 \right]^2 & : T_r < 1 \\ \left[1 + c_1 \left(1 - \sqrt{T_r} \right) \right]^2 & : T_r \geq 1 \end{cases} \tag{2.60}$$

and the g^E mixing rule

$$a_m = b_m \sum_i \frac{x_i (a\alpha)_i}{b_i} + \frac{b_m}{q_1} \left[g^E + RT \sum_i x_i \ln \frac{b_m}{b_i} \right] \qquad b_m = \sum_i x_i b_i \tag{2.61}$$

with the constant factor $q_1 = -0.64663$. The Gibbs excess energy $g^E = RT \sum_i x_i \ln \gamma_i$ is computed using the UNIFAC activity coefficient model, see section 2.7.2.

Thermodynamic Equilibrium Calculations

The second law of thermodynamics defines that in a closed system the entropy S will evolve towards its maximum. This is equivalent to the condition that in a thermodynamic equilibrium state an energy function will evolve towards its minimum. In order to compute the thermodynamic equilibrium of a system a thermodynamic potential has to be minimized, depending of the choice of the independent state variables. A summary of the independent state variables and the related thermodynamic potential is shown in Tab. 3.1, see also Walas (1985, p. 131).

Table 3.1: Independent variables and the corresponding thermodynamic potential that reaches its minimum in equilibrium state. The intensive state variables$^{(\star)}$ are indicated by a star.

independent variables		minimum
entropy S	volume V	internal energy U
pressure$^{(\star)}$ P	entropy S	enthalpy H
temperature$^{(\star)}$ T	volume V	Helmholtz energy A
temperature$^{(\star)}$ T	pressure$^{(\star)}$ P	Gibbs energy G

In technical devices, it is much easier to control the intensive state variables temperature and pressure than the extensive ones. Therefore, it is common to minimize the Gibbs energy G to find the thermodynamic equilibrium for a given temperature T and pressure P

$$\min_{n_\alpha^\pi} G \tag{3.1}$$

subject to stoichiometric constraints.

In the case of pure phase equilibrium calculations, instead of the Gibbs energy minimization the solution of the isofugacity condition

$$f_\alpha^\pi = f_\alpha^{\pi'} \tag{3.2}$$

is a common problem formulation, see e. g. Walas (1985, p. 301) or Gmehling et al. (2012, p. 161). For chemical reactions the use of the equilibrium constant is also a commonly used equilibrium condition

$$K_{\text{eq},\rho} = \exp\left(\frac{-\Delta_\text{r}g_\rho}{RT}\right) = \prod_\alpha \left(\frac{f_\alpha}{f_\alpha^\circ}\right)^{\nu_{\alpha\rho}}, \tag{3.3}$$

see e. g. Walas (1985, p. 466) or Gmehling et al. (2012, pp. 533–534). In the next section, the minimization of the Gibbs energy is exemplified for a chemical reaction system. After that, the Dynamic Method is introduced which is based on the solution of set of differential equations that satisfies in its steady state the algebraic equilibrium conditions above.

3.1   Gibbs Energy Minimization

This section gives a brief overview of the Gibbs energy minimization method for chemical systems in one phase, e. g. in a vapour phase, see also Lwin (2000). The chemical equilibrium composition is reached when the Gibbs energy of a system reaches its minimum, i. e. when the composition n_α is chosen in a way that the corresponding Gibbs energy is minimal. The resulting mathematical problem can be formulated by

$$\min_{n_\alpha} n_\text{t}g \tag{3.4a}$$

subject to

$$\mathbf{A}\mathbf{n} = \mathbf{b} \qquad \text{elemental balances,} \tag{3.4b}$$

$$n_\alpha \geq 0 \quad \forall \alpha \qquad \text{non-negativity constraints.} \tag{3.4c}$$

Here, $n_\text{t}g$ refers to the Gibbs energy of the system

$$n_\text{t}g = \sum_{\alpha \in \mathscr{S}} n_\alpha \Delta_\text{f}g_\alpha^\circ(T) + RT n_\alpha \ln \frac{f_\alpha}{f_\alpha^\circ} \tag{3.5}$$

and $n_\text{t} = \sum_\alpha n_\alpha$ refers to the total molar amount of substance This non-linear programming problem (NLP) is constrained by the elemental balances. The matrix $\mathbf{A} = [a_{\varepsilon\alpha}]$ is the so-called elemental matrix where $a_{\varepsilon\alpha}$ refers to the number of atoms ε in species α. The vector $\mathbf{n} = [n_\alpha]$ refers to the actual composition of the system and the vector $\mathbf{b}$ refers to the elemental composition of the initial state $\mathbf{n}^0$, i. e. $\mathbf{b} = \mathbf{A}\mathbf{n}^0$. Of course, negative amounts of substance are not allowed, and therefore the non-negativity constraints $n_\alpha \geq 0$ is included into the problem formulation.

3.1.1 Example

Assuming a system containing the five species $\mathscr{S} = \{CO_2, H_2, CH_4, H_2O, CO\}$, the elemental matrix of this system is given by

$$\mathbf{A} = \begin{bmatrix} 1 & 0 & 1 & 0 & 1 \\ 2 & 0 & 0 & 1 & 1 \\ 0 & 2 & 4 & 2 & 0 \end{bmatrix} \tag{3.6}$$

where each column describes one of the considered species and the rows refer to the atoms carbon (C), oxygen (O) and hydrogen (H), respectively. For the sake of simplicity, we assume ideal gas behaviour in this example, i. e. $\phi_\alpha = 1$. This leads to the objective function

$$n_t g = \sum_{\alpha \in \mathscr{S}} n_\alpha \Delta_f g_\alpha^\circ(T) + RT \sum_{\alpha \in \mathscr{S}} n_\alpha \ln x_\alpha + RT n_t \ln \frac{P}{P^\circ} \tag{3.7}$$

which has to be minimized. An implementation in MATLAB is given in Listing 3.1. This example makes use of the NLP-solver `fmincon` of the Optimization Toolbox applying the algorithm `'interior-point'`. For more details on this optimization algorithm, see also Byrd et al. (1999, 2000) and Waltz et al. (2006).

Listing 3.1: Example for the Gibbs energy minimization in MATLAB.

```matlab
 1  function gibbs_min
 2
 3  T = 500;                    % define temperature in K
 4  P = 101325;                 % and pressure in Pa
 5
 6  % Gibbs energies of formation at T = 500K.
 7  GIG  = [ -397291 -1642 -36396 -221592 -156935 ]';
 8
 9  logp = log(P / 101325);     % define composed variables with
10  RT   = 8.3144621 * T;       % p0 = 101325 Pa and R = 8.314471 J/mol K
11
12  A  = [ 1 0 1 0 1            % elemental matrix, and,
13         2 0 0 1 1
14         0 2 4 2 0 ];
15  n0 = [ 1 4 0 0 0 ]';        % initial condition
16
17  ops = optimset( ...              % set algorithm to interior-point
18    'Algorithm','interior-point'); % and solve the problem.
19  n = fmincon( ...
20    @Gibbs,  n0, ...          % objective function, initial guess
21    -eye(5), zeros(5,1), ...  % lin inequality constraints
22    A, A*n0, ...              % lin equality constraints
23    [], [], [], ...           % boundaries, nonlinear constraints
```

```
24    ops)                      % solver options

25

26    function nG = Gibbs(n)    % objective fcn: Gibbs energy
27      n(n<=0) = eps;          % avoid log(0)
28      sn = sum(n);
29      nG = sum(n.*GIG) + RT*(sum(n.*log(n/sn)) + sn*logp);
30    end
31  end
```

This example uses a feed of $n_{CO2}/n_{H2} = 1/4$, which is a stoichiometric feed ratio of the methanation of carbon dioxide according to

$$CO_2 + 4\,H_2 \rightleftharpoons CH_4 + 2\,H_2O\,, \tag{3.8}$$

and returns the composition in thermodynamic equilibrium, which is

$$\mathbf{n}_{eq} = \begin{pmatrix} n_{CO2} \\ n_{H2} \\ n_{CH4} \\ n_{H2O} \\ n_{CO} \end{pmatrix} = \begin{pmatrix} 0.0176 \\ 0.0703 \\ 0.9824 \\ 1.9648 \\ 0.0000 \end{pmatrix}. \tag{3.9}$$

The calculation is performed at a temperature of $T = 500\,\mathrm{K}$ and at ambient pressure $P = P^\circ = 101325\,\mathrm{Pa}$. This means that at this conditions a CO_2 conversion of the methanation reaction of approximately 98% is thermodynamically feasible.

3.2   Dynamic Method

The main parts of this section are based on Zinser et al. (2015), Zinser et al. (2016a), and Zinser and Sundmacher (2016), publications of the author.

We assume a set of phases $\mathscr{P}$ which defines the phases that may occur in the considered system, e. g. $\mathscr{P} = \{V, L\}$ for a vapour-liquid system. The total number of phases is denoted by $p = |\mathscr{P}|$. Some examples for the phase sets $\mathscr{P}$ are given in Tab. 3.2. Additionally, for each phase $\pi \in \mathscr{P}$, a set of species $\mathscr{S}^\pi$ is defined which describes the allowed species in the considered phase.

In many cases, it is a feasible assumption that every compound can exist in every phase, i. e. that $\mathscr{S} = \mathscr{S}^\pi \, \forall \pi \in \mathscr{P}$. In this case only one set of species $\mathscr{S}$ is required. Some other systems require that not every species is allowed to exist in every phase. Examples for such systems include

- non-condensable gases, and

- ions, dissolved in a liquid phase.

For systems that define one common set so species $\mathscr{S}$ the number of species is given by $s = |\mathscr{S}|$. In this case, a total number of $sp(p-1)/2$ rate expressions $r_\alpha^{\pi,\pi'}$ are required to compute the molar fluxes of all species $\alpha \in \mathscr{S}$ between the phases $\pi, \pi' \in \mathscr{P}$. If all these molar fluxes are in equilibrium with each other the thermodynamic equilibrium of the overall system is reached.

Additionally, in each phase $\pi \in \mathscr{P}$, a set of chemical reactions $\mathscr{R}^\pi$ may take place. Here, for every reaction, one molar flux r_ρ^π due to the corresponding chemical reaction is required. This molar flux must fulfil the following requirements:

- it must be thermodynamically consistent, and

- kinetic information, such as a reaction constant or an Arrhenius term, is not required to obtain the thermodynamic equilibria.

The dynamic method for solving thermodynamic equilibria problems is formulated as a set of ordinary differential equations

$$\frac{\mathrm{d}\mathbf{n}}{\mathrm{d}\tau} = \mathbf{A}\mathbf{r} \qquad\qquad \mathbf{n}\,(\tau = 0) = \mathbf{n}_0 \qquad\qquad (3.10)$$

that describes the evolution of the molar composition in each phase

$$\mathbf{n} = [\mathbf{n}^\pi]_{\pi \in \mathscr{P}} \,, \qquad\qquad \text{with } \mathbf{n}^\pi = [n_\alpha^\pi]_{\alpha \in \mathscr{S}^\pi} \,. \qquad\qquad (3.11)$$

In Eq (3.10), the stoichiometric matrix $\mathbf{A}$ describes all connections of species in the different phases with respect to the molar fluxes as a consequence of phase transitions and/or chemical reactions. This stoichiometric matrix

$$\mathbf{A} = \begin{bmatrix} \mathbf{A}_\mathrm{p} & \mathbf{A}_\mathrm{r} \end{bmatrix} \qquad\qquad (3.12)$$

consist of a part $\mathbf{A}_\mathrm{p}$ that describes the connections between the phases. The second part $\mathbf{A}_\mathrm{r}$ refers to the stoichiometry of the chemical reactions in each phase. The indices p and r refer to the phase transitions and to the chemical reactions, respectively. In the same manner, the vector of

Table 3.2: Some examples of systems containing different numbers of phases p and their phase set $\mathscr{P}$.

p	type	$\mathscr{P}$
1	pure vapour systems	{V}
2	vapour-liquid systems	{V,L}
3	vapour-liquid-liquid systems	{V,L1,L2}
3	liquid-liquid-liquid systems	{L1,L2,L3}

rate expressions

$$\mathbf{r} = \begin{bmatrix} \mathbf{r}_\mathrm{p} \\ \mathbf{r}_\mathrm{r} \end{bmatrix} \tag{3.13}$$

consists of two parts: the upper one that describes the rate expressions due to phase transitions $\mathbf{r}_\mathrm{p}$, and, the lower one that formulates the fluxes because of the chemical reactions $\mathbf{r}_\mathrm{r}$.

All rate expressions in the resulting system of ordinary differential equations, Eq. (3.10), must be formulated in a thermodynamic consistent way, such that the steady state of this system corresponds to the thermodynamic equilibrium of the considered system. Since we are only interested in the steady state, note that it is not required to apply a "real" reaction kinetic while a thermodynamic consistent one is sufficient. In the following sections, the derivations of the required rate expressions are given for both, phase transitions, and chemical reactions.

3.2.1 Phase Transitions

This section deals with the derivation of a set of thermodynamic consistent rate expressions for the transition of a species α between two phases π and π'. The vector of rate expressions $\mathbf{r}_\mathrm{p}$ is composed of the rate expressions at each interface,

$$\mathbf{r}_\mathrm{p} = \left[\mathbf{r}^{\pi,\pi'} \right]_{\substack{\pi,\pi' \in \mathscr{P} \\ \pi \neq \pi'}} \tag{3.14}$$

while the rate expressions at a given interface (π, π') is composed of all species α that may cross this interface. The set of species α that may cross the interface between the phases π and π' is defined by

$$\mathscr{I}^{\pi,\pi'} = \mathscr{S}^\pi \cap \mathscr{S}^{\pi'}. \tag{3.15}$$

This leads to the vector of rate expressions at a given interface as follows:

$$\mathbf{r}^{\pi,\pi'} = \left[r_\alpha^{\pi,\pi'} \right]_{\alpha \in \mathscr{I}^{\pi,\pi'}} \tag{3.16}$$

The rate expressions $r_\alpha^{\pi,\pi'}$ are directly derived from the thermodynamic equilibrium condition, i. e. the equality the partial fugacities, between the two phases π and π', see also Walas (1985, p. 301) or Gmehling et al. (2012, p. 161),

$$f_\alpha^\pi = f_\alpha^{\pi'}, \qquad \forall \alpha \in \mathscr{I}^{\pi,\pi'}. \tag{3.17}$$

In order to establish the phase equilibria, the rate expression can be obtained by reformulation of the equilibrium condition and yields to

$$r_\alpha^{\pi,\pi'} = k_\alpha^{\pi,\pi'} \left(f_\alpha^\pi - f_\alpha^{\pi'} \right), \qquad \forall \alpha \in \mathscr{I}^{\pi,\pi'} \tag{3.18}$$

which is a measure for the distance between the actual state, i.e. a non-equilibrium state, and the equilibrium state. This rate expression becomes $r_\alpha^{\pi,\pi'} = 0$ if the thermodynamic phase equilibrium is reached, i.e. the isofugacity condition, Eq. (3.17), is fulfilled. The rate constant $k_\alpha^{\pi,\pi'}$ is a measure for the speed of the mass transfer between the phases π and π'. While we are only interested in the steady state of the ODE system (3.10), this constant can be set to an arbitrary value $k_\alpha^{\pi,\pi'} > 0$, e.g. $k_\alpha^{\pi,\pi'} = 1$. Furthermore, this value can also be used to adjust the numerical performance of the ODE solver.

Finally, the stoichiometric matrix $\mathbf{A}_\mathrm{p}$ of a given system has to be constructed. In case of a two-phase system, the stoichiometric matrix is given by

$$\mathbf{A}_\mathrm{p} = \begin{bmatrix} -\mathbf{J}^{\pi_1,\pi_2} \\ \mathbf{J}^{\pi_2,\pi_1} \end{bmatrix} \tag{3.19}$$

where the submatrices $\mathbf{J}^{\pi,\pi'} \in \mathbb{R}^{|\mathscr{S}^\pi| \times |\mathscr{I}^{\pi,\pi'}|}$ are constructed by

$$\mathbf{J}^{\pi,\pi'} = \left[\delta_{\alpha,\alpha'} \right]_{\substack{\alpha \in \mathscr{S}^\pi \\ \alpha' \in \mathscr{I}^{\pi,\pi'}}}, \tag{3.20}$$

and

$$\delta_{\alpha,\alpha'} = \begin{cases} 1 & : \alpha = \alpha' \\ 0 & : \text{otherwise} \end{cases} \tag{3.21}$$

refers to the Kronecker delta. Analogously, in the case of a three-phase system, the stoichiometric matrix $\mathbf{A}_\mathrm{p}$ yields to

$$\mathbf{A}_\mathrm{p} = \begin{bmatrix} -\mathbf{J}^{\pi_1,\pi_2} & -\mathbf{J}^{\pi_1,\pi_3} & \mathbf{0} \\ \mathbf{J}^{\pi_2,\pi_1} & \mathbf{0} & -\mathbf{J}^{\pi_2,\pi_3} \\ \mathbf{0} & \mathbf{J}^{\pi_3,\pi_1} & \mathbf{J}^{\pi_3,\pi_2} \end{bmatrix}. \tag{3.22}$$

In a general p-phase system, the stoichiometric matrix $\mathbf{A}_\mathrm{p}$ is constructed from $p \times i$ submatrices, where i refers to the number of interfaces between the phases. The functional relationship between the number of phases p and the number of interfaces between two distinct phases, i, is displayed in Tab. 3.3.

Table 3.3: Number of interfaces i between two distinct phases π and π' as a function of the total number of phases p.

Phases p	1	2	3	4	5	p
Interfaces i	0	1	3	6	10	$\frac{1}{2}p(p-1)$

3.2.1.1 Special Case $\mathscr{S}^\pi = \mathscr{S}$

In the special case that all species α are allowed to occur in every phase $\pi \in \mathscr{P}$, i.e. $\mathscr{S}^\pi = \mathscr{S}$ for all phases $\pi \in \mathscr{P}$, the derivation above simplifies as follows.

- There is one set of substances $\mathscr{S}$ which is valid for all phases. Of course, this was the precondition.

- The set of species that may cross an interface is also equal to the set of substances in the system, i. e. $\mathscr{I}^{\pi,\pi'} = \mathscr{S}$.

- The submatrices of the stoichiometric matrix $\mathbf{A}_{\mathrm{p}}$ have all the same dimension and are equal to the $s \times s$ identity matrix $\mathbf{J}^{\pi,\pi'} = \mathbf{I}$.

3.2.2 Chemical Reactions

Beside of the transfer of substances between the phases, in every phase a set of chemical reactions $\mathscr{R}^{\pi}$ may occur. Therefore, the vector of rate expressions due to chemical reactions,

$$\mathbf{r}_{\mathrm{r}} = \left[\mathbf{r}^{\pi}\right]_{\pi \in \mathscr{P}} \tag{3.23}$$

consists of a subvector $\mathbf{r}^{\pi}$ that refers to the chemical reactions of the corresponding phase π. The vector of rate expressions in the given phase π collects all rate expressions of the chemical reactions ρ that take place in this phase,

$$\mathbf{r}^{\pi} = \left[r_{\rho}^{\pi}\right]_{\rho \in \mathscr{R}^{\pi}} . \tag{3.24}$$

Starting of the equilibrium condition for a single reaction ρ, see also Walas (1985, p. 466) or Gmehling et al. (2012, pp. 533–534),

$$K_{\mathrm{eq},\rho}^{\pi} = \exp\left(\frac{-\Delta_{\mathrm{r}} g_{\rho}^{\pi}}{RT}\right) = \prod_{\alpha \in \mathscr{S}^{\pi}} \left(\frac{f_{\alpha}^{\pi}}{f_{\alpha}^{\circ\pi}}\right)^{v_{\alpha\rho}^{\pi}} \tag{3.25}$$

which has its origin in the law of mass action by Guldberg and Waage (1879). Here, $v_{\alpha\rho}^{\pi}$ refers to the stoichiometric coefficient of species α in reaction ρ of phase π. The stoichiometric coefficients of the reactants are negative, i. e. $v_{\alpha\rho}^{\pi} < 0$, while the coefficients of the products have a positive sign, $v_{\alpha\rho}^{\pi} > 0$. By separation of the contributions of the reactants and the products in Eq. (3.25), one gets

$$K_{\mathrm{eq},\rho}^{\pi} = \frac{\prod_{\substack{\alpha \in \mathscr{S}^{\pi} \\ v_{\alpha\rho}^{\pi} > 0}} \left(\frac{f_{\alpha}^{\pi}}{f_{\alpha}^{\circ\pi}}\right)^{v_{\alpha\rho}^{\pi}}}{\prod_{\substack{\alpha \in \mathscr{S}^{\pi} \\ v_{\alpha\rho}^{\pi} < 0}} \left(\frac{f_{\alpha}^{\pi}}{f_{\alpha}^{\circ\pi}}\right)^{|v_{\alpha\rho}^{\pi}|}} . \tag{3.26}$$

This can be reformulated to an expression for the rate expressions for chemical reactions, analo-

gously to a power law kinetic

$$r_\rho^\pi = k_\rho^\pi \times \left[\prod_{\substack{\alpha \in \mathscr{S}^\pi \\ v_{\alpha\rho}^\pi < 0}} \left(\frac{f_\alpha^\pi}{f_\alpha^{\circ\pi}} \right)^{|v_{\alpha\rho}^\pi|} - \frac{1}{K_{\text{eq},\rho}^\pi} \prod_{\substack{\alpha \in \mathscr{S}^\pi \\ v_{\alpha\rho}^\pi > 0}} \left(\frac{f_\alpha^\pi}{f_\alpha^{\circ\pi}} \right)^{v_{\alpha\rho}^\pi} \right]. \tag{3.27}$$

When the chemical equilibrium is reached, this rate expressions becomes $r_\rho^\pi = 0$. The rate constant k_ρ^π defines the velocity of the chemical reaction.

While in chemical reaction engineering this information is usually modelled by an Arrhenius equation, this information is not required within our methodological framework. Therefore, this constant can be set to an arbitrary value, e.g. $k_\rho^\pi = 1$. If the equilibrium constants $K_{\text{eq},\rho}^\pi$ of a given system of reactions are distributed on a large range, e.g. $K_{\text{eq},\rho}^\pi = 10^{-10} \ldots 10^{10}$, it is useful to apply a kind of normalization of the rate expressions by setting

$$k_\rho^\pi = \sqrt{K_{\text{eq},\rho}^\pi}. \tag{3.28}$$

In each phase $\pi \in \mathscr{P}$, a different set of reactions $\mathscr{R}^\pi$ may occur. Therefore, the overall stoichiometric matrix $\mathbf{A}_r$ is constructed from the stoichiometric matrices of the phase specific matrices $\mathbf{A}_r^\pi$, i.e.

$$\mathbf{A}_r = \text{diag}\left(\mathbf{A}_r^{\pi_1}, \mathbf{A}_r^{\pi_2}, \ldots \right) \tag{3.29}$$

with the phase-specific stoichiometric matrices

$$\mathbf{A}_r^\pi = \left[v_{\alpha\rho}^\pi \right]_{\substack{\alpha \in \mathscr{S}^\pi \\ \rho \in \mathscr{R}^\pi}} \tag{3.30}$$

The stoichiometric matrices $\mathbf{A}_r$ as well as the vectors of rate expressions $\mathbf{r}_r$ for one-phase, two-phase and three-phase systems are given by

$$\mathbf{A}_r = \mathbf{A}_r^{\pi_1} \qquad\qquad \mathbf{r}_r = \mathbf{r}^{\pi_1}, \tag{3.31}$$

$$\mathbf{A}_r = \begin{bmatrix} \mathbf{A}_r^{\pi_1} & \mathbf{0} \\ \mathbf{0} & \mathbf{A}_r^{\pi_2} \end{bmatrix} \qquad\qquad \mathbf{r}_r = \begin{pmatrix} \mathbf{r}^{\pi_1} \\ \mathbf{r}^{\pi_2} \end{pmatrix}, \text{ and} \tag{3.32}$$

$$\mathbf{A}_r = \begin{bmatrix} \mathbf{A}_r^{\pi_1} & \mathbf{0} & \mathbf{0} \\ \mathbf{0} & \mathbf{A}_r^{\pi_2} & \mathbf{0} \\ \mathbf{0} & \mathbf{0} & \mathbf{A}_r^{\pi_3} \end{bmatrix} \qquad\qquad \mathbf{r}_r = \begin{pmatrix} \mathbf{r}^{\pi_1} \\ \mathbf{r}^{\pi_2} \\ \mathbf{r}^{\pi_3} \end{pmatrix}, \tag{3.33}$$

respectively.

3.2.3 Fugacities

All of the rate expressions that were derived in the previous sections are functions of the partial fugacities f_α^π of the species α in the considered phase π. There are two main approaches to quantify these fugacities. The first approach, the so-called ϕ-approach, quantifies the fugacity in terms of the fugacity coefficients ϕ_α^π, see Walas (1985, p. 141) or Gmehling et al. (2012, p. 188),

$$f_\alpha^\pi = x_\alpha^\pi \phi_\alpha^\pi P \tag{3.34}$$

while the so-called γ-approach the fugacities in terms of the activity coefficients γ_α^π formulates,

$$f_\alpha^\pi = x_\alpha^\pi \gamma_\alpha^\pi f_\alpha^{\circ\pi}, \tag{3.35}$$

see Walas (1985, p. 167). Here, the standard fugacity $f_\alpha^{\circ\pi}$ can be chosen arbitrarily (Gmehling et al., 2012, p. 188). Note, that the standard fugacity is only used when combining the ϕ-approach with a γ-approach, e. g. the ϕ-approach for a gaseous phase and the γ-approach for a liquid phase. For systems that apply Eq. (3.35) to all phases, the standard fugacities cancel out. For an ideal gas, the standard fugacity can be set to the ambient pressure, $f_\alpha^{\circ\pi} = P^\circ = 1013235\,\mathrm{Pa}$ (Gmehling et al., 2012, p. 533). Dependent on the system, it is also common to relate the standard fugacity to the vapour pressure, $f_\alpha^{\circ\pi} = \phi_\alpha^{\mathrm{vap}} P^{\mathrm{vap}}$, or to a Henry coefficient, $f_\alpha^{\circ\pi} = \tilde{k}_\mathrm{H}$, see also Gmehling et al. (2012, p. 189) or Rönsch (2015, p. 118).

Since the fugacity coefficients ϕ_α^π can be computed from cubic Equations of State, which describe both, vapour and liquid phases, the ϕ-approach is favourable for vapour (V) as well as vapour-liquid (VL) systems. Additionally, with the assumption of an ideal gas behaviour, i. e. $\phi_\alpha^\mathrm{V} = 1$, the partial fugacities from Eq. (3.34) simplifies for an ideal vapour phase ($\pi = \mathrm{V}$) to

$$f_\alpha^\mathrm{V} = x_\alpha^\mathrm{V} P. \tag{3.36}$$

Usually, the activity coefficients γ_α^π are obtained from an activity coefficient model such as NRTL, UNIQUAC or the group contribution model UNIFAC. The γ-approach is the common approach for liquid systems or systems incorporating multiple liquid phases. With the assumption of an ideal system, i. e. $\gamma_\alpha^\pi = 1$, the expression (3.35) can be simplified to

$$f_\alpha^\pi = x_\alpha^\pi f_\alpha^{\circ\pi} \tag{3.37}$$

which is an analogous formulation of Raoult's law, $P_\alpha = x_\alpha P_\alpha^\circ$. The assumption of infinite dilution,

$$f_\alpha^\pi = x_\alpha^\pi \gamma_\alpha^{\circ\pi} f_\alpha^{\circ\pi} = k_\mathrm{H} x_\alpha^\pi \tag{3.38}$$

yields to a formulation which is of the same form as Henry's law, see also Walas (1985, p. 167). Within the scope of this thesis, in the most cases, the full approaches, Eq. (3.34) and Eq. (3.35) are applied.

3.2.4 Analogies between Phase Transitions and Chemical Reactions

In the derivations in sections 3.2.1 and 3.2.2, the rate expressions for the phase transitions and for the chemical reactions are derived separately. It is also possible to consider a phase transition of species α between the phases π and π' as a kind of "chemical reaction"

$$\alpha^{(\pi)} \rightleftharpoons \alpha^{(\pi')}. \tag{3.39}$$

According to Eq. (3.25), this leads to the "chemical" equilibrium condition

$$K_{\text{eq}} = \frac{f_\alpha^\pi}{f_\alpha^{\pi'}} \tag{3.40}$$

while the condition for the "phase" equilibrium is given by Eq. (3.17),

$$1 = \frac{f_\alpha^\pi}{f_\alpha^{\pi'}}. \tag{3.41}$$

Combining those equilibrium conditions, the equilibrium constant of a phase transition yields

$$K_{\text{eq}} = 1. \tag{3.42}$$

With this information, we can compute the Gibbs energy of "reaction", i. e. the Gibbs energy of a phase transition $\Delta_{\text{trs}}g$, which yields from Eq. (3.25) to

$$\Delta_{\text{trs}}g = -RT\ln(1) = 0. \tag{3.43}$$

3.3 Examples

The application of the dynamic method for thermodynamic equilibria, which was introduced in the section 3.2, is demonstrated here for some examples of different type and complexity.

All the examples were implemented in MATLAB and solved using the MATLAB ODE solver suite. If not stated in the example explicitly, the solver `ode15s` was used to solve the resulting system. The solver `ode15s` is based on the numerical differentiation formulas, for a detailed description of the algorithm, see Shampine and Reichelt (1997).

3.3.1 Methanol Synthesis Reaction

The first example shows a reactive system in a vapour phase. More precisely, the methanol synthesis reaction from carbon dioxide is considered. The overall reaction network is given by

$$CO_2 + 3\,H_2 \rightleftharpoons CH_3OH + H_2O \tag{3.44a}$$

$$CO_2 + H_2 \rightleftharpoons CO + H_2O \tag{3.44b}$$

$$CO + 2\,H_2 \rightleftharpoons CH_3OH \tag{3.44c}$$
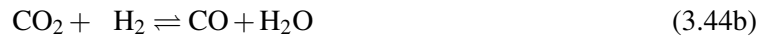
Besides the methanol synthesis from CO_2, Eq. (3.44a), the reverse water-gas shift (RWGS) reaction, Eq. (3.44b), as well as the methanol synthesis from carbon monoxide, Eq. (3.44c), is taken into account. Due to the fact, that only two of those three reactions are linearly independent it is sufficient to take only a set of two linear independent chemical reactions, e. g. Eq. (3.44a)–(3.44b), which is used in the following computations. For the formulation of the dynamic method for this example, we define the set of phases $\mathscr{P} = \{V\}$ which consists only of $p = 1$ phase. Additionally, in this system $s = 5$ species may occur. Hence, the set of species is given by $\mathscr{S} = \{CO_2, H_2, CH_3OH, H_2O, CO\}$. Since in this example exists only one phase, the superscript which refers to the vapour phase is omitted in this example for better readability.

Due to the fact that we consider only a single-phase system, no phase transitions occur in the system and the stoichiometric matrix of the phase transitions is empty, $\mathbf{A}_p = \emptyset_{s \times 0}$, as well as the vector of fluxes between the phases $\mathbf{r}_p = \emptyset_{0 \times 1}$.

With the assumption of ideal gas behaviour, $\phi_\alpha = 1$, the rate expressions of the chemical reactions yield to

$$r_1 = k_1 \times \left[x_{CO2} x_{H2}^3 \left(\frac{P}{P^\circ} \right)^4 - \frac{x_{CH3OH} x_{H2O}}{K_{eq,1}} \left(\frac{P}{P^\circ} \right)^2 \right], \tag{3.45a}$$

$$r_2 = k_2 \times \left[x_{CO2} x_{H2} - \frac{x_{CO} x_{H2}}{K_{eq,2}} \right] \left(\frac{P}{P^\circ} \right)^2. \tag{3.45b}$$

A normalization of the reaction rates is not applied, i. e. the rate constants are set to unity $k_\rho = 1$. The stoichiometric matrix and the vector of rate equations is given by

$$\mathbf{A} = \mathbf{A}_r = \begin{bmatrix} -1 & -3 & 1 & 1 & 0 \\ -1 & -1 & 0 & 1 & 1 \end{bmatrix}^T, \text{ and } \qquad \mathbf{r} = \mathbf{r}_r = \begin{pmatrix} r_1 \\ r_2 \end{pmatrix}, \tag{3.46}$$

respectively. The equilibrium calculation of this system was performed with an initial composition which corresponds to the stoichiometric feed of the methanol synthesis of carbon dioxide,

$$\mathbf{x}(\tau = 0) = \mathbf{x}_0 = [1/4, 3/4, 0, 0, 0]^T \tag{3.47}$$

and a pressure of $P = 4\,\text{MPa}$. The high pressure was chosen due to the fact, that the methanol
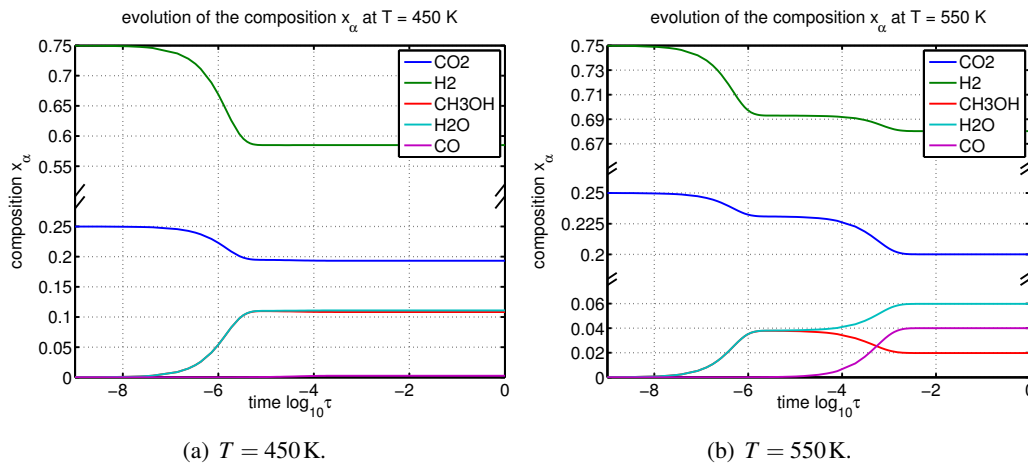
(a) $T = 450\,\text{K}$.   (b) $T = 550\,\text{K}$.

Figure 3.1: Evolution of the mixture compositions x_α over time τ at (a) $T = 450\,\text{K}$ and at (b) $T = 550\,\text{K}$.

synthesis reaction is thermodynamically favoured at higher pressures. The evolution of the composition x_α with respect to time τ is shown in Fig. 3.1(a) at the temperature $T = 450\,\text{K}$ and in Fig. 3.1(b) at $T = 550\,\text{K}$. At the lower temperature $T = 450\,\text{K}$, the reverse water-gas shift reaction is completely unfavoured, while at $T = 550\,\text{K}$, both reactions, the methanol synthesis from CO_2 as well as the reverse water-gas shift reaction to carbon monoxide will take place in the reactor simultaneously.

Fig. 3.1(b) illustrates also that the methanol synthesis reaction takes place on a time range of $10^{-7}\ldots 10^{-5}$ while the reverse water-gas shift reaction occurs on the time range of $10^{-4}\ldots 10^{-3}$. One should note that the time ranges have no physical meaning because we did not provide any kinetic information, but it illustrates how the method attains the thermodynamic equilibrium.

3.3.1.1 Eigenvalue Analysis

The example problem at $P = 4\,\text{MPa}$ and $T = 550\,\text{K}$, see also Fig. 3.1(b), was used to investigate the mathematical properties of the resulting set of differential equations. The eigenvalues λ of an ODE system are defined by

$$\det(\mathbf{J} - \lambda \mathbf{I}) = 0 \tag{3.48}$$

were $\mathbf{J}$ refers to the Jacobian matrix of the ODE system and $\mathbf{I}$ is the identity matrix. For the definition and numerical approximation of the Jacobian matrix, see also Appendix B.2.

The evolution of the eigenvalues, more precisely the absolute values of the real parts of the eigenvalues, with respect to time τ are shown in Fig. 3.2(a). It can be seen that two of the eigenvalues are distinctly different from zero while the other three eigenvalues are — within a numerical noise — zero. Concluding from the findings in Fig. 3.2, the dynamics of this system of five coupled differential equations could also be described by a system of only two differential equations. Here, the system of five compounds which are connected with each other by two linear independent

(a) Eigenvalues.
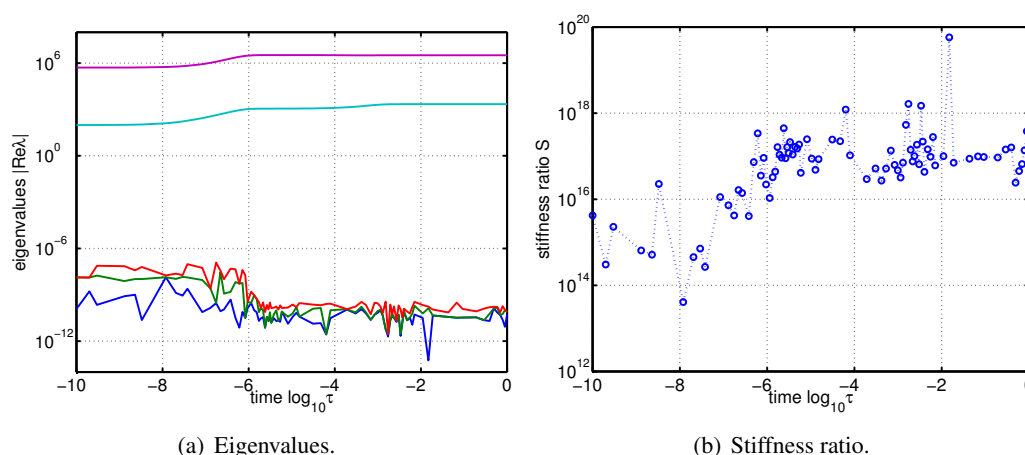
(b) Stiffness ratio.

Figure 3.2: (a) Evolution of the eigenvalues $|\Re(\lambda_k)|$ w. r. t. time τ and (b) the evolution of the stiffness ratio S.

chemical reactions. Hence, it is possible to transform the original five-dimensional state space $\mathbf{n}$ to a two-dimensional state space ξ which is spanned by the extents of reaction of two linear independent chemical reactions.

The stiffness ratio S of a set of ordinary differential equations is defined by

$$S = \frac{\max_k |\Re(\lambda_k)|}{\min_k |\Re(\lambda_k)|} \tag{3.49}$$

where λ_k refer to the eigenvalues of the differential equations at a given state. A set of differential equations is called stiff, if the stiffness ratio is $S \geq 10^3$, see also Hermann (2004, p. 157). Due to the fact that the eigenvalues λ_k depend on the state of a set of differential equations, the stiffness of the equations may change also w. r. t. time τ.

The evolution of the stiffness ratio S of the given example is shown in Fig. 3.2(b) with respect to time. The fluctuations of the stiffness ratio results from the numerical noise in small eigenvalues. Here, the stiffness ratio is in a range of $10^{13} < S < 10^{20}$, so the set of differential equations is "stiff".

3.3.1.2   Influence of the ODE Solver

The MATLAB ODE suite provides four algorithms that are suitable to solve stiff systems of differential equations. Those are:

- `ode15s` implements the numerical differentiation formulas of variable order,

- `ode23s` is a modified Rosenbrock formula of second order,

- `ode23t` is an implementation of the trapezoidal rule, and

- `ode23tb` is an implicit Runge-Kutta formula.

For more details of those algorithms, see also Shampine and Hosea (1996); Shampine and Reichelt (1997); Shampine et al. (1999).

The efficiencies of these four algorithms were compared for the current example of the methanol synthesis. Therefore, the problem was solved at $P = 4\,\text{MPa}$ and $N_T = 101$ different temperatures from the interval $T/\text{K} \in [300, 700]$. For every computation, the CPU time and the number of function evaluations was measured. The CPU time is shown in Fig. 3.3(a) as a function of the number of function evaluations for each algorithm. As expected, those values correlate linearly. The algorithms `ode15s` and `ode23t` are the most efficient algorithms in terms of number of function evaluations. When comparing the CPU time the solvers `ode15s` and `ode23tb` show the best performance. The mean value as well as the extrema of the CPU time for each algorithm is shown in Fig. 3.3(b). Since the ODE solver `ode15s` gives good performances in both measures, CPU time and number of function evaluations, it is used as the default solver in the following problems.

3.3.1.3 Normalization of the Reaction Rates

In the next study, the original ODE system was modified in several ways. The first modification was the normalization of the two reaction rates using the rate constant

$$k_\rho = \sqrt{K_{\text{eq},\rho}}\,. \tag{3.50}$$

In the second modification, the full model of the chemical reaction rates was applied. This includes the third reaction rate

$$r_3 = x_{\text{CO}} x_{\text{H2}}^2 \left(\frac{P}{P^\circ}\right)^3 - \frac{x_{\text{CH3OH}}}{K_{\text{eq},3}} \left(\frac{P}{P^\circ}\right) \tag{3.51}$$

(a) CPU time as function of function evaluations.
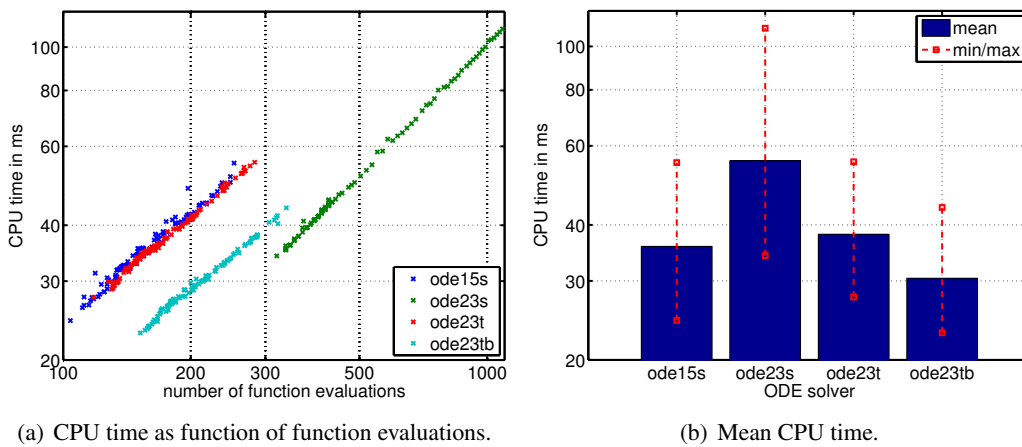
(b) Mean CPU time.

Figure 3.3: Computational performance of the MATLAB ODE solvers: (a) CPU time as function of the number of function evaluations, and (b) mean CPU time and extrema.

(a) CPU time as a function of the function evaluations.   (b) Mean CPU times.
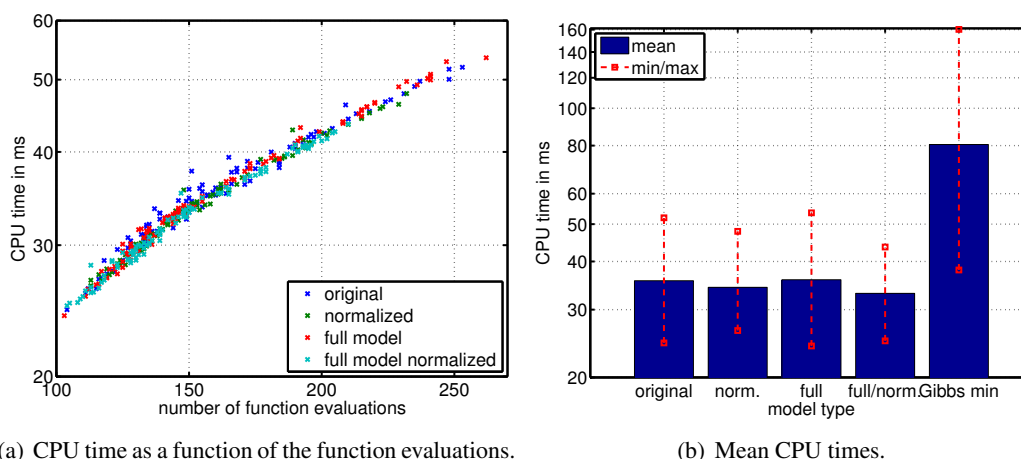
Figure 3.4: (a) CPU time as a function of the number of function evaluations, and (b) average CPU times
of the five compared methods including minimum and maximum CPU time.

to the system of differential equations. This is not necessary for reaching the chemical equilibrium, but it may have an impact on the convergence towards the thermodynamic equilibrium by providing an additional degree of freedom in the state space. A third modification of the original system was achieved by incorporating both, the normalization of the rate expressions, Eq.(3.50), and the third reaction rate, Eq. (3.51). Those three modifications, the original formulation and the Gibbs energy minimization technique were applied on the $N_T = 101$ different temperatures of the study above. The average numerical efficiencies of those five methods were compared with each other. The results in terms of CPU time are displayed in Tab. 3.4.

The CPU time as a function of the number of function evaluations is given in Fig. 3.4(a). It can be seen that there are only small differences between the different formulations of the dynamic method. The normalized full model with 94% of the CPU time of the original model leads to the best efficiency. The lowest CPU time was required by the full model without normalization with 103% of the CPU time of the reference case. The four formulations of the dynamic method as well as the Gibbs energy minimization are compared in Fig. 3.4(b). It can be seen, that all formulations of the dynamic method are in the same order of magnitude in terms of computational costs while the Gibbs energy minimization technique needs the double CPU time for solving this chemical equilibrium problem.

Table 3.4: Average CPU times for computation of the chemical equilibrium using the four different formulations of the dynamic method as well es the Gibbs energy minimization. All values in ms.

	original	full	Gibbs minimization
$k_\rho = 1$	35.1 (100%)	36.0 (103%)	80.5 (229%)
$k_\rho = \sqrt{K_{eq,\rho}}$	33.8 (96%)	33.0 (94%)	
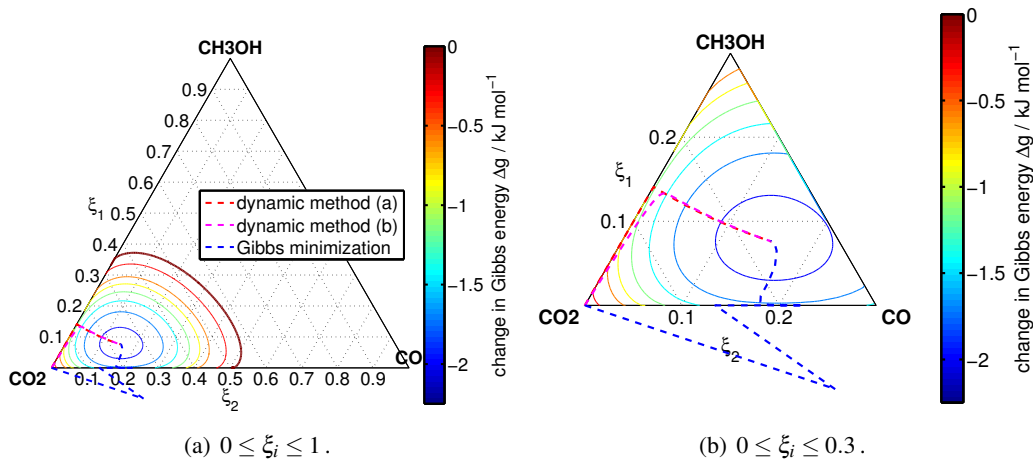
Figure 3.5: Trajectories of the evolution from initial composition to the chemical equilibrium for different algorithms. (a) full state space and (b) zoomed state space on the region $0 \leq \xi_i \leq 0.3$.

3.3.1.4   Comparison with Gibbs Energy Minimization Technique

With the assumption of a stoichiometric feed ratio $CO_2 : H_2 = 1/3$ the 5-dimensional state space $\mathbf{n}$ can be reduced to a 2-dimensional state space $\xi = [\xi_1, \xi_2]^T$

$$\xi_1(\tau) = \frac{n_{CH3OH}(\tau)}{n_{CO2}(0)}, \qquad\qquad \xi_2(\tau) = \frac{n_{CO}(\tau)}{n_{CO2}(0)}. \qquad (3.52)$$

Here, ξ_1 refers to the extend of reaction of the methanation reaction from CO_2, Eq. (3.44a), while ξ_2 refers to the extend of reaction of the reverse water-gas shift reaction, Eq. (3.44b). While Eq. (3.52) defines the transformation from the $\mathbf{n}$-space to the ξ-space, the back-transformation can be done according to

$$\mathbf{n}(\tau) = \begin{bmatrix} 1 - \xi_1 - \xi_2 \\ 3 - 3\xi_1 - \xi_2 \\ \xi_1 \\ \xi_1 + \xi_2 \\ \xi_2 \end{bmatrix} \mathbf{n}_{CO2}(0). \qquad (3.53)$$

With the stoichiometric limitations, i. e.

$$0 \leq \xi_1 \leq 1, \qquad\qquad 0 \leq \xi_2 \leq 1, \qquad\qquad 0 \leq \xi_1 + \xi_2 \leq 1 \qquad (3.54)$$

all possible compositions ξ of the system can be defined by a point in a ternary diagram.

The trajectories from the initial composition $\xi = [0,0]^T$ starting from CO_2 towards the chemical equilibrium are shown in Fig. 3.5 in a ternary diagram. In the calculations a condition of $T = 550\,\mathrm{K}$ and $P = 4\,\mathrm{MPa}$ is assumed. Fig. 3.5 shows the trajectories of the dynamic method in the original formulation, i. e. implementing the two linear independent chemical reactions, with the two rate constants:
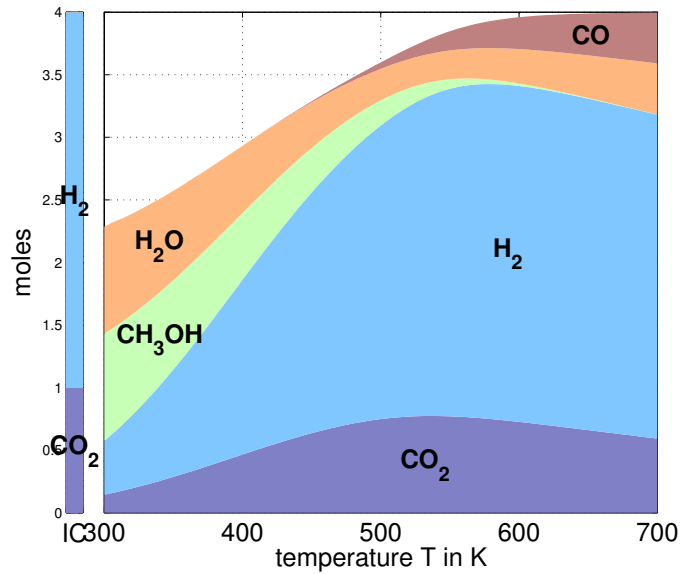
Figure 3.6: Chemical equilibrium of the methanol synthesis as a function of temperature for $P = 4\,\text{MPa}$. The initial composition (IC) is given on the left bar.

(a) $k_\rho = 1$ — the original formulation, red curves in Fig. 3.5, and

(b) $k_\rho = \sqrt{K_{\text{eq},\rho}}$ — the normalized formulation, magenta curves in Fig. 3.5.

It can be seen that the two curves follow closely to each other. The original formulation changes the direction of the system composition in a sharp corner while the normalized formulation changes the direction in the state space smoother. Additionally, the trajectory from the initial composition towards the solution of using the Gibbs energy minimization method is shown in the figure as well and is indicated by the blue curves. It can be seen that the trajectory of the Gibbs energy minimization violates the stoichiometric boundary conditions, i. e. jumps towards negative extends of reaction. The reason for this effect is that the algorithm which is used for the Gibbs energy minimization has actually no information of the physics occurring in the system while the proposed dynamic method relies on a physical motivation, i. e. the mass fluxes due to chemical reactions. In case of the dynamic method, the evolution equations are formulated in a way that the trajectories can not violate the stoichiometry.

Beside of the trajectories in the state space ξ the change in Gibbs energy, compared to the initial composition,

$$\Delta g(T) = g(T, \mathbf{n}(\tau)) - g(T, \mathbf{n}(0)) \tag{3.55}$$

is shown using the iso-Gibbs energy curves in the diagram. While the overall ternary diagram defines the stoichiometric limitations, the thermodynamic limitation is defined by the region of the isolines, i. e. $\Delta g \leq 0$. It can be seen that the final equilibrium point of the different algorithms fully agrees with the point of minimum Gibbs energy.

The chemical equilibrium at $P = 4\,\text{MPa}$ on the temperature interval $T/\text{K} \in [300, 700]$ is shown in Fig. 3.6 for a stoichiometric initial condition. It can be seen that the methanol synthesis is

thermodynamically favoured at lower temperatures while at higher temperatures the reverse water-gas shift reaction dominates the system.

3.3.2 VLE of the methanol synthesis products

In this example, the dynamic method is applied on a phase equilibria problem. More precisely, the vapour-liquid equilibrium (VLE) of the product spectrum of the methanol synthesis, section 3.3.1, is computed.

Accordingly, the set of species $\mathscr{S}$ is equal to the last example problem, i. e.

$$\mathscr{S} = \{CO_2, H_2, CH_3OH, H_2O, CO\}. \tag{3.56}$$

The set of the phases is given by $\mathscr{P} = \{V, L\}$. The chemical equilibrium of the system at $T = 450\,K$ and $P = 4\,MPa$ is given by

$$\mathbf{x}_0 = \begin{pmatrix} 0.1933 \\ 0.585 \\ 0.1083 \\ 0.1109 \\ 0.0026 \end{pmatrix} \tag{3.57}$$

In this separation problem, the partition of the species between the vapour and the liquid phases is calculated. Here, the product methanol (CH_3OH) and the side-product water (H_2O) are concentrated in the liquid phase while the non-reacted gases carbon dioxide (CO_2) and hydrogen (H_2) as well as traces of carbon monoxide (CO) remain in the gaseous phase. In a technical process these non-reacted gases are recycled back to the reactor.

In this example, no chemical reactions occur and therefore the stoichiometric matrix $\mathbf{A}_r$ as well as the vector giving the rate expressions $\mathbf{r}_r$ due to chemical reactions are empty,

$$\mathbf{A}_r = \emptyset_{2s \times 0}, \qquad\qquad \mathbf{r}_r = \emptyset_{0 \times 1}. \tag{3.58}$$

For this system, rate expressions for the fluxes through the interface $V \leftrightarrow L$ has to be formulated. The vector of rate expression for the phase transitions in this example are given by

$$\mathbf{r}_p = \left[r_\alpha^{V,L} \right]_{\alpha \in \mathscr{S}}. \tag{3.59}$$

In this example, the fugacities are formulated using the ϕ-ϕ-approach, Eq. (3.34),

$$r_\alpha^{V,L} = P \left(x_\alpha^V \phi_\alpha^V - x_\alpha^L \phi_\alpha^L \right). \tag{3.60}$$

The fugacity coefficients ϕ_α^π are obtained from the predictive Soave-Redlich-Kwong (PSRK) equa-

tion of state, section 2.8, via

$$\ln \phi_\alpha^\pi = \frac{(nb)'}{b}(Z^\pi - 1) - \ln[Z^\pi - B] - \frac{A}{Z^\pi}\left[\frac{(n^2a)'}{na} - \frac{(nb)'}{b}\right]\ln\left[\frac{Z^\pi + B}{Z^\pi}\right], \qquad (3.61)$$

where Z^π refers to the compressibility factor of phase π. A and B are the dimensionless equation of state parameters, and

$$(.)' \equiv \frac{\partial(.)}{\partial n_\alpha} \qquad (3.62)$$

are the partial derivatives of the mixing rule. A summary of the required parameters for the PSRK equation of state is given in Appendix A.4.

3.3.2.1   Initialization

When solving the resulting ODE system for a multiphase system the initial composition, i. e. the feed composition, has to be defined for the valid phases $\pi \in \mathscr{P}$ to initiate the calculation. In the given example, the feed composition, which is defined by the reactor, has to be distributed among the vapour and the liquid phase to start the computation. In simple systems, the initial partition can be done randomly. In general, an additional physical information should be used to set up the initial composition in each phase. Some examples for such physical properties may be

- the normal boiling point T_b or the vapour pressure P_{vap} for VLE systems,

- the polarity p in case of LLE systems, or

- the solubility S in case of SLE systems.

In order to set the initial composition in each phase up, a function κ is defined that assigns each component $\alpha \in \mathscr{S}$ to a preferred phase $\pi \in \mathscr{P}$

$$\kappa : \mathscr{S} \to \mathscr{P} \qquad (3.63)$$

In this VLE example, the normal boiling point $T_{b,\alpha}$ of the species α is applied to select a preferred phase

$$\kappa : \alpha \mapsto \begin{cases} \text{V} & : T_{b,\alpha} < T \quad \text{vapour} \\ \text{L} & : \text{else} \qquad\quad \text{liquid} \end{cases} \qquad (3.64)$$

where the component α is a key component of the phase $\pi = \kappa(\alpha)$. With the definition of the key components for each phase $\pi \in \mathscr{P}$ the initial composition for each phase can be formulated by

$$n_\alpha^{\pi,0} = n_\alpha^0 \times \begin{cases} K & : \kappa(\alpha) = \pi \text{ (preferred phase)} \\ 1 - K & : \text{else} \end{cases} \qquad (3.65)$$

(a) Dynamic evolution.   (b) Equilibrium composition.
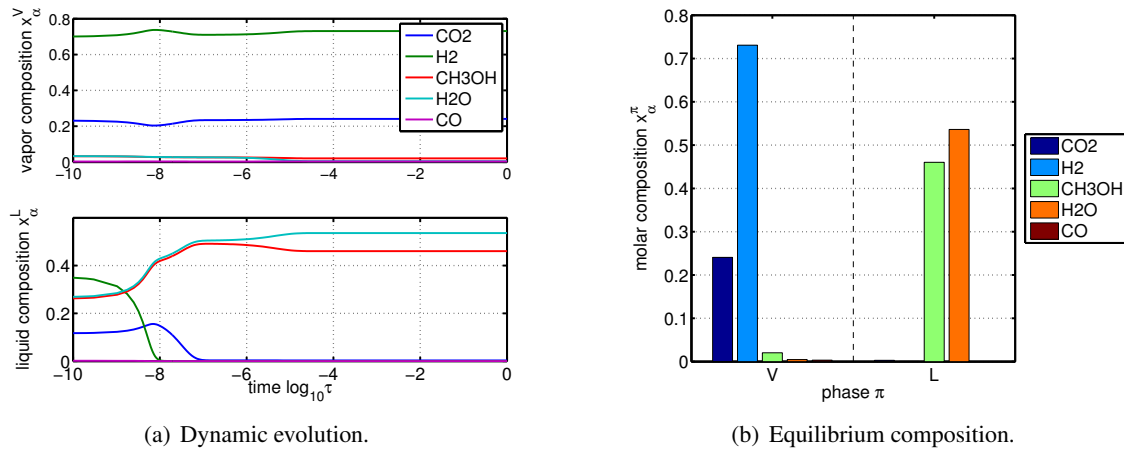
Figure 3.7: (a) Evolution of the composition in both phases, and (b) equilibrium composition of the VLE system.

with $K = 0.8$. Note, that Eq. (3.65) holds only for two-phase systems. A general expression for systems with $p = |\mathscr{P}|$ phases is given by

$$n_\alpha^{\pi,0} = n_\alpha^0 \times \begin{cases} K & : \kappa(\alpha) = \pi \\ \frac{1}{p-1}(1-K) & : \text{else} \end{cases}. \tag{3.66}$$

3.3.2.2   Simulation Results

The vapour-liquid equilibrium of the methanol system with the feed composition according to Eq. (3.57) was calculated at a temperature of $T = 300\,\text{K}$ and a pressure of $P = 0.5\,\text{MPa}$. The evolution of the composition in the vapour phase as well as in the liquid phase is given in Fig. 3.7(a). The final composition, i.e. the equilibrium composition, is shown in Fig. 3.7(b).

3.3.3   VLLE of Fischer-Tropsch Products

In this section, the dynamic method is utilized for the computation of a phase equilibrium involving a vapour and two distinct liquid phases. Therefore the phase equilibrium of the Fischer-Tropsch synthesis is calculated. The Fischer-Tropsch synthesis by Fischer and Tropsch (1926) is a process which converts carbon monoxide and hydrogen into hydrocarbons, i.e. in the case of alkanes only the net reaction is given by

$$i\,\text{CO} + (2i+1)\,\text{H}_2 \rightleftharpoons \text{C}_i\text{H}_{2i+2} + i\,\text{H}_2\text{O} \tag{3.67}$$
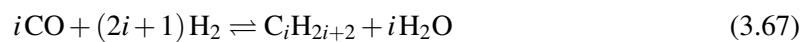
The resulting distribution of alkanes is commonly described by the Flory distribution (Flory, 1936)

$$n_{\text{C}i}^0 = n_{\text{total}}\,(1-\alpha)\,\alpha^{i-1} \tag{3.68}$$
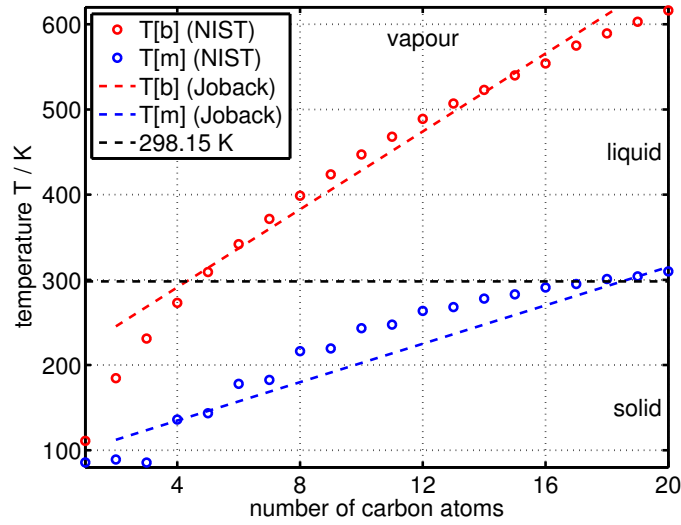
Figure 3.8: Boiling point T_b and melting point T_m as a function of the number of carbon atoms of the n-alkanes.

where α is the chain growth probability and i is the number of carbon atoms of the hydrocarbon. The subscript Ci refers to the n-alkane C_iH_{2i+2}. The state of matter of the hydrocarbons reaches from vapour over the liquid phase up to the solid phase. The boiling points T_b as well as the melting points T_m are given in Fig. 3.8 as a function of the number of the carbon atoms N_C of the n-alkanes. Here, the experimental data points (dots) from the NIST Webbook (Linstrom and Mallard, 2015) are compared to linear estimations using the group contribution method of Joback and Reid (1987), which gives

$$T_b^{\text{Joback}}/K = 199.6 \; + 22.88 N_C \text{ and} \tag{3.69a}$$

$$T_m^{\text{Joback}}/K = \; 89.76 + 11.27 N_C. \tag{3.69b}$$

for $N_C \geq 2$. It can be seen that the alkanes

- C1 (methane) to C4 (butane) are in vapour phase in the standard state,

- C5 (pentane) to C16...18 are in liquid phase at standard state, and

- longer alkanes are in solid state at ambient conditions.

In this example, we assume a typical Fischer-Tropsch product distribution of n-alkanes from methane (C1) up to hexadecane (C16) with $\alpha = 0.8$ which can be described without the presence of a solid phase. Additionally, we assume that the amount of water

$$n_{\text{H2O}}^0 = \sum_i i \cdot n_{\text{C}i} \tag{3.70}$$

which is formed as a side product is also part of the initial composition.

The proposed dynamic method on the vapour-liquid-liquid equilibrium of the Fischer-Tropsch product distribution is now applied. Here, the set of the three valid phases is given in form of a vapour (V), an organic liquid (L1), as well as an aqueous liquid phase (L2):

$$\mathcal{P} = \{V, L1, L2\}. \tag{3.71}$$

The set of $s = 17$ species in this system is given by

$$\mathcal{S} = \{H_2O, C_iH_{2i+2} \,\forall i = 1 \dots 16\} \tag{3.72}$$

The interactions between the vapour phase and the liquid phases is modelled using the ϕ-ϕ-approach

$$r_\alpha^{V,Li} = P\left(x_\alpha^V \phi_\alpha^V - x_\alpha^{Li} \phi_\alpha^{Li}\right), \quad i \in \{1,2\} \tag{3.73}$$

and the fugacity coefficients ϕ_α^π are calculated using the predictive Soave-Redlich-Kwong equation of state, see also section 2.8. The interactions between the two liquid phases are modelled using the γ-γ-approach

$$r_\alpha^{L1,L2} = P^\circ \left(x_\alpha^{L1} \gamma_\alpha^{L1} - x_\alpha^{L2} \gamma_\alpha^{L2}\right) \tag{3.74}$$

where the activity coefficients are computed using the UNIFAC group contribution method, see section 2.7.2.

For this system with $p = 3$ phases and $s = 17$ species, we get a system with 51 (3×17) coupled ordinary differential equations. The stoichiometric matrix for this system is given by

$$\mathbf{A} = \mathbf{A}_p = \begin{bmatrix} -\mathbf{I} & -\mathbf{I} & \mathbf{0} \\ \mathbf{I} & \mathbf{0} & -\mathbf{I} \\ \mathbf{0} & \mathbf{I} & \mathbf{I} \end{bmatrix}, \tag{3.75}$$

where $\mathbf{I}$ refers to the identity matrix of dimension 17.

3.3.3.1 Initialization

A general initialization procedure for multiphase systems was already exemplified in section 3.3.2 for methanol synthesis.

In the present example, the key components are partitioned by the normal boiling point $T_{b,\alpha}$ for the vapour phase and by the polarity p_α between the liquid phases. More precisely, the function that assigns the key components to the phases is defined by

$$\kappa : \alpha \mapsto \begin{cases} V & : T_{b,\alpha} < T \quad \text{vapour} \\ L1 & : p_\alpha \approx 0 \quad \text{liquid, non-polar} \\ L2 & : p_\alpha > 0 \quad \text{liquid, polar} \end{cases} \tag{3.76}$$

and the initial distribution of the composition among the three phases is done by

$$n_\alpha^{\pi,0} = n_\alpha^0 \times \begin{cases} K & : \kappa(\alpha) = \pi \\ \frac{1}{2}(K-1) & : \text{else} \end{cases}. \tag{3.77}$$

with $K = 0.8$. Hence, the short hydrocarbons methane (C1) to butane (C4) are initially assigned to the vapour phase (V), the longer hydrocarbons pentane (C5) to hexadecane (C16) are assigned to the first liquid phase (L1), i. e. the organic liquid phase, and the water is assigned to the second liquid phase (L2), which represents the aqueous liquid phase. Exemplary, the initial distribution of propane (C_3H_8) between the three phases $(V, L1, L2)$ is $(0.8, 0.1, 0.1)$ while the initial distribution of tetradecane ($C_{14}H_{30}$) is given by $(0.1, 0.8, 0.1)$.

3.3.3.2   Simulation Results

The resulting set of ODEs was solved with MATLAB for ambient temperature $T = 298.15\,\text{K}$ ($25\,^\circ\text{C}$) and a pressure of $P = 0.1\,\text{MPa}$. The temporal evolution of the composition in each phase is given in Fig. 3.9(a)–3.9(c). The steady state composition, i. e. the thermodynamic equilibrium, is shown in Fig. 3.9(d). It can be seen that the water forms its own liquid phase (L2) and the long-chained hydrocarbons will be found in the organic liquid phase (L1). Short alkanes with low boiling points are preferably found in the vapour phase (V).

3.3.3.3   Reduction of the Model

We assume a multiphase system with p phases in thermodynamic equilibrium with each other. Then, the isofugacity conditions are fulfilled at all binary interfaces between two phases

$$f_\alpha^\pi = f_\alpha^{\pi'}, \quad \forall \pi, \pi' \in \mathscr{P}. \tag{3.78}$$

The idea of reduction of the complexity of the resulting model is based on the fact, that if a phase π is in thermodynamic equilibrium with two other phases π' and π'', these two other phases are also in equilibrium with each other,

$$f_\alpha^\pi = f_\alpha^{\pi'} \quad \wedge \quad f_\alpha^\pi = f_\alpha^{\pi''} \quad \Rightarrow \quad f_\alpha^{\pi'} = f_\alpha^{\pi''}. \tag{3.79}$$

Therefore, the system can be solved thermodynamically correct also by considering only those rate expressions where the first π phase is involved. In the example of the vapour-liquid-liquid separation of the Fischer-Tropsch products, only the interaction of the vapour phase with the phases L1 and L2 is considered.

(a) Evolution of the vapour phase.

(b) Evolution of the organic liquid phase.

(c) Evolution of the aqueous liquid phase.

(d) Equilibrium composition.
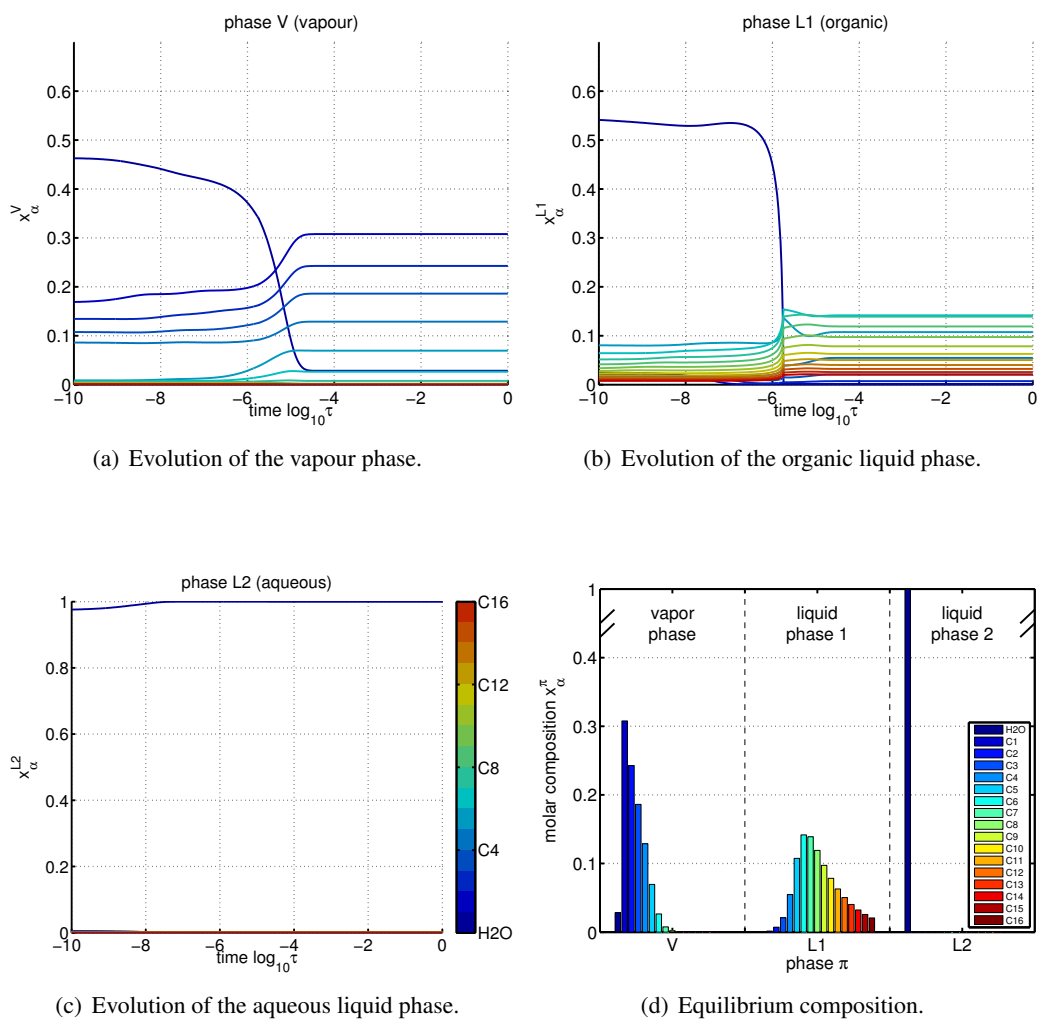
Figure 3.9: Evolution of the compositions (a) in the vapour phase, (b) in the organic liquid phase, and (c) in the aqueous liquid phase. (d) shows the equilibrium composition of the given vapour-liquid-liquid system.

Table 3.5: Density ρ of the structural Jacobian of the reduced system as a function of the number of phases p.

number of phases p	2	3	4	5	6
density of Jacobian ρ	100%	77.78%	62.5%	52%	44.44%

The Jacobian matrix $\mathbf{J}$ of the full model

$$\mathbf{J}^{\text{full}}_{p=3} = \begin{bmatrix} \star & \star & \star \\ \star & \star & \star \\ \star & \star & \star \end{bmatrix} \tag{3.80}$$

has a dimension of $sp \times sp$ and consists of $p \times p$ blocks, where $\star$ refers to a $s \times s$ matrix of non-zero values. Note that the number of phases is $p = 3$ in this example. Each matrix $\star$ describes the coupling of two defined phases and are fully allocated due to the strong coupling between mole fractions of the species in the thermodynamic models.

The Jacobian of the reduced model can be given by the following pattern:

$$\mathbf{J}^{\text{reduced}}_{p=3} = \begin{bmatrix} \star & \star & \star \\ \star & \star & \\ \star & & \star \end{bmatrix}. \tag{3.81}$$

More generally, the pattern of the Jacobian of a reduced system with p phases can be given by

$$\mathbf{J}^{\text{reduced}}_{p} = \begin{bmatrix} \star & \star & \cdots & \star & \star \\ \star & \star & & & \\ \vdots & & \ddots & & \\ \star & & & \star & \\ \star & & & & \star \end{bmatrix} \tag{3.82}$$

where the first row, the first column, and the main diagonal of the submatrices are non-zero submatrices. The density of such a Jacobian matrix can be given by

$$\rho\left(\mathbf{J}^{\text{reduced}}_{p}\right) = \frac{3p - 2}{p^2} \tag{3.83}$$

an tabulated in Tab. 3.5. The separation of the Fischer-Tropsch products was also solved by applying the reduced set of equations. The numerical performance of the full and the reduced model is compared in Tab. 3.6. In both cases, the MATLAB-solver ode15s was applied.

It can be seen, that a mentionable improvement in terms of computational costs can be achieved. The solver ode15s is able to deal with structural pattern matrices of the Jacobian and to lower the computational expenses in computing the partial derivatives of the right hand side of the ODE system (Coleman et al., 1984). In a three phase system, the density of the Jacobian $\rho(\mathbf{J}) \approx 78\%$

Table 3.6: Comparison of the numerical costs of the full and reduced model of the Fischer-Tropsch example.

	full	reduced	rel.
steps	285	227	80%
function evaluations	1 048	880	84%
partial derivatives	10	8	80%
CPU time	2.04 s	1.51 s	74%

was still too high to take advantages from such specialized algorithms. This was also the reason why no structural information of the Jacobian was provided to the ODE solver in those simulations. Nevertheless, an improvement of the computational efficiency was obtained. The stoichiometric matrix as well as the vector of rate expressions for the full model are

$$
\mathbf{A} = \begin{bmatrix} -\mathbf{I} & -\mathbf{I} & \mathbf{0} \\ \mathbf{I} & \mathbf{0} & -\mathbf{I} \\ \mathbf{0} & \mathbf{I} & \mathbf{I} \end{bmatrix} \text{, and} \qquad \mathbf{r} = \begin{bmatrix} \mathbf{r}^{V,L1} \\ \mathbf{r}^{V,L2} \\ \mathbf{r}^{L1,L2} \end{bmatrix}, \qquad (3.84)
$$

while it simplifies for the reduced model to

$$
\mathbf{A} = \begin{bmatrix} -\mathbf{I} & -\mathbf{I} \\ \mathbf{I} & \mathbf{0} \\ \mathbf{0} & \mathbf{I} \end{bmatrix} \text{, and} \qquad \mathbf{r} = \begin{bmatrix} \mathbf{r}^{V,L1} \\ \mathbf{r}^{V,L2} \end{bmatrix}. \qquad (3.85)
$$

In the equations of the reduced model, the direct coupling of the two liquid phases is neglected. This means that a mass transfer between the two liquid phases cannot be realized directly but has to make a detour through the vapour phase.

Due to the fact that the amount of water in the overall system is very large compared to the amount of hydrocarbons, see also Eq. (3.70), the initial amount of water in the vapour phase as well as in the organic phase is extensive. This can be seen in the evolution diagrams of the composition of the full model, Fig. 3.9. Large amount of this water has to be transferred into the aqueous liquid phase L2 which can also be seen in the evolution diagrams.

In the reduced model, the thermodynamic equilibrium is expectedly the same as in the full model. Therefore, the water transfer $L1 \rightarrow L2$ has to take the route $L1 \rightarrow V \rightarrow L2$. This effect can be seen in the evolution diagrams of the reduced model in Fig. 3.10. It can be concluded, that

(i) it takes longer to reach the thermodynamic equilibrium in terms of physical time τ, not in terms of computational time. The steady state is attained in $\log_{10} \tau \approx -4$ in case of the full model and $\log_{10} \tau \approx -3$ in case of the reduced model. Additionally,

(ii) the amount of water in the organic phase increases in the beginning. After the equilibration of vapour V and aqueous liquid L2 is done, the indirect water transfer from the organic liquid L1 via vapour V to its destination L2 takes place. This effect can be seen at the peak

(a) Evolution of the vapour phase.   (b) Evolution of the organic liquid phase.
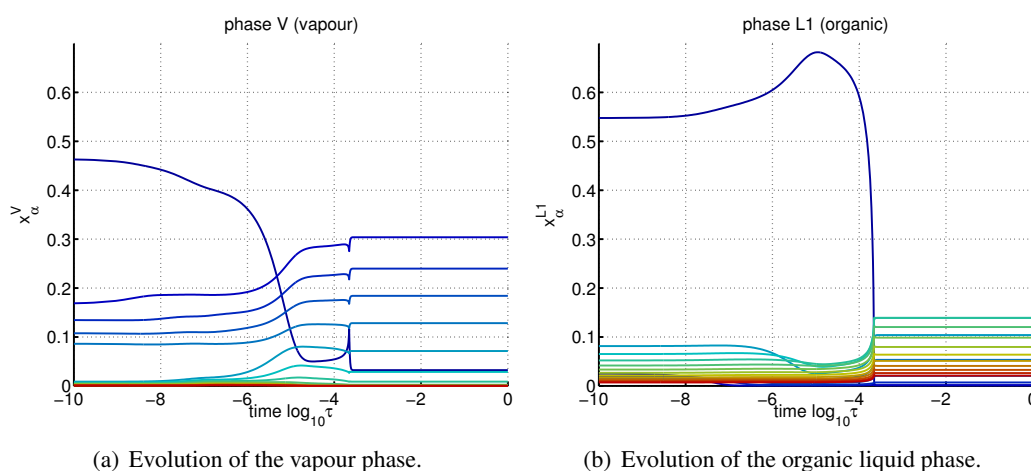
Figure 3.10: Evolution of the compositions (a) in the vapour phase, (b) in the organic liquid phase, when
          using the reduced model equations. The evolution in the aqueous liquid phase shows no men-
          tionable difference to the full model, see Fig. 3.9(c). Therefore, it is not shown explicitly
          here.

of the amount of water in the vapour phase at $\log_{10} \tau \approx -4 \ldots -3$ which has its origin in the
water transfer between the two liquid phases.

It can be summarized that the *physical* way how the thermodynamic equilibrium is attained has
more degrees of freedom in case of the full model than in the reduced model. The reason is that
the full model has a higher number of rate expressions and a stronger coupling among the phases.

Nevertheless, the *computational* way to reach the thermodynamic equilibrium is better in case of
the reduced model, due to the the decoupling of the describing equations.

3.3.4 LLLE of *n*-Heptane–Aniline–Water

In order to demonstrate the ability of the proposed method to deal with multicomponent systems
containing more than two liquid phases in thermodynamic equilibrium, one ternary system is
addressed here. Sørensen et al. (1979) reported that the system *n*-heptane–aniline–water forms
three coexisting liquid phases and Lucia et al. (2000) used the system also as a test problem for
their multiphase calculations. For the molecular structures of *n*-heptane and aniline, see Fig. 3.11.
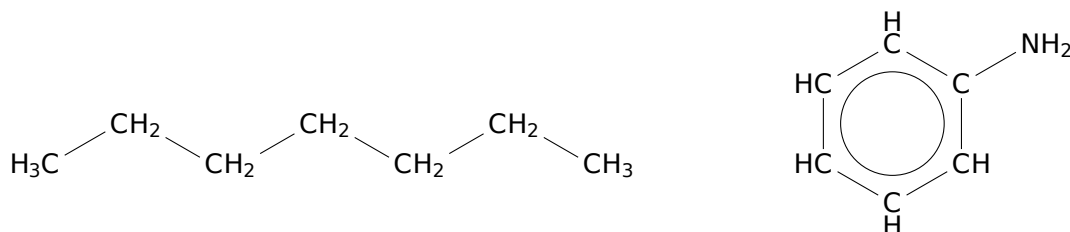
Figure 3.11: Molecular structures of *n*-heptane (left) and aniline (right).

The set of $s = 3$ species is given by

$$\mathscr{S} = \{C_7H_{14}, C_6H_5NH_2, H_2O\} \tag{3.86}$$

and we have $p = 3$ liquid phases

$$\mathscr{P} = \{L1, L2, L3\}. \tag{3.87}$$

The stoichiometric matrix is given by

$$\mathbf{A} = \mathbf{A_p} = \begin{bmatrix} -\mathbf{I} & -\mathbf{I} & \mathbf{0} \\ \mathbf{I} & \mathbf{0} & -\mathbf{I} \\ \mathbf{0} & \mathbf{I} & \mathbf{I} \end{bmatrix} \tag{3.88}$$

where $\mathbf{I}$ refers to the 3×3 identity matrix and the rate expressions for the phase transitions $\mathbf{r_p}$ are computed via the γ-γ-approach

$$r_\alpha^{L1,L2} = P\left(x_\alpha^{L1}\gamma_\alpha^{L1} - x_\alpha^{L2}\gamma_\alpha^{L2}\right) \tag{3.89a}$$

$$r_\alpha^{L1,L3} = P\left(x_\alpha^{L1}\gamma_\alpha^{L1} - x_\alpha^{L3}\gamma_\alpha^{L3}\right) \tag{3.89b}$$

$$r_\alpha^{L2,L3} = P\left(x_\alpha^{L2}\gamma_\alpha^{L2} - x_\alpha^{L3}\gamma_\alpha^{L3}\right) \tag{3.89c}$$

where the activity coefficients γ_α^π are obtained from the UNIFAC model. The considered ternary system of n-heptane–aniline–water was used as an example to explain this group contribution method in section 2.7.2.

As for all multiphase systems, the initial composition for each phase has to be set up. In this ternary system with three liquid phases one species α is assigned as key component to one of the liquid phases, i. e.

$$\kappa : \alpha \mapsto \begin{cases} L1 & : \alpha = C_7H_{14} \\ L2 & : \alpha = C_6H_5NH_2 \\ L3 & : \alpha = H_2O \end{cases} \tag{3.90}$$

For an equimolar feed composition of $n_\alpha^0 = 1\,\text{mol}\,\forall\alpha$ the evolution of the composition in the three liquid phases is shown in Fig. 3.12(a)–3.12(c). The steady state solution, i. e. the thermodynamic equilibrium, of the system is depicted in Fig. 3.12(d).

By variation of the feed composition n_α^0 a ternary phase diagram can be constructed and the regimes of coexistence of two and three liquid phases can be determined. The Gibbs energy of the mixture is defined by

$$\Delta g = \sum_\alpha x_\alpha \ln x_\alpha + \sum_\alpha x_\alpha \ln \gamma_\alpha. \tag{3.91}$$

The ternary phase diagram as well as the isolines of constant Gibbs energy of the mixture Δg are shown in Fig. 3.13.

(a) Evolution in phase L1.

(b) Evolution in phase L2.

(c) Evolution in phase L3.
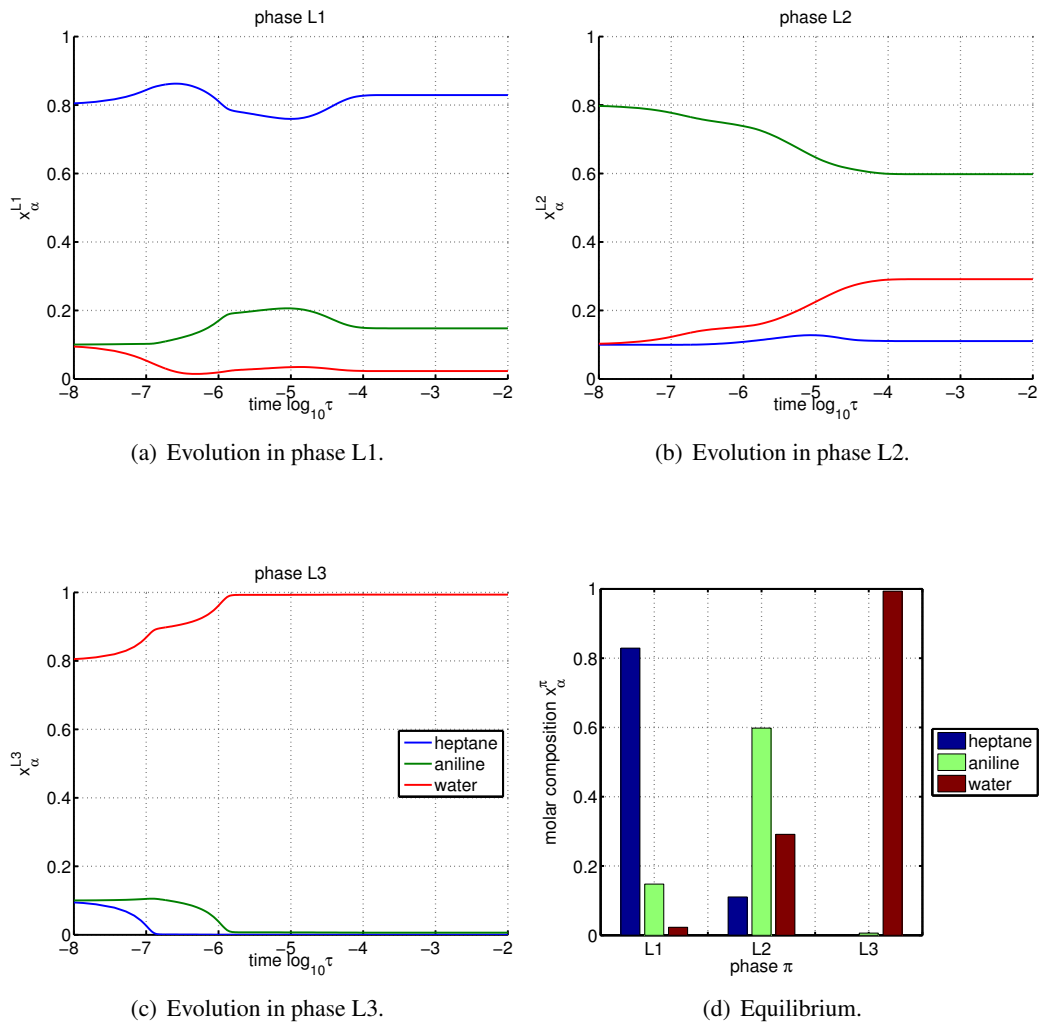
(d) Equilibrium.

Figure 3.12: (a) (b) (c) Evolution of the composition in the three liquid phases w. r. t. time τ. (d) Molar composition x_α^π in each phase in thermodynamic equilibrium.
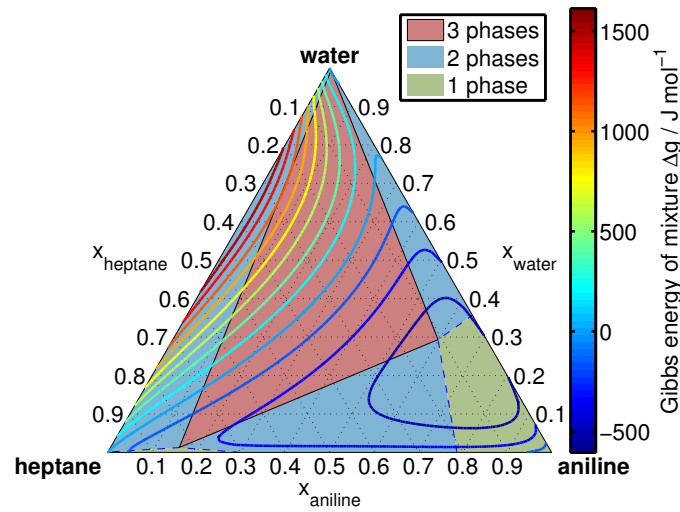
Figure 3.13: Ternary phase diagram of the system n-heptane–aniline–water shows the number of liquid phases that coexist for a given feed composition and the Gibbs energy of the mixture Δg.

3.3.5 Simultaneous Reaction and Vapour-Liquid Equilibrium of Methanation

In this example, the ability of the proposed method to solve simultaneous chemical and phase equilibrium problems is demonstrated. Here, the chemical equilibrium of the methanation reaction as well as the vapour-liquid equilibrium of the condensation of the side-product water under high pressures is solved simultaneously. Hence, the set of the $p = 2$ phases is set to

$$\mathscr{P} = \{V, L\}. \tag{3.92}$$

In this example, the $s = 5$ species

$$\mathscr{S} = \{CO_2, H_2, CH_4, H_2O, CO\} \tag{3.93}$$

are connected with each other by the two gas-phase reactions, the methanation reaction from CO_2 and the reverse water-gas shift reaction,

$$CO_2 + 4\,H_2 \rightleftharpoons CH_4 + 2\,H_2O, \tag{3.94a}$$

$$CO_2 + H_2 \rightleftharpoons CO + H_2O. \tag{3.94b}$$

This leads to the rate expressions $\mathbf{r}^V = \left[r_1^V, r_2^V\right]^T$ due to chemical reactions in the vapour phase,

$$r_1^V = (x\phi)_{CO2}^V \left((x\phi)_{H2}^V\right)^4 \left(\frac{P}{P^\circ}\right)^5 - \frac{(x\phi)_{CH4}^V \left((x\phi)_{H2O}^V\right)^2}{K_{eq,1}} \left(\frac{P}{P^\circ}\right)^3 \tag{3.95a}$$

$$r_2^V = (x\phi)_{CO2}^V (x\phi)_{H2}^V \left(\frac{P}{P^\circ}\right)^2 - \frac{(x\phi)_{CO}^V (x\phi)_{H2O}^V}{K_{eq,2}} \left(\frac{P}{P^\circ}\right)^2 \tag{3.95b}$$

where $(x\phi)_\alpha^\pi$ refers to $x_\alpha^\pi \phi_\alpha^\pi$. The stoichiometric matrix of the chemical reactions in the vapour phase is given by

$$\mathbf{A}_r^V = \begin{bmatrix} -1 & -4 & 1 & 2 & 0 \\ -1 & -1 & 0 & 1 & 1 \end{bmatrix}^T \tag{3.96}$$

and since no chemical reactions are considered in the liquid phase, the stoichiometric matrix of the chemical reactions in the liquid phase is empty, $\mathbf{A}_r^L = \emptyset_{5\times0}$. This combines to the stoichiometric matrix due to chemical reactions of the overall system to

$$\mathbf{A}_r = \begin{bmatrix} \mathbf{A}_r^V & \mathbf{0} \\ \mathbf{0} & \mathbf{A}_r^L \end{bmatrix} = \begin{bmatrix} \mathbf{A}_r^V & \mathbf{0} \\ \mathbf{0} & \emptyset_{5\times0} \end{bmatrix} = \begin{bmatrix} \mathbf{A}_r^V \\ \mathbf{0}_{5\times2} \end{bmatrix} \tag{3.97}$$

Additionally, the rate expressions of the mass transfer between the vapour and the liquid phase $\mathbf{r}^{V,L} = \left[r_\alpha^{V,L}\right]$ are defined by applying the ϕ-ϕ-approach,

$$r_\alpha^{V,L} = P\left((x\phi)_\alpha^V - (x\phi)_\alpha^L\right) \tag{3.98}$$

and the corresponding stoichiometric matrix is

$$\mathbf{A}_p = \begin{bmatrix} -\mathbf{I} \\ \mathbf{I} \end{bmatrix}, \tag{3.99}$$

where $\mathbf{I}$ refers to the 5×5 identity matrix. By combining the stoichiometric matrices and the rate equations, one gets for the overall system

$$\mathbf{A} = \begin{bmatrix} \mathbf{A}_r^V & -\mathbf{I} \\ \mathbf{0}_{5\times2} & \mathbf{I} \end{bmatrix}, \text{ and } \qquad \mathbf{r} = \begin{bmatrix} \mathbf{r}^V \\ \mathbf{r}^{V,L} \end{bmatrix}. \tag{3.100}$$

In this example, the fugacity coefficients ϕ_α^π are computed by applying the predictive Soave-Redlich-Kwong (PSRK) Equation of State, see section 2.8. The initial composition of this integrated reaction-separation unit is assumed to be the stoichiometric ratio of $CO_2 : H_2 = 1 : 4$ which is present in the vapour phase,

$$\mathbf{n}_0 = [1, 4, 0, 0, 0]^T. \tag{3.101}$$

While in the initial state of this system no water is available, there does no liquid phase exist at
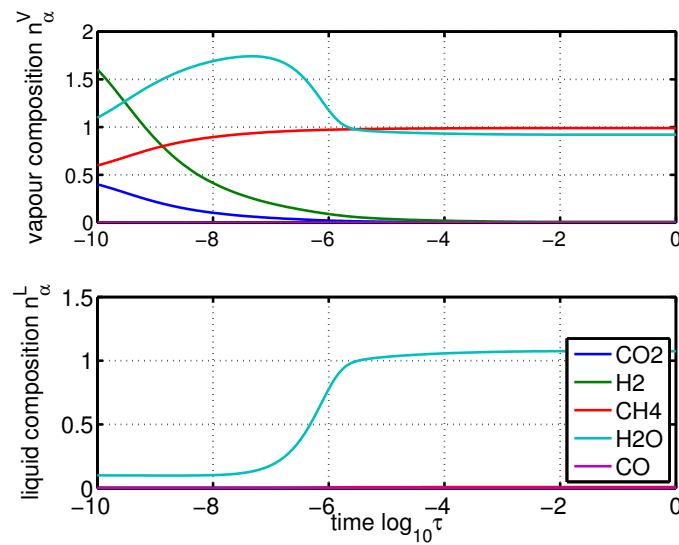
Figure 3.14: Evolution of the composition in the vapour phase (top) as well as in the liquid phase (bottom).

this point. It is common to assume the extent of reaction to be zero at the initial condition in pure phase systems, which is no feasible set-up in this case. Therefore, an initial extent of reaction ξ of the methanation reaction is assumed. Additionally, the key component of the liquid phase is set to water with a split fraction K. This leads to an initial set-up of the equilibrium problem at $\tau = 0$ of

$$
\mathbf{n}^V(0) = \begin{bmatrix} 1-\xi \\ 4(1-\xi) \\ \xi \\ 2\xi(1-K) \\ 0 \end{bmatrix}, \text{ and } \qquad \mathbf{n}^L(0) = \begin{bmatrix} 0 \\ 0 \\ 0 \\ 2\xi K \\ 0 \end{bmatrix}. \tag{3.102}
$$

The simultaneous chemical and phase equilibria of the methanation system was computed at a temperature of $T = 550\,\mathrm{K}$ and a pressure of $P = 18\,\mathrm{MPa}$ using an initial set-up of $\xi = 0.5$ and $K = 0.1$. The evolution of the composition in the vapour phase and in the condensed phase is shown in Fig. 3.14. It can be seen, that nearly full conversion is achieved while approximately the half amount of the side product water is condensed into the liquid phase at given process conditions.

3.3.5.1   Reduction of the Model

As shown in Fig. 3.14, in the liquid phase mainly the side-product water occurs in which only some traces of the gases are dissolved. While the general derivation of the proposed dynamic method allows different sets of the occurring species $\mathscr{S}^\pi$ for each phase $\pi \in \mathscr{P}$, this is demonstrated now at the given example problem.

While the model reduction which was introduced in the VLL-separation example of the Fischer-

Tropsch products, section 3.3.3, only reduces the complexity of the problem formulation, the model reduction which is done here makes additional assumptions on the particular system.

We assume, that water is the only species which is allowed to exist in the liquid phase. The last simulation, see Fig. 3.14, showed already that this is a feasible assumption on the given system. Therefore, the set of valid pphases is still the same,

$$\mathscr{P} = \{V, L\} \,, \tag{3.103}$$

while the sets of allowed species in the two phases will differ from each other, namely

$$\mathscr{S}^{V} = \{CO_2, H_2, CH_4, H_2O, CO\} \,, \tag{3.104a}$$

$$\mathscr{S}^{L} = \{H_2O\} \,. \tag{3.104b}$$

While the equations for the chemical reactions, Eqs. (3.95a)–(3.96), are still valid in this case, the rate equations due to the mass transfer between the phases has to be reformulated. The interface $\mathscr{I}^{V,L}$ of the vapour and the liquid phase is defined by the intersection of the species of these phases

$$\mathscr{I}^{V,L} = \mathscr{S}^{V} \cap \mathscr{S}^{L} = \{H_2O\} \,, \tag{3.105}$$

which is water only. Therefore, only one rate expression for the phase transition has to be formulated, namely that one of the water

$$r_{H2O}^{V,L} = P \left((x\phi)_{H2O}^{V} - (x\phi)_{H2O}^{L} \right) \tag{3.106}$$

Note, that now in the liquid phase the pure compound fugacity coefficient is applied. For the reduced model, the equilibrium composition was also computed using the same conditions in terms of temperature, pressure and initial set-up. The evolution of the composition w. r. t. time τ is shown in Fig. 3.15. It can be seen that the evolution as well as the steady state composition is qualitatively the same as in the full model case, Fig. 3.14.

A comparison of the numerical expenses of the full model and the reduced model was performed and is shown in Tab. 3.7.

Table 3.7: Comparison of the numerical costs of the full model and the reduced model.

	full	reduced	rel.
dynamic states	10	6	60%
steps	188	180	96%
function evaluations	456	406	89%
partial derivatives	7	6	85%
CPU time	0.491 s	0.338 s	69%
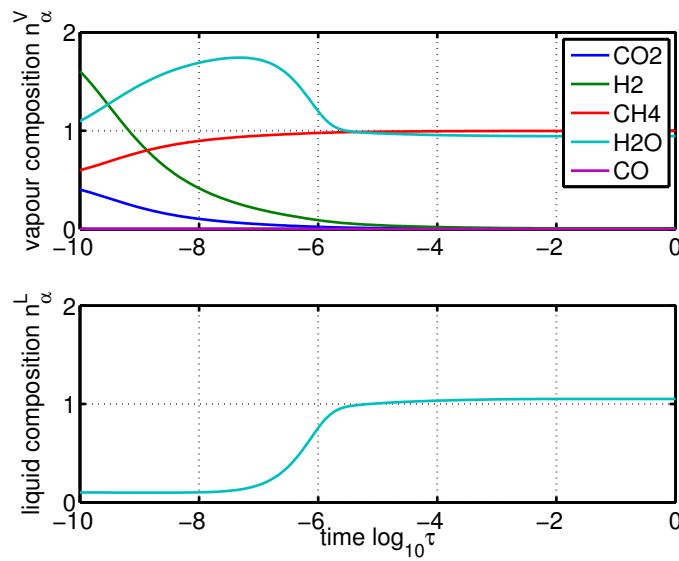
Figure 3.15: Evolution of the composition in both phases applying the reduced model.

3.3.5.2   Case Study: Existence of the two-phase Regime

Fig. 3.16 shows the different regimes of existence of the different phases. The black dashed line refers to the vapour pressure of water. Below this line all pure compounds of the system, even water, are in gaseous state. Above this line pure water would exist as a liquid, but a liquid phase does not necessarily exist for the resulting product mixture water–methane. The red region refers to a supercritical regime. Here, the simulation leads to a coexistence of liquid and vapour phase with identical composition, which means that a supercritical state is reached. In the region where no liquid phase exists, the simulation leads to an equilibrium composition with the molar amount of zero in the liquid phase.

The region of coexistence of vapour and liquid phase is depicted in Fig. 3.16 by the isolines of the liquid fraction

$$L = \frac{\sum\limits_{\alpha \in \mathscr{S}^{\mathrm{L}}} n_{\alpha}^{\mathrm{L}}}{\sum\limits_{\pi \in \mathscr{P}} \sum\limits_{\alpha \in \mathscr{S}^{\pi}} n_{\alpha}^{\pi}} \tag{3.107}$$

of the system. Assuming a full stoichiometric conversion and a full separation between the products methane and water, a maximum liquid fraction of $L = 2/3$ can be obtained.

In this process, the removal of water from the reactive vapour phase leads to a higher conversion of CO_2 to methane. From a thermodynamic point of view, the best separation performance and consequently the highest conversion is achieved at low temperatures and high pressures, e. g. in the upper left corner of Fig. 3.16, which corresponds to $T = 500\,\mathrm{K}$ and $P = 20\,\mathrm{MPa}$. It should be emphasized, that this analysis only shows the thermodynamic limitations of this process. When designing such a process with simultaneous reaction and separation by water condensation, also kinetic and energetic limitations must be considered:
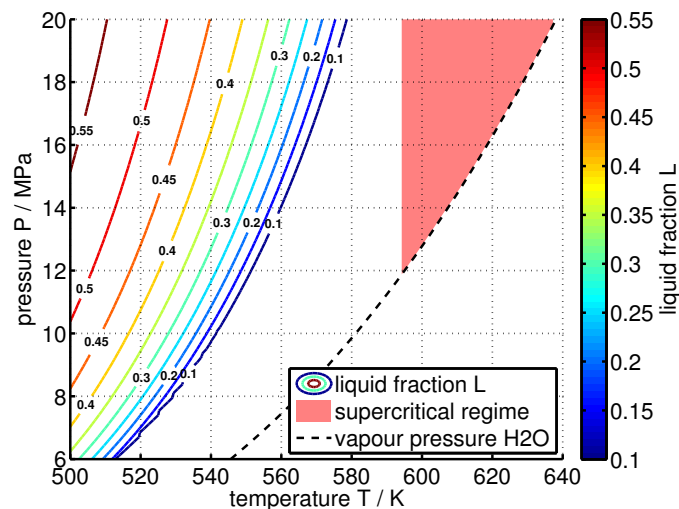
Figure 3.16: Different regimes of the existence of the phases as function of temperature T and pressure P.

(i) **kinetic limitations:** lower temperatures leads to lower reaction rates and therefore higher residence times and larger reactors are required to achieve a given conversion.

(ii) **energetic limitations:** higher pressures leads to higher energy demands for the compression of the reactants.

3.4 Summary

In this chapter, the Dynamic Method was introduced and its feasibility was exemplified at several examples of different type and complexity. A summary of the considered systems is shown in Tab. 3.8. For example 1, see section 3.3.1, also a comparison of the Dynamic Method with the conventional Gibbs energy minimization method is done. It was shown, that the computational costs are in the same order of magnitude. Additionally, it was shown that the Dynamic Method does not violate stoichiometric constraints on the way from the initial composition towards the equilibrium composition. In contrast it can be seen, that the algorithm that was used for the Gibbs energy minimization violates the stoichiometry in its first step which leads to negative molar amounts of substances.

Additionally, the proposed method was successfully applied on complex phase equilibrium calculations, such as VLLE and LLLE, as well as on a simultaneous chemical reaction and phase equilibrium problem.

Table 3.8: Overview of the considered systems and their properties. The number of dimensions gives the number of dynamic states of the corresponding ODE system.

	System	Reaction	Phases	Species	Dimensions
Ex. 1	Methanol synthesis, reaction	✓	V (1)	H_2, H_2O, CO, CO_2, CH_3OH (5)	5
Ex. 2	Methanol synthesis, separation	—	VL (2)	H_2, H_2O, CO, CO_2, CH_3OH (5)	10
Ex. 3	VLLE of Fischer-Tropsch products	—	VLL (3)	H_2O, CH_4, C_2H_6, ..., $C_{16}H_{34}$ (17)	51
Ex. 4	LLLE of heptane–aniline–water	—	LLL (3)	H_2O, C_6H_7N, C_7H_{16} (3)	9
Ex. 5	Reactive VLE of methanation	✓	VL (2)	H_2, H_2O, CO, CO_2, CH_3OH (5)	10

Chapter **4**

Process Simulation

The main parts of this section are based on Zinser et al. (2016b), a publication of the author.

In chapter 3, a dynamic method for computing thermodynamic equilibria for single process units was developed. In this chapter the Dynamic Method will be extended to a method, which is able to solve overall process flowsheets into their thermodynamic equilibrium. This method is called Simultaneous Dynamic Method (SDM) within this work.

In the first part of this chapter, some conventional approaches for computing process flowsheets are introduced, the so-called tearing methods. After that, the Dynamic Method is extended from closed systems to open systems. The SDM is able to solve the overall process flowsheet including recycle streams into its equilibrium. The conventional tearing methods are compared to with the Simultaneous Dynamic Method and the influences of properties like the recycle ratio or the initial set-up of the process simulation are investigated in detail.

4.1 Process Types

4.1.1 Linear Processes

In a linear process structure without recycle streams, the molar compositions in all streams can be calculated easily step by step, starting at the first unit. An example for such an process is the methanation process with intermediate cooling and water condensation, see also El-Sibai et al. (2015). A simplified process flowsheet of this process assuming full conversion is depicted in Fig. 4.1.

— 63 —
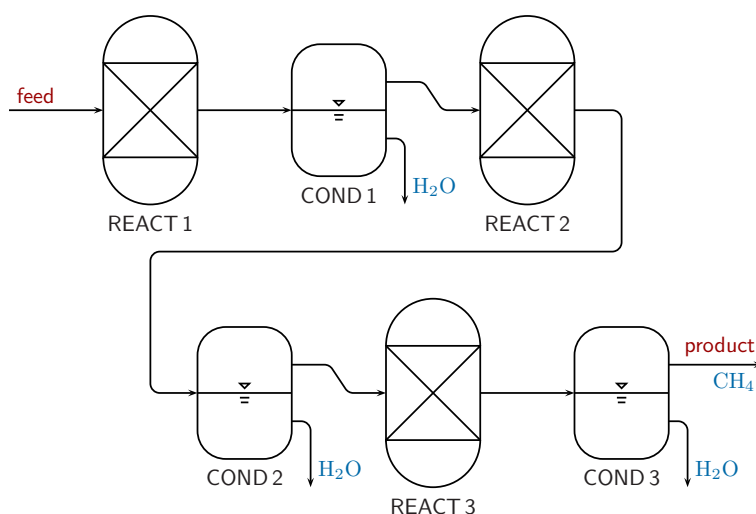
Figure 4.1: Simplified process flowsheet of a methanation process.

4.1.2 Processes including Recycle Streams

In general, chemical reactions and separation steps do not have full conversion or perfect separation. In process engineering, it is common to overcome these thermodynamic limitations by recycling of unreacted material or by a complex interconnection of different separation steps. This leads to process structures with recycle streams, which are not known a priori and have to be computed iteratively.

A simple example for a process that requires a recycle loop is the methanol synthesis process from carbon dioxide, see also Rihko-Struckmann et al. (2010). Here, the synthesis reaction

$$CO_2 + 3\,H_2 \rightleftharpoons CH_3OH + H_2O \tag{4.1}$$

reaches approximately 50% conversion in its chemical equilibrium at a temperature of $T = 450\,\mathrm{K}$. After a reaction step, the products methanol and water are separated by condensation from the remaining, non-reacted gases. The non-reacted reactants carbon dioxide and hydrogen are recycled back into the reactor. By this technique, the thermodynamic limitation of the reaction can be overcome and the overall process can achieve almost full conversion. A simplified process flowsheet of the methanol synthesis process is shown in Fig. 4.2.

The methanol synthesis process is used in this chapter to demonstrate the applicability of the Simultaneous Dynamic Method to perform process simulations.

4.1.3 Complex Processes

In the industrial practice, there are numerous processes with many nested recycle loops. An example of such a process is the BASF process for the production of formic acid (HCOOH). A process
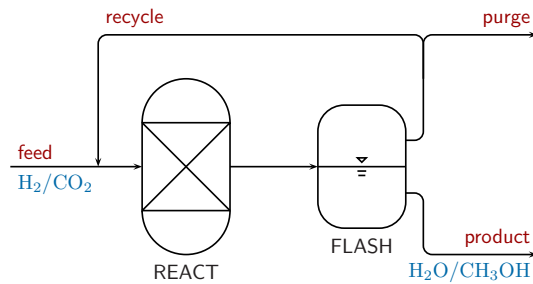
Figure 4.2: Simplified process flowsheet of the methanol synthesis process.
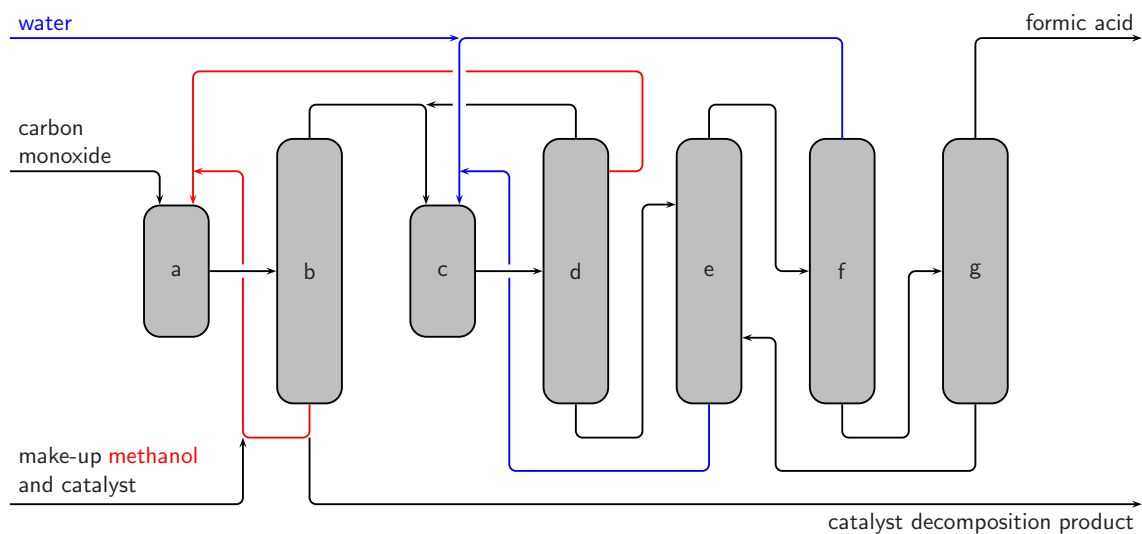
Figure 4.3: Flowsheet of the BASF process for the production of formic acid.

flowsheet is given in Fig. 4.3. This process is based on the carbonylation of methanol and the hydrolysis of methyl formate:

$$CH_3OH + CO \rightleftharpoons HCOOCH_3 \tag{4.2a}$$

$$HCOOCH_3 + H_2O \rightleftharpoons CH_3OH + HCOOH \tag{4.2b}$$

The two reactions, Eq. (4.2a) and Eq. (4.2b), are performed in the two reactors, (a) and (c) in Fig. 4.3. The five distillation columns, (b), (d), (e), (f), and (g), are required to realize the complex separation between remaining reactants and products, and for the purification of the formic acid. For more details of this process, see Reutemann and Kieczka (2000). In highly complex process structures which include also nested recycle loops, conventional tearing method have also been applied in a nested manner. The proposed Simultaneous Dynamic Method can be formulated independently of the complexity of any specific process topology.

4.2   Tearing Methods

In the case of a linear process topology without any recycle loops, the outlet streams of each unit can be computed subsequently. In the general case with at least one recycle loop, an iterative strategy for computing a process flowsheet is required in order to quantify the steady state process conditions. A conventional approach to solve such process flowsheets is the class of the so-called tearing methods. This class of solution strategies is introduced at the example of the methanol synthesis process, Fig. 4.2.

When the process flowsheet is initialized, the feed into the process is typically known while the molar composition of the recycle stream is unknown so far. The basic idea of the tearing methods is to "tear" the recycle stream, i.e. to set its molar composition simply to zero

$$\mathbf{n}_{\text{recycle}}^{(0)} = \mathbf{0}. \tag{4.3}$$

In the next step, the subsequent units and streams are calculated according to the unit models and in the end of this iteration cycle an updated value $\mathbf{n}_{\text{recycle}}^{\text{update}}$ for the recycle stream is available. The next iteration cycle is repeated using a new value for the recycle stream composition

$$\mathbf{n}_{\text{recycle}}^{(k+1)} = (1-\lambda)\,\mathbf{n}_{\text{recycle}}^{(k)} + \lambda\,\mathbf{n}_{\text{recycle}}^{\text{update}} \tag{4.4}$$

where $\lambda \in (0,2)$ is a parameter which allows an adjustment of the convergence properties of the method.

- $\lambda = 1$ leads to the most simple tearing method: The updated recycle stream $\mathbf{n}_{\text{recycle}}^{\text{update}}$ is directly used in the next iteration cycle $\mathbf{n}_{\text{recycle}}^{(k+1)} = \mathbf{n}_{\text{recycle}}^{\text{update}}$.

- $0 < \lambda < 1$ leads to a so-called relaxation method. This method uses a weighted average between the old value $\mathbf{n}_{\text{recycle}}^{(k)}$ and the updated one $\mathbf{n}_{\text{recycle}}^{\text{update}}$. This approach leads to higher robustness of the solution algorithm, but also implies a lower convergence speed.

- $1 < \lambda < 2$ refers to the class of over-relaxation methods, which may lead to a faster convergence.

4.2.1   Basic (linear) Example

In this section, the application of the tearing methods is demonstrated for a simple process as shown in Fig. 4.4. We assume an exhaust gas treatment process which converts a toxic compound A into a non-toxic compound B according to

$$\mathrm{A} \rightleftharpoons \mathrm{B}. \tag{4.5}$$

This process consists of a reactor unit which reduces the amount of compound A by a cleaning ratio or conversion $C \in (0, 1]$. In the next step the gas mixture is separated and unreacted reactants are recycled. The amount of the recycle stream is defined by the recycle ratio $R \in (0, 1)$. A process flowsheet of this process is depicted in Fig. 4.4. The equations for the molar streams in this process can be written as

$$\dot{n}_1 = \dot{n}_3 + \dot{n}_{\text{feed}}, \qquad \dot{n}_2 = C\dot{n}_1, \qquad \dot{n}_3 = R\dot{n}_2, \text{ and} \qquad \dot{n}_{\text{out}} = (1-R)\dot{n}_2. \tag{4.6}$$

For the computation of the recycle loop it is sufficient to consider the streams within the loop, i.e. $\dot{n}_1$, $\dot{n}_2$, and $\dot{n}_3$. The equations for these three streams can be written as a linear set of equations of the form $\mathbf{A}\dot{\mathbf{n}} = \mathbf{b}$, where $\dot{\mathbf{n}} = [\dot{n}_1, \dot{n}_2, \dot{n}_3]^{\mathrm{T}}$:

$$\underbrace{\begin{bmatrix} -1 & & 1 \\ C & -1 & \\ & R & -1 \end{bmatrix}}_{\mathbf{A}:=} \dot{\mathbf{n}} = \underbrace{\begin{bmatrix} -\dot{n}_{\text{feed}} \\ 0 \\ 0 \end{bmatrix}}_{\mathbf{b}:=}. \tag{4.7}$$

For this case, the system of linear equations can be solved analytically by

$$\dot{\mathbf{n}} = \mathbf{A}^{-1}\mathbf{b} = \frac{1}{RC-1} \begin{bmatrix} 1 & R & 1 \\ C & 1 & C \\ RC & R & 1 \end{bmatrix} \begin{bmatrix} -\dot{n}_{\text{feed}} \\ 0 \\ 0 \end{bmatrix} = \frac{\dot{n}_{\text{feed}}}{1-RC} \begin{bmatrix} 1 \\ C \\ RC \end{bmatrix}. \tag{4.8}$$

The model equations in a general process scheme are typically highly non-linear, and cannot be solved analytically. Hence, in the present example it is also focused on iterative methods for systems of linear equations. Such iterative methods (Dahmen and Reusken, 2006) are

- the Jacobi method,

- the Gauss–Seidel method, and

- the method of successive over-relaxation (SOR).

General, formal descriptions as well as MATLAB implementations of the three methods are given
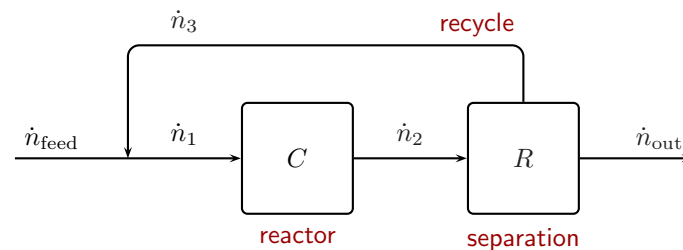
Figure 4.4: Process flowsheet of the exhaust gas treatment process.
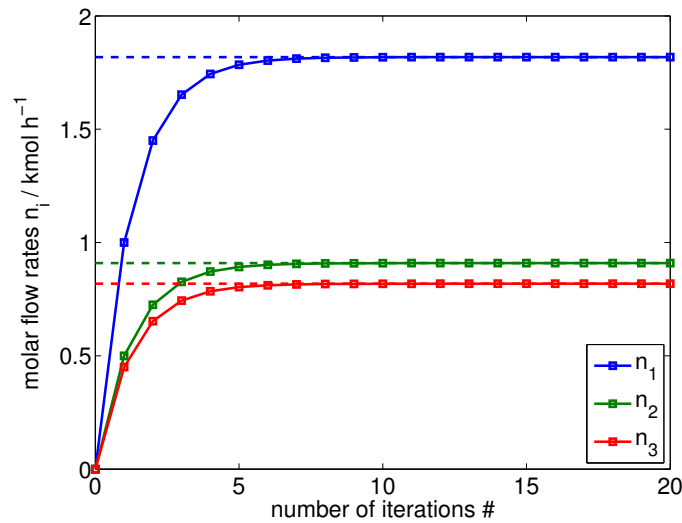
Figure 4.5: Evolution of the molar flow rates of the process towards the solution applying the Gauss-Seidel method. The exact solutions of each stream are depicted by the dashed lines.

in the appendix, see section B.3. While the Jacobi method and the Gauss-Seidel method do not require any additional parameter, the method of successive over-relaxation (SOR) needs a relaxation parameter $\lambda \in (0, 2)$. In case of the choice of $\lambda = 1$ the method of SOR simplifies to the Gauss-Seidel method.

4.2.1.1   Iterative Solution using the Gauss-Seidel Method

In order to illustrate the application and solution of a process model using iterative algorithms, the given model, Eq. (4.7), is solved numerically by applying the three algorithms, as mentioned above. The process parameters, namely the cleaning ratio C, the recycle ratio R, and the molar feed stream $\dot{n}_{\text{feed}}$ are set to

$$C = 1/2, \qquad\qquad R = 9/10, \text{ and} \qquad\qquad \dot{n}_{\text{feed}} = 1\,\text{kmol}/\text{h}, \qquad (4.9)$$

respectively. Hence, the analytical solution yields to

$$\frac{\dot{\mathbf{n}}}{\text{kmol h}^{-1}} = \begin{bmatrix} 20/11 \\ 10/11 \\ 9/11 \end{bmatrix}. \qquad (4.10)$$

In the numerical simulations, the *a posteriori* error estimation

$$\text{err}(k) := \sum_{j=1}^{n} \left| x_j^k - x_j^{k-1} \right| \overset{!}{<} M \qquad (4.11)$$

was applied with a threshold of $M = 10^{-6}$. The Gauss-Seidel method reached the threshold within
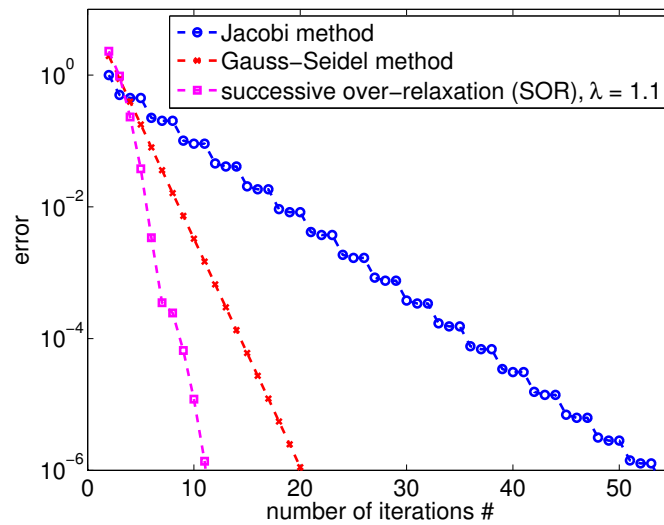
Figure 4.6: Evolution of the error estimation of the three methods w. r. t. the number of iterations.

20 iterations. The evolution of the molar flow rates w. r. t. the number of iterations is shown in Fig. 4.5 for all three molar streams. The exact values of the molar streams are depicted by dashed lines.

4.2.1.2   Comparison of the Different Iterative Methods

For comparison, the process system was also solved using the Jacobi method and the method of successive over-relaxation (SOR). The evolution of the error estimations $\mathrm{err}(k)$ for the three methods is shown in Fig. 4.6. While the Gauss-Seidel method reaches the threshold M in 20 iterations, the Jacobi method needs more than 50 iterations. The efficiency of the method of successive over-relaxation depends on the choice of the relaxation parameter λ. At the given process model, the best efficiency was observed using a relaxation parameter of $\lambda = 1.1$ which meets the predefined error tolerance of $M = 10^{-6}$ already within 11 iterations. The influence of the relaxation parameter λ on the convergence speed of the method of successive over-relaxation is examined in the next section in detail.

4.2.1.3   Influence of the Relaxation Parameter

In order to examine the influence of the relaxation parameter λ on the efficiency of the method of successive over-relaxation (SOR), the given process model was solved using different values of λ on the range $1/2 \leq \lambda \leq 3/2$. The number of iterations that are necessary in order to meet the threshold M w. r. t. the relaxation parameter λ is depicted in Fig. 4.7. For $\lambda = 1$, SOR simplifies to the Gauss-Seidel method and requires 20 iterations to reach the given threshold of $M = 10^{-6}$.

Since for $\lambda < 1$, the method of successive over-relaxation leads to a weighted average of the Gauss-Seidel method ($\lambda = 1$) and "doing nothing" ($\lambda = 0$), the number of iterations are higher
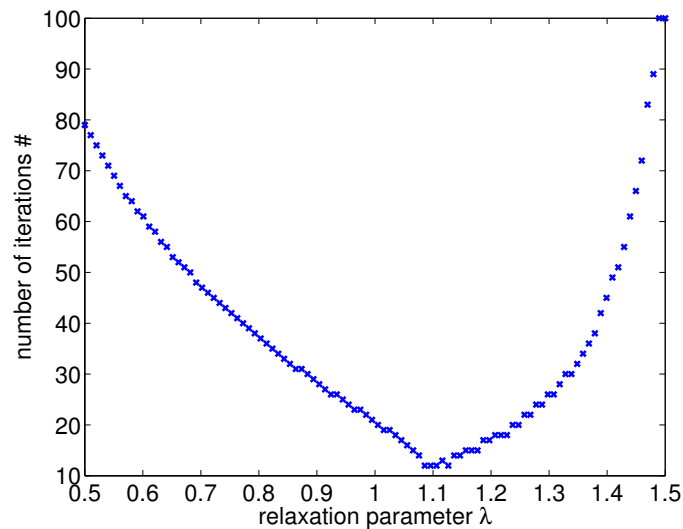
Figure 4.7: Number of iterations of the method of successive relaxation w. r. t. the relaxation parameter λ.

for smaller values of λ.

In the over-relaxed case, $1 < \lambda < 2$, there can be found an optimal value for the relaxation parameter λ. At the example of the given process, this optimal relaxation parameter is located at $\lambda \approx 1.1$ and the resulting method meets the given error tolerance in only 11 iterations.

4.2.2   Methanol Synthesis Process

Section 4.2.1 gave an example for a linear process model and used the well-known iterative solution algorithms for systems of linear equations in order to compute the unknown molar streams in the flowsheet. These methods are known in literature (e. g. Dahmen and Reusken, 2006) as the Jacobi method, the Gauss-Seidel method, and the method of successive over-relaxation (SOR), respectively. While these methods are designed for solving systems of linear equations, their principles can also applied to general non-linear systems of equations. Hence, the method of successive over-relaxation leads in the non-linear case to the tearing method described by Eq. (4.4).

In this section, a methanol synthesis process from carbon dioxide and hydrogen is investigated, see also Rihko-Struckmann et al. (2010). A simplified process flowsheet is given in Fig. 4.8. The process consists basically of a reactor unit and a vapour-liquid-separation unit. Besides the overall process, both steps are already investigated separately in section 3.3.1 and 3.3.2. The methanol synthesis reactor was investigated in section 3.3.1 (page 36), and the vapour-liquid-separation of the products was examined in section 3.3.2 (page 43), respectively.

Within this methanol synthesis process, the five species

$$\mathscr{S} = \{CO_2, H_2, CH_3OH, H_2O, CO\} \tag{4.12}$$
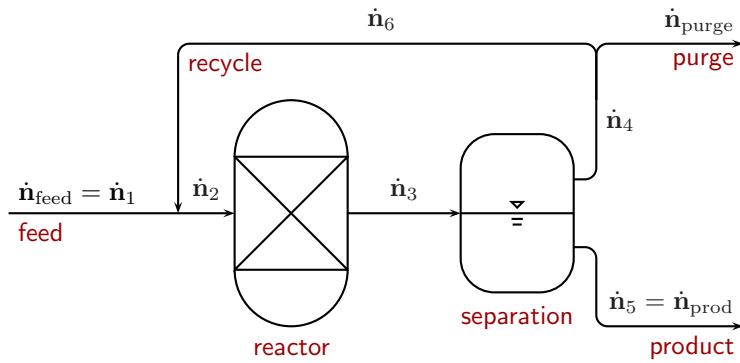
Figure 4.8: Flowsheet of the methanol synthesis process.

may occur while in the chemical reactor the three chemical reactions

$$CO_2 + 3\,H_2 \rightleftharpoons CH_3OH + H_2O \tag{4.13a}$$

$$CO + 2\,H_2 \rightleftharpoons CH_3OH \tag{4.13b}$$

$$CO_2 + H_2 \rightleftharpoons CO + H_2O \tag{4.13c}$$
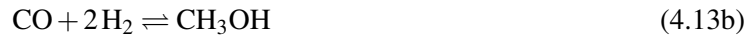
can take place: The synthesis reactions of methanol from carbon dioxide and carbon monoxide, as well as the reverse water-gas shift reaction. Therefore, the vector $\dot{\mathbf{n}}$ describing the molar flow rates in the process consists of five elements for each species

$$\dot{\mathbf{n}} = [\dot{n}_\alpha]_{\alpha \in \mathscr{S}}\,. \tag{4.14}$$

The numbering and nomenclature of all streams is defined in Fig. 4.8. With the fact that chemical reactions only take place in the chemical reactor, the molar amounts of substance are conserved in the rest of the process, the following relations can be derived from the mass balances in the process

$$\dot{\mathbf{n}}_1 = \dot{\mathbf{n}}_{\text{feed}} \tag{4.15a}$$

$$\dot{\mathbf{n}}_2 = \dot{\mathbf{n}}_1 + \dot{\mathbf{n}}_6 \tag{4.15b}$$

$$\dot{\mathbf{n}}_6 = (1 - \xi)\,\dot{\mathbf{n}}_4 \tag{4.15c}$$

$$\dot{\mathbf{n}}_{\text{prod}} = \dot{\mathbf{n}}_5 \tag{4.15d}$$

$$\dot{\mathbf{n}}_{\text{purge}} = \xi\,\dot{\mathbf{n}}_4 \tag{4.15e}$$

where ξ refers to the purge ratio and, consequently, $(1 - \xi)$ refers to the recycle ratio in this process. Beside of these mass balances that describe the flowsheet connectivity, some additional relationships has to be formulated in order to describe the thermodynamics of the reactor and the

separation unit, i. e.

$$F_{\text{react}}(\dot{\mathbf{n}}_2, \dot{\mathbf{n}}_3) = 0, \tag{4.16a}$$

$$F_{\text{sep}}(\dot{\mathbf{n}}_3, \dot{\mathbf{n}}_4, \dot{\mathbf{n}}_5) = 0. \tag{4.16b}$$

Note that F_{react} and F_{sep} are not necessarily represented by conventional algebraic expression, but also can incorporate an optimization problem or a differential equation. Therefore, the relations between the streams that are connected by the relations F_{react} and F_{sep} have to be solved iteratively by applying suitable numerical methods. In the given example, these relations describe the thermodynamic equilibrium conditions, which can be computed by a feasible approach such as the Gibbs energy minimization technique, a non-linear algebraic set of equations, or the dynamic method which was introduced in chapter 3 of this work.

In this section, the models of the reactor and the separation from sections 3.3.1 and 3.3.2 are connected by the mass balances, Eq. (4.15), to an overall process model.

While the thermodynamic model describing the vapour-liquid-equilibrium in the separation stage, section 3.3.2, applies the predictive Soave-Redlich-Kwong (PSRK) Equation of State, the reaction model in section 3.3.1 used the ideal gas law to describe the gaseous phase in the reactor.

For the sake of consistency, the reactor model is also extended here to apply the PSRK Equation of State. Therefore, the rate expressions r_ρ, Eq. (3.45), describing the two linear independent chemical reactions is extended by the fugacity coefficients ϕ_α to

$$r_1 = (x\phi)_{\text{CO2}} (x\phi)_{\text{H2}}^3 \left(\frac{P}{P^\circ}\right)^4 - \frac{(x\phi)_{\text{CH3OH}} (x\phi)_{\text{H2O}}}{K_{\text{eq},1}} \left(\frac{P}{P^\circ}\right)^2, \tag{4.17a}$$

$$r_2 = \left[(x\phi)_{\text{CO2}} (x\phi)_{\text{H2}} - \frac{(x\phi)_{\text{CO}} (x\phi)_{\text{H2}}}{K_{\text{eq},2}}\right] \left(\frac{P}{P^\circ}\right)^2. \tag{4.17b}$$

with $(x\phi)_\alpha = x_\alpha \phi_\alpha$ and the fugacity coefficients ϕ_α are computed from the PSRK Equation of State.

This process flowsheet was solved with an initial guess of the recycle stream of $\dot{\mathbf{n}}_6 = \mathbf{0}$ and the purge ratio was set to $\xi = 0.1$. As in the linear example in the previous section, a threshold for the error according to Eq. (4.11) was also set to $M = 10^{-6}$ and a maximum number of 100 iteration cycles was allowed. Therefore the value of 100 iterations in the following diagrams means that the given error threshold was not achieved within 100 iterations.

In the following calculations, the process conditions in the two units are set to $T_{\text{react}} = 450\,\text{K}$ and $P_{\text{react}} = 4\,\text{MPa}$ in the reactor and $T_{\text{sep}} = 300\,\text{K}$ and $P_{\text{sep}} = 0.5\,\text{MPa}$ in the separation unit. The feed stream is assumed to be in stoichiometric ratio $CO_2/H_2 = 1/3$.
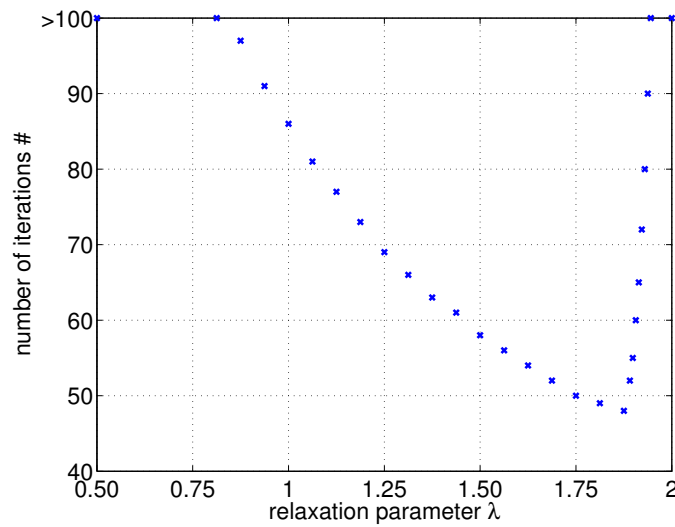
Figure 4.9: Number of iterations over the relaxation parameter λ.

4.2.2.1 Influence of the Relaxation Parameter

In order to investigate the efficiency of the different tearing methods, the method parameter λ was varied. The results in terms of number of iterations w.r.t. the relaxation parameter λ is shown in Fig. 4.9. While the direct substitution method ($\lambda = 1$) needs 86 iterations, the over-relaxation method with $\lambda = 1.875$ shows the fastest convergence for the given process simulation with 48 iteration cycles.

These simulations were performed on a system with the following configuration:

Hardware: Intel® Core™ Processor i3-560 (4 MiB Cache, 3.33 GHz), 4 GiB RAM.

Operating System: Microsoft Windows 7 Version 6.1 (Build 7601: Service Pack 1).

Software: MATLAB Version 7.12.0.635 (R2011a), Java 1.6.0_17-b04 with Sun Microsystems Inc. Java HotSpot™ 64-Bit Server VM mixed mode.

Here, an average CPU time per iteration of $t_{CPU} \approx 201 \text{ ms}$ was measured. This means an overall simulation time of approximately $10 \ldots 20 \text{ s}$, dependent on the choice of the relaxation parameter.

4.2.2.2 Influence of the Purge Ratio

In a further study, the relaxation parameter λ was fixed to $\lambda = 1.8$ while the purge ratio ξ — or the recycle ratio $(1 - \xi)$, respectively — was varied on the range $0.05 \leq \xi \leq 0.5$. The results in terms of the number of iterations over the purge ratio is depicted in Fig. 4.10. It can be seen that the number of iterations for larger purge streams, $\xi \geq 0.15$, is approximately constant at ≈ 30 iterations, while the numerical costs increase rapidly for small purge ratios, $\xi \leq 0.15$. Due to the fact, that large purge streams often correspond with large losses of valuable reactants, the
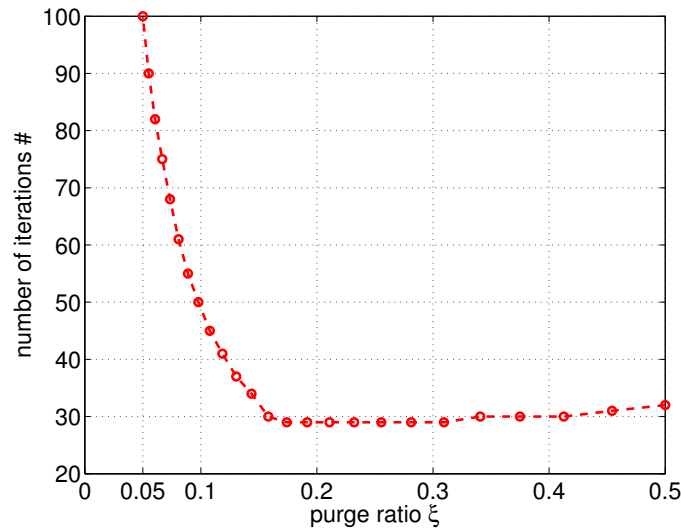
Figure 4.10: Number of iterations over the purge ratio ξ.

purge streams in technical applications are usually very small, e. g. $\xi \leq 0.01$. This may lead to high numerical costs. A simple strategy for handling such small purge streams is to start with a larger purge ratio, e. g. $\xi = 0.3$, and decrease it stepwise until the final value is reached during the iterations.

4.2.2.3   Simultaneous Influence of Relaxation Parameter and Purge Ratio

In this study, both parameters (λ, ξ) are varied on the region

$$\Omega = \{(\lambda, \xi) \,|\, 0.5 \leq \lambda \leq 2 \wedge 0.05 \leq \xi \leq 0.5\} \,. \tag{4.18}$$

The number of iterations which is required to meet the error threshold M as function of the relaxation parameter λ and the purge ratio ξ is shown in Fig. 4.11 as a three-dimensional surface plot (top) as well as a two-dimensional contour plot (bottom). Here, a minimum number of iteration cycles of only 10 cycles can be found at $(\lambda, \xi) \approx (1.3, 0.5)$. Additionally, for each purge ratio ξ, a range of optimal relaxation parameters $\lambda_{\mathrm{opt}} = f(\xi)$ can be identified. This range is depicted in Fig. 4.11 by the black regions. The width of this regions fluctuates with varying the purge ratio ξ. The reason for this fluctuation is the nature of the objective function: the number of iterations is always a natural number.

As mentioned above, one strategy for fast convergence of a process simulation with a small given purge ratio ξ is to start with a large purge ratio ξ and decrease it stepwise with each iteration. As we have seen in this case study, it could improve the efficiency additionally, when a fixed relaxation parameter λ is replaced by an adaptive relaxation parameter $\lambda_{\mathrm{opt}} = f(\xi)$.
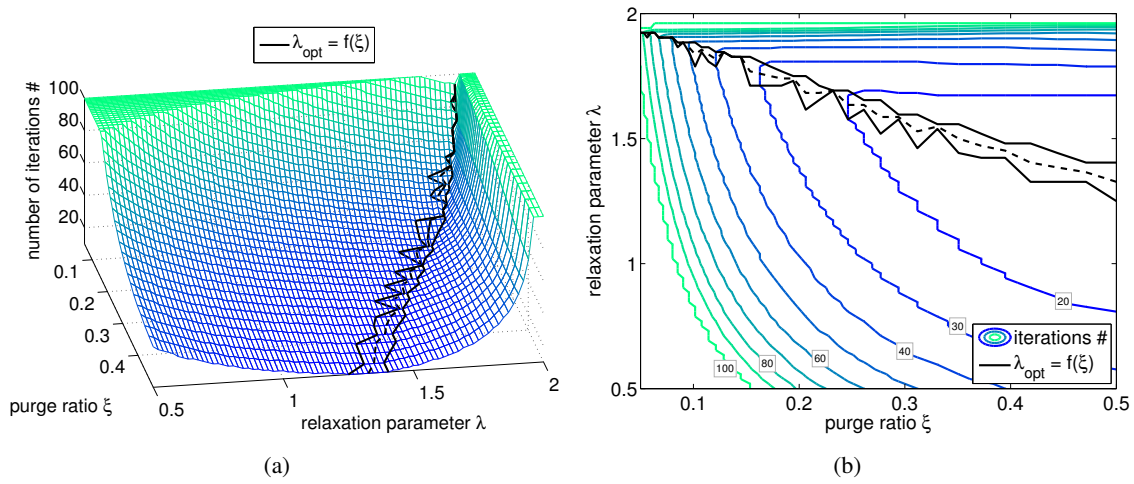
Figure 4.11: The number of iterations of the methanol synthesis process as a function of relaxation parameter λ and purge ratio ξ, displayed as a mesh grid plot (a) and a contour plot (b). Additionally, the black curves mark a range for an optimal relaxation parameter λ_{opt} as function of the purge ratio ξ.

4.2.2.4 Influence of the Initial Set-up of the Recycle Stream

In order to examine the influence of the initial set-up of the recycle stream, the simulation was performed with different initial values for the recycle stream $\dot{\mathbf{n}}_6^{(0)} = \left[\dot{n}_{6,\alpha}^{(0)}\right]$. The relaxation parameter as well as the purge ratio were fixed to $\lambda = 1.8$ and $\xi = 0.1$, respectively. The three initial set-ups

$$\dot{n}_{6,\alpha}^{(0)} = 0, \qquad \dot{n}_{6,\alpha}^{(0)} = |X|, \text{ and} \qquad \dot{n}_{6,\alpha}^{(0)} = \left|\dot{n}_{6,\alpha}^{\text{final}} + X\right| \qquad (4.19)$$

were tested. Here, X refers to a standard normally distributed random variable and $\dot{n}_{6,\alpha}^{\text{final}}$ refers to the molar streams in the steady state of the process. Note, that in general the steady state of the process is not known a priori. The numbers of iteration for each initial set-up is depicted in Fig. 4.12 as a function of the distance between the initial set-up and the final solution

$$d = \left\|\dot{\mathbf{n}}_6^{(0)} - \dot{\mathbf{n}}_6^{\text{final}}\right\|_2, \qquad (4.20)$$

where $\|\cdot\|_2$ refers to the Euclidean norm

$$\|\mathbf{x}\|_2 := \sqrt{\sum_{i=1}^{n} x_i^2}. \qquad (4.21)$$

It can be seen that the distance of the chosen initial value from the final value in steady state has no influence of the efficiency of the tearing method. Additionally, an initial value of simply zero (0) leads to a faster convergence to the steady state, ≈ 50 iterations, than a random initialization with approximately 65 to 80 iterations.
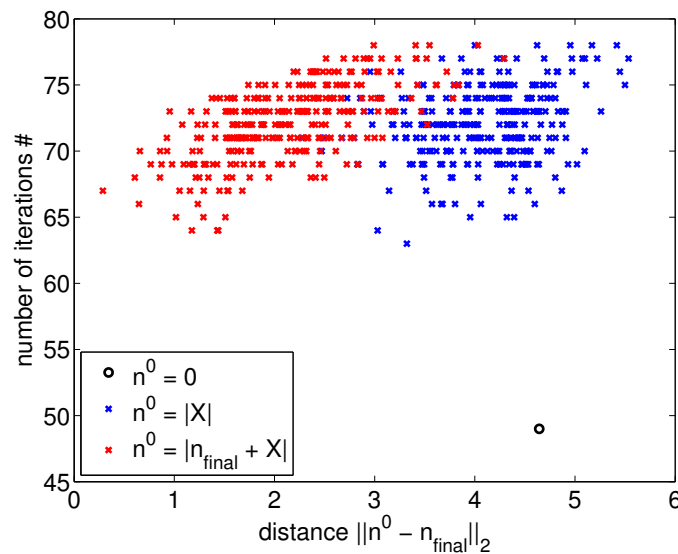
Figure 4.12: Number of iterations as a function of the initial set-up.

4.2.2.5 Summary

At the example of the given methanol synthesis process the properties of the tearing methods were investigated. These can be summarized as follows.

- Every process has an optimal relaxation parameter λ_{opt}.

- Small purge ratios ξ, i.e. high recycle ratios, lead to slow convergence speed.

- Technical relevant configurations have small purge ratios ξ. Therefore, strategies for efficient computation are required. Adaptive variations of ξ and λ through the iteration process are suggested.

- Initial values for the recycle stream of zero are a good choice. Random initial set-ups lead to lower convergence speed, also the distance to the final state has not necessarily an influence of the convergence properties.

- Simulation time is approximately $200\,\mathrm{ms}$ for one iteration and $10\ldots20\,\mathrm{s}$ for the overall process.

4.3 Simultaneous Dynamic Method

In the previous part of this chapter, in section 4.2, the so-called tearing methods were investigated. In the present section, the Dynamic Method which was introduced in chapter 3 is extended to a Simultaneous Dynamic Method (SDM). This approach enables the simultaneous computation of the thermodynamic equilibria in every unit within a process, i.e. the presented approach does not
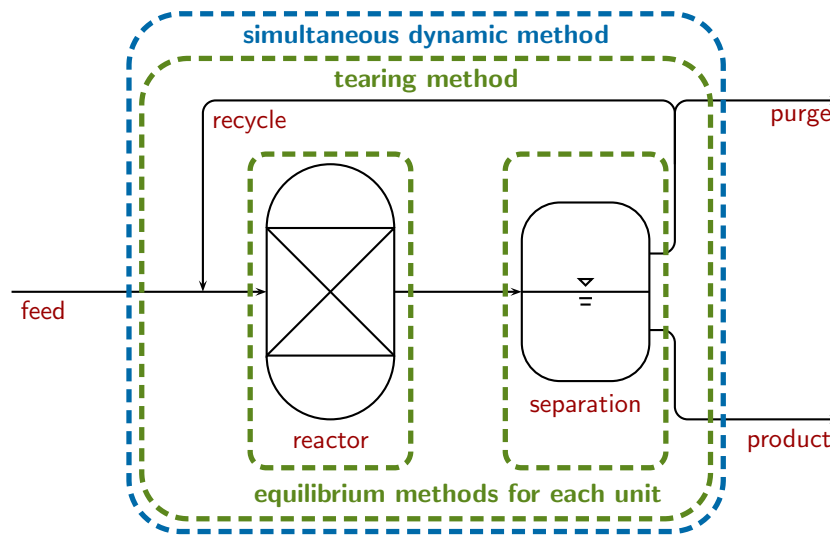
Figure 4.13: Simplified flowsheet of the methanol synthesis process and calculation procedures of the sequential approaches (green) and the Simultaneous Dynamic Method (blue).

require any iteration between the unit level and the process level. In this simultaneous approach, the mass balances of the overall process are always fulfilled implicitly. By elimination of the iteration between the unit level and the process level, it is shown in the following that the Simultaneous Dynamic Method is significantly more efficient than iterating any tearing methods throughout the process model.

A comparison of the different calculation procedures is depicted in Fig. 4.13 at the example of the methanol synthesis. The sequential tearing approach implements equilibrium models on the unit level and mass balance models on the process level which are connected with each other and require an iterative solution. A sequential approach has the advantage that the individual unit models can have an arbitrary mathematical structure, e. g. a Gibbs energy minimization model for the reactor and a set of algebraic equations for the vapour-liquid separation model. Nevertheless, in case of a simultaneous simulation approach it is recommended to use the same mathematical type of problem formulation in every unit model throughout the process. Hence, the unit models can easily combined to an overall process model and only the dimensionality of the overall mathematical model increases. The ODE based approach of the Dynamic Method is such a type of model formulation which can be applied to all types of thermodynamic equilibrium problems efficiently.

In an overall process simulation, the distinct unit models are connected by molar streams according to the process topology. Therefore, the thermodynamic view has to be shifted from a closed system to an open system. Hence, the model of a single unit $u \in \mathcal{U}$ is formulated using additional inlet and outlet streams beside of the sinks and sources due to chemical reactions and phase transitions

$$\frac{d\mathbf{n}^{(u)}}{d\tau} = \dot{\mathbf{n}}_{\text{in}} - \dot{\mathbf{n}}_{\text{out}} + \mathbf{A}^{(u)}\mathbf{r}^{(u)}.$$

(4.22)

In spatially lumped systems, the outlet $\dot{\mathbf{n}}_{\text{out}}$ composition is always considered as equal to the composition in the unit, i. e.

$$\dot{\mathbf{n}}_{\text{out}} = \frac{1}{\theta^{(u)}} \mathbf{n}^{(u)} \tag{4.23}$$

where $\theta^{(u)}$ refers to the residence time of the considered unit. In case of a multiphase unit such as a vapour-liquid separation unit there is a unique outlet stream for each phase of the unit, which sums up to the overall outlet stream

$$\dot{\mathbf{n}}_{\text{out}} = \sum_{\pi \in \mathscr{P}} \frac{1}{\theta^{(u)}} \dot{\mathbf{n}}^{\pi,(u)} . \tag{4.24}$$

The feed stream into a multiphase unit may be assigned to an arbitrary phase or it may distributed among the phases in a random split fraction. The assignment of the feed streams to a phase may have a small impact on the computational performance of the process simulation, but not on the steady state of the phase composition since we are only interested in the thermodynamic equilibrium and not on a dynamic behaviour of the system.

In the case of the Simultaneous Dynamic Method, we consider two types of dynamic behaviours:

- the dynamic evolution of the composition in each unit into the thermodynamic equilibrium subject to chemical reactions and phase transitions, and

- the dynamic evolution of the molar streams which are connecting the different units in the overall process flowsheet.

Technically, the thermodynamic equilibrium of a system is achieved by assuming an infinite residence time or infinite reaction volume. Practically, the Dynamic Method uses a long enough time span. Additionally, the Dynamic Method has the property that the time range can be adjusted by modifying the rate constants $k_{\alpha}^{\pi,\pi'}$ and k_{ρ}^{π}, respectively. In case of the Simultaneous Dynamic Method there are already immanent time constants in the system: the residence times of the individual units. Hence, the rate constants of the fluxes due to chemical reactions and phase transitions have to be chosen in a way, that the thermodynamic equilibria is reached much faster than the equilibration of the overall mass balances of the process.

In the following, the application of the Simultaneous Dynamic Method at the example of the methanol synthesis process is demonstrated.

4.3.1   Methanol Synthesis Process

The methanol synthesis from carbon dioxide and hydrogen was already simulated using the tearing methods in section 4.2.2. Here, this process is simulated applying the Simultaneous Dynamic Method. The process flowsheet and the numbering of the individual streams is shown in Fig. 4.14.
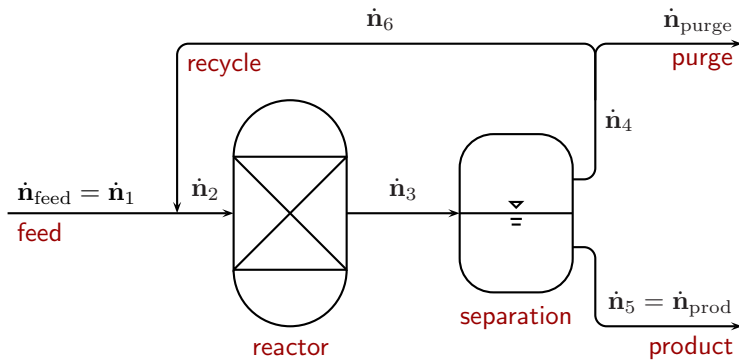
Figure 4.14: Flowsheet of the methanol synthesis process.

The simplified process consists of two process units, a reactor and a vapour-liquid-separation unit,

$$\mathscr{U} = \{\text{react}, \text{sep}\} \tag{4.25}$$

while the set of chemical compounds is constant for all phases in all units,

$$\mathscr{S} = \{CO_2, H_2, CH_3OH, H_2O, CO\} . \tag{4.26}$$

The phases that may occur in the different process units are unit-dependent. In the chemical reactor only the vapour phase is considered while in the separation unit both, a vapour phase as well as a liquid phase, may coexist,

$$\mathscr{P}^{(\text{react})} = \{V\} , \qquad\qquad \mathscr{P}^{(\text{sep})} = \{V, L\} . \tag{4.27}$$

This leads to an overall set of 15 dynamic states: the molar amounts of the five species in the reactor $\mathbf{n}^{(\text{react})}$ and the molar amounts in both phases in the separation unit, $\mathbf{n}^{V,(\text{sep})}$, and $\mathbf{n}^{L,(\text{sep})}$, respectively.

Since we are interested in the equilibrium compositions in the units, we can set the mean residence time of the units $\theta^{(u)}$ to an arbitrary value as long as the thermodynamic equilibration is much faster than the equilibration of the mass balances of the overall process. For the sake of simplicity, the mean residence times of all units in this process were set to unity, i. e. $\theta^{(u)} = \theta = 1\,\text{s}$. Therefore, the streams in this process are given by

$$\dot{\mathbf{n}}_1 = \dot{\mathbf{n}}_{\text{feed}} , \qquad\qquad \dot{\mathbf{n}}_2 = \dot{\mathbf{n}}_1 + \dot{\mathbf{n}}_6 , \tag{4.28a}$$

$$\dot{\mathbf{n}}_3 = \frac{1}{\theta}\,\mathbf{n}^{(\text{react})} , \qquad\qquad \dot{\mathbf{n}}_4 = \frac{1}{\theta}\,\mathbf{n}^{V,(\text{sep})} , \tag{4.28b}$$

$$\dot{\mathbf{n}}_5 = \frac{1}{\theta}\,\mathbf{n}^{L,(\text{sep})} , \qquad\qquad \dot{\mathbf{n}}_6 = (1 - \xi)\,\dot{\mathbf{n}}_4 , \tag{4.28c}$$

$$\dot{\mathbf{n}}_{\text{purge}} = \xi\,\dot{\mathbf{n}}_4 , \text{ and} \qquad\qquad \dot{\mathbf{n}}_{\text{prod}} = \dot{\mathbf{n}}_5 . \tag{4.28d}$$

With this information, the set of ordinary differential equations of the overall process simulation can be formulated as follows:

$$\frac{d\mathbf{n}^{(\text{react})}}{d\tau} = \dot{\mathbf{n}}_2 - \dot{\mathbf{n}}_3 + \mathbf{A}^{(\text{react})}\mathbf{r}^{(\text{react})} \tag{4.29a}$$

$$\frac{d\mathbf{n}^{\text{V,(sep)}}}{d\tau} = \dot{\mathbf{n}}_3 - \dot{\mathbf{n}}_4 + \mathbf{A}^{\text{V,(sep)}}\mathbf{r}^{(\text{sep})} \tag{4.29b}$$

$$\frac{d\mathbf{n}^{\text{L,(sep)}}}{d\tau} = \quad - \dot{\mathbf{n}}_5 + \mathbf{A}^{\text{L,(sep)}}\mathbf{r}^{(\text{sep})} \tag{4.29c}$$

Note, that the feed stream into the vapour-liquid separation unit is fully assigned to the vapour phase of the unit. This choice has no influence on the steady-state of the process as long as the thermodynamic equilibrium of the separation unit is reached.

The stoichiometric matrices of this process are given by

$$\mathbf{A}^{(\text{react})} = \begin{bmatrix} -1 & -1 \\ -3 & -1 \\ 1 & 0 \\ 1 & 1 \\ 0 & 1 \end{bmatrix}, \tag{4.30a}$$

$$\mathbf{A}^{\text{V,(sep)}} = \begin{bmatrix} -1 & & 0 \\ & \ddots & \\ 0 & & -1 \end{bmatrix}, \text{ and} \tag{4.30b}$$

$$\mathbf{A}^{\text{L,(sep)}} = \begin{bmatrix} 1 & & 0 \\ & \ddots & \\ 0 & & 1 \end{bmatrix}, \tag{4.30c}$$

respectively. The rate expressions for the reactor unit can be formulated by $\mathbf{r}^{(\text{react})} = [r_1, r_2]^\text{T}$ with

$$r_1 = (x\phi)_{\text{CO2}} (x\phi)_{\text{H2}}^3 \left(\frac{P}{P^\circ}\right)^4 - \frac{(x\phi)_{\text{CH3OH}} (x\phi)_{\text{H2O}}}{K_{\text{eq},1}} \left(\frac{P}{P^\circ}\right)^2, \text{ and} \tag{4.31a}$$

$$r_2 = \left[(x\phi)_{\text{CO2}} (x\phi)_{\text{H2}} - \frac{(x\phi)_{\text{CO}} (x\phi)_{\text{H2}}}{K_{\text{eq},2}}\right] \left(\frac{P}{P^\circ}\right)^2, \tag{4.31b}$$

while the rate expressions for the vapour-liquid separation unit can be written as $\mathbf{r}^{(\text{sep})} = [r_\alpha]$ with

$$r_\alpha = P\left((x\phi)_\alpha^\text{V} - (x\phi)_\alpha^\text{L}\right). \tag{4.32}$$

Here, the symbol $(x\phi)_\alpha^\pi$ abbreviates $(x\phi)_\alpha^\pi = x_\alpha^\pi \phi_\alpha^\pi$ and the fugacity coefficients are computed using the predictive Soave-Redlich-Kwong (PSRK) Equation of State (EoS).

The structural Jacobian matrix of the resulting ODE system has the structure

$$
\mathbf{J} = \begin{bmatrix}
\star & \cdots & \star & \star & & & & & & \\
\vdots & \ddots & \vdots & & \ddots & & & & & \\
\star & \cdots & \star & & & \star & & & & \\
\star & & & \star & \cdots & \star & \star & \cdots & \star \\
& \ddots & & \vdots & \ddots & \vdots & \vdots & \ddots & \vdots \\
& & \star & \star & \cdots & \star & \star & \cdots & \star \\
& & & \star & \cdots & \star & \star & \cdots & \star \\
& & & \vdots & \ddots & \vdots & \vdots & \ddots & \vdots \\
& & & \star & \cdots & \star & \star & \cdots & \star
\end{bmatrix}
\tag{4.33}
$$

where $\star$ refers to an non-zero value. A very strong coupling of the evolution equations can be seen at the square submatrices. The reason for this strong coupling are the highly non-linear thermodynamic models for the reactor and the vapour-liquid separation. The upper left 5×5 submatrix refers to the evolution equations of the chemical reactor while the lower right 10×10 submatrix arise from the two phases in the separation unit. Additionally, the interconnection of both units can be seen by the diagonal submatrices: The middle left diagonal submatrix is caused by the forward connection from the reactor to the vapour phase of the separation unit and the upper centre submatrix refers to the recycle loop of the remaining gases from the vapour-liquid separation back to the reactor.

In general, the structural Jacobian of the resulting equations of the Simultaneous Dynamic Method has the following structure:

- Every process units has a full square submatrix which is aligned at the diagonal of the entire Jacobian matrix. The size of this submatrix depends on the number of species and phases in the considered unit. In case of units with three or even more coexisting phases, this submatrix can also reduced as shown in Eq. (3.82) on page 50.

- Every stream between two units is represented in the Jacobian matrix by a diagonal submatrix whose position corresponds to its source unit and target unit. While the row of the submatrix in the entire Jacobian refers to the target unit of the stream and the column of the submatrix refers to the source unit of the stream.

- Feed streams into the process model are independent of the internal states of the process. Therefore, they have no influence on the structural Jacobian. Same holds for product streams of the overall process since they can be represented as a linear combination of the internal states.

Hence, a larger number of process units in an overall process leads to a smaller density of the Jacobian matrix of the resulting set of evolution equations. Therefore, the knowledge of the structural Jacobian is especially in case of large processes a valuable information in order to reduce

the computational expenses when integrating the resulting evolution equations, see also Coleman et al. (1984).

Similar to the tearing methods, the process conditions in the two units were set to $T_{\text{react}} = 450\,\text{K}$ and $P_{\text{react}} = 4\,\text{MPa}$ in the reactor and $T_{\text{sep}} = 300\,\text{K}$ and $P_{\text{sep}} = 0.5\,\text{MPa}$ in the separation unit. The feed stream was assumed to be in stoichiometric ratio $CO_2/H_2 = 1/3$.

In the following, the evolution equations are solved numerically, as well as

- the influence of the initial set-up of the evolution equations, and

- the influence of the purge ratio ξ

are analysed in detail.

4.3.1.1 Simulation of the Evolution Equations

The evolution equations of the methanol synthesis process were solved into their steady state using the following initial set-up:

- The feed stream is stoichiometric, i.e. $\dot{\mathbf{n}}_{\text{feed}} = [1,3,0,0,0]^{\text{T}}\,\text{mol}/\text{h}$.

- The initial guess of to outlet stream of the chemical reactor assumes a conversion of 50% of the feed stream towards the desired product, i.e. $\dot{\mathbf{n}}_3(\tau = 0) = \dot{\mathbf{n}}_{\text{react}}^0 = \frac{1}{2}[1,3,1,1,0]^{\text{T}}\,\text{mol}/\text{h}$.

- The initial guesses of the outlet streams of the separation unit assumes a perfect separation between the remaining gases (carbon dioxide and hydrogen) and the liquids (water and methanol), i.e. $\dot{\mathbf{n}}_4 = \dot{\mathbf{n}}_{\text{sep}}^{\text{V},0} = \frac{1}{2}[1,3,0,0,0]^{\text{T}}\,\text{mol}/\text{h}$ and $\dot{\mathbf{n}}_5 = \dot{\mathbf{n}}_{\text{sep}}^{\text{L},0} = \frac{1}{2}[0,0,1,1,0]^{\text{T}}\,\text{mol}/\text{h}$, respectively.

The resulting evolution equations were solved in MATLAB using the ODE solver `ode15s`. The evolution of the composition of the outlet stream of the reactor is shown in Fig. 4.15 while the evolution of the two outlet streams of the separation unit are depicted in Fig. 4.16 as well. Here, it can be seen, that the thermodynamics of each single unit equilibrates on a time scale of $10^{-10} < \tau < 10^{-6}$. The final stream composition due to the flowsheet connectivity, namely the recycle stream in this special case, equilibrates on the time range $10^{-2} < \tau < 10^3$. As we can see, the requirement of the Simultaneous Dynamic Method that the fluxes due to chemical reaction and phase transitions must be much faster than the fluxes between the units is fulfilled.

This simulation was performed on a system with the following configuration:

Hardware: Intel® Core™ Processor i7-4710MQ (6 MiB Cache, 2.5 GHz), 16 GiB RAM.

Operating System: Microsoft Windows 7 Version 6.1 (Build 7601: Service Pack 1).
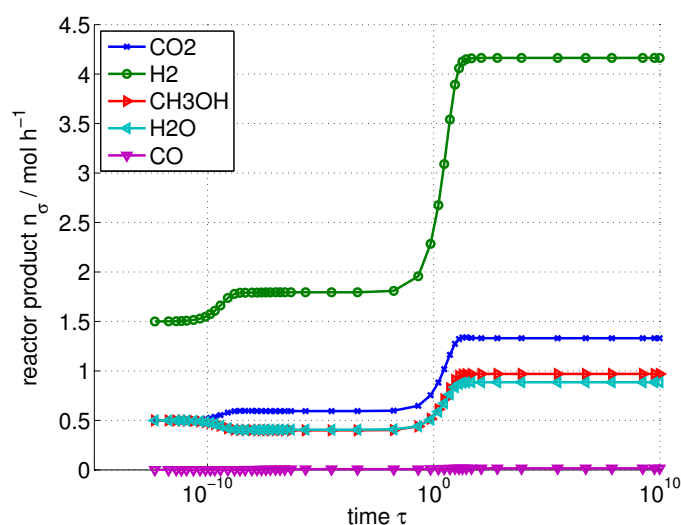
Figure 4.15: Evolution of the composition of the outlet stream of the chemical reactor w. r. t. time τ.

(a) vapour phase

(b) liquid phase
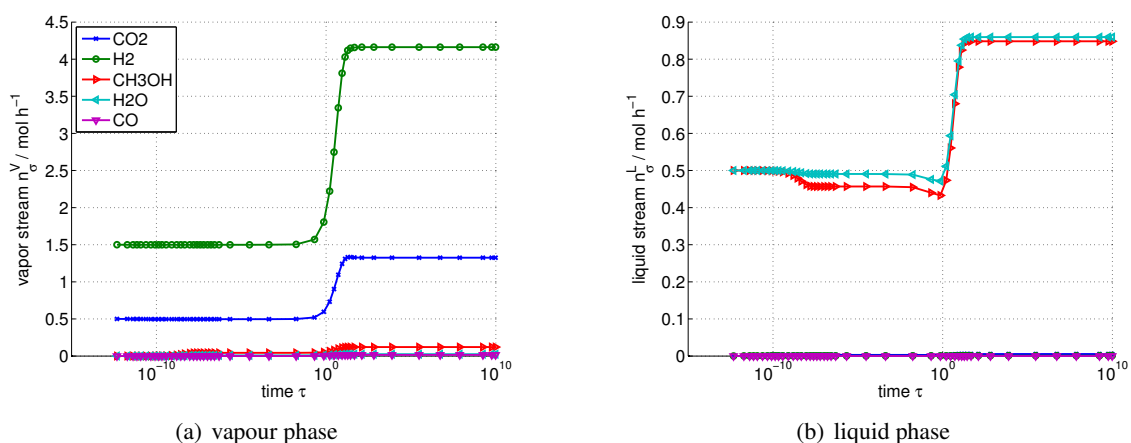
Figure 4.16: Evolution of the composition of the (a) vapour and (b) liquid outlet streams of the separation unit w. r. t. time τ.

Software: MATLAB Version 8.2.0.701 (R2013b), Java 1.7.0_11-b21 with Oracle Corporation Java HotSpot™ 64-Bit Server VM mixed mode.

In this configuration, a CPU time of 144 ms for the overall process simulation was measured. Note, that this value cannot be directly compared to the values form the case of the tearing methods with 201 ms per iteration and 10 . . . 20 s for the overall simulation due to a different hard- and software configuration on which the calculations are performed. Nevertheless, it indicates clearly that the overall CPU time in case of the Simultaneous Dynamic Method is in the same order of magnitude as the CPU time of a single iteration in the case of a tearing method. The computational performance of the two approaches on a consistent simulation environment is compared later in detail.
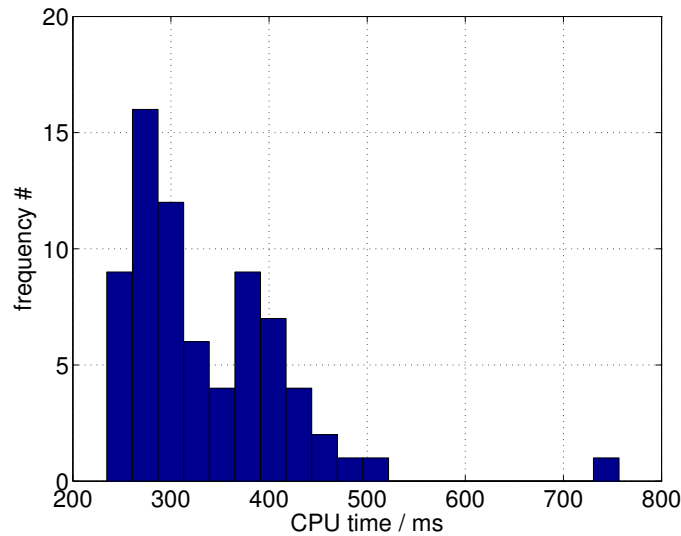
Figure 4.17: Histogram of the measured CPU times for different random initial conditions.

4.3.1.2 Variation of the Initial Condition

While the initial set-up of the simulation in the previous section 4.3.1.1 already contained knowledge of the process, namely an approximate conversion of the chemical reaction and the separation of the components among the phases, in this study the initial conditions of the resulting evolution equations are set randomly. Therefore, the initial conditions of the streams $s \in \{3,4,5\}$ was set to

$$\dot{n}_{s,\alpha}(\tau = 0) = |X|, \tag{4.34}$$

were X refers to a standard normally distributed random variable and the absolute value $|X|$ is used in order to avoid non-physical initial conditions. The CPU time was measured for 73 different random initial conditions. A histogram of the CPU times is depicted in Fig. 4.17. The average of the measured CPU times is 336 ms which is approximately two times higher than in the case of the process-based reasonable initial conditions. The evolution of the compositions in the three streams for a random initial set-up is showed exemplary in Fig. 4.18 for the chemical reactor outlet and in Fig. 4.19 for the outlet streams of the separation unit. A comparison of these evolutions with the graphs of the previous study, Fig. 4.15 and 4.16, shows that the equilibrium compositions are — of course — identical. Only the way how they are reached is a different one.

4.3.1.3 Influence of the Purge Ratio

The influence of the purge ratio ξ on the computational performance of the Simultaneous Dynamic Method was examined. Therefore, the purge ratio ξ was varied on the range $10^{-4} \leq \xi \leq 1/2$. The initial condition was chosen randomly, but kept constant for the different purge ratios. The required CPU times for the different purge ratios is shown in Fig. 4.20. It can be seen, that the influence of the purge ratio on the computational performance is very small. The average measured CPU time
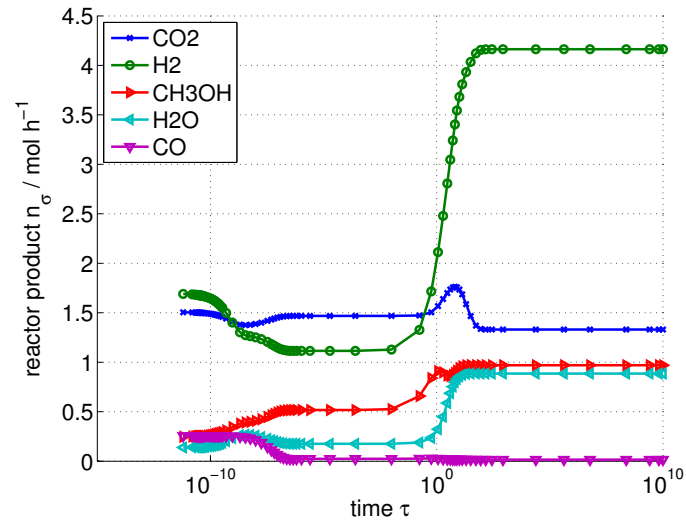
Figure 4.18: Evolution of the composition of the outlet stream of the chemical reactor w. r. t. time τ for a random initial set-up.

(a) vapour phase

(b) liquid phase
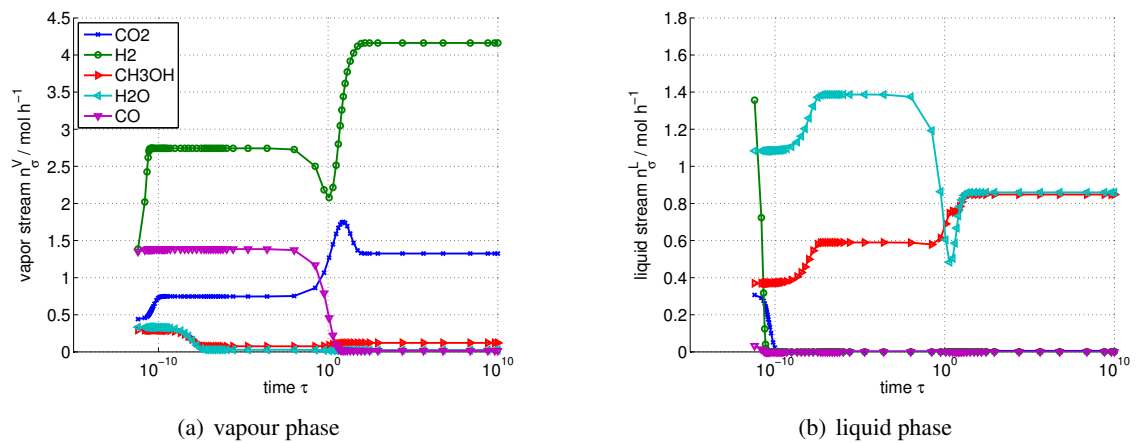
Figure 4.19: Evolution of the composition of the (a) vapour and (b) liquid outlet streams of the separation unit w. r. t. time τ for a random initial set-up.
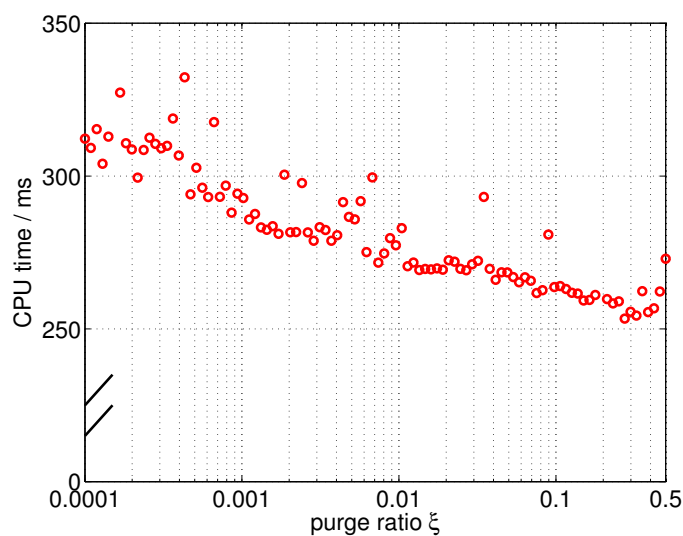
Figure 4.20: CPU times for different purge ratios ξ.

was 282 ms. Note, that the tearing methods were already infeasible for purge ratios of $\xi < 0.05$.

4.4   Comparison and Summary

In this chapter, conventional approaches for process simulation, the so-called tearing methods, were introduced and illustrated at the example of the methanol synthesis process. After that, the Dynamic Method which was introduced in chapter 3 was extended to a Simultaneous Dynamic Method. The assets of this new approach compared to the iterative tearing methods were also shown on the example of the methanol synthesis process.

The computational performances of the different approaches were compared against each other on a system using the following configuration:

Hardware: Intel® Pentium® Processor E5400 (2 MiB Cache, 2.70 GHz), 3.0 GiB RAM.

Operating System: Ubuntu 10.04.1 LTS, Linux Kernel 2.6.32-24-generic-pae, GNOME 2.30.2.

Software: MATLAB 7.14.0.739 (R2012a), Java 1.6.0 17-b04 with Sun Microsystems Inc. Java HotSpot™ Client VM mixed mode.

A comparison of the computational costs of two tearing methods as well as the Simultaneous Dynamic Method is summarized in Tab. 4.1. The initial set-up of the Simultaneous Dynamic Method was set the process-based reasonable initial conditions as described on p. 82. A random initial set-up would increase the CPU time of the Simultaneous Dynamic Method to approximately 1000 ms. Nevertheless, it can be clearly seen, that the Simultaneous Dynamic Method is able to speed up the computational performance in terms of CPU time by a factor of 20 to 100, depending on the set-up of the competing approaches.

Table 4.1: Computational performances of two tearing methods and the Simultaneous Dynamic Method.

Method	Direct Substitution	Over- Relaxation	Simultaneous Dynamic Method
λ	1	1.8	—
Iterations	85	48	1
Time/Iteration	$\approx 400\,\text{ms}$		$\approx 400\,\text{ms}$
CPU time	34 s	19 s	0.4 s

Process Optimization

A Dynamic Method for computing thermodynamic equilibrium problems was introduced in chapter 3. This approach is based on the relaxation of the isofugacity conditions as a set of ODEs, while the isofugacity condition results from the necessary optimality condition of the Gibbs minimization problem. In chapter 4, this approach is extended to the Simultaneous Dynamic Method, which formulates the ODEs for each process unit and connects them according to the flowsheet connectivity of the overall process. The Simultaneous Dynamic Method solves the molar compositions in all streams within the process flowsheet for a given set of process parameters such as

- pressures $P^{(u)}$ and

- temperatures $T^{(u)}$ for each unit $u \in \mathscr{U}$, or

- other process-related parameters, e. g. the recycle ratio ξ.

An important task in process engineering is the identification of an optimal set of the process parameters $\mathbf{p}$ for a given objective function F, e. g.

- the electrical energy demand,

- the heating or cooling duty within the process units,

- the operating costs of the process, which include the costs for energy supply, reactants, or disposal of possible side-products.

In order to identify an optimal set of process parameters $\mathbf{p}$ the following optimization problem has to be solved:

$$\min_{\mathbf{p}} F(\mathbf{p}, \mathbf{n}_{\text{eq}}) \tag{5.1a}$$

subject to

$$\mathbf{g}(\mathbf{p}, \mathbf{n}_{\text{eq}}) = \mathbf{0} \qquad\qquad \text{equality constraints,} \tag{5.1b}$$

$$\mathbf{h}(\mathbf{p}, \mathbf{n}_{\text{eq}}) \leq \mathbf{0} \qquad\qquad \text{inequality constraints,} \tag{5.1c}$$

and the equilibrium composition $\mathbf{n}_{\text{eq}}$ according to the Simultaneous Dynamic Method

$$\frac{d\mathbf{n}}{d\tau} = \mathbf{Ar} + \mathbf{Bn} \qquad\qquad \mathbf{n}(\tau = 0) = \mathbf{n}_0 \qquad\qquad \mathbf{n}(\tau \to \infty) = \mathbf{n}_{\text{eq}}. \tag{5.1d}$$

In the formulation (5.1d) of the SDM the term $\mathbf{Ar}$ refers to the fluxes due to the thermodynamic behaviour in each unit, while the term $\mathbf{Bn}$ refers to the mass flows between the different process units. In order to solve the optimization problem (5.1) a large variety of algorithms of different complexity is available. Optimization methods can be divided into local and global optimization methods. Local optimization methods use only local informations of the objective function such as function value, Jacobian matrix, or the Hessian matrix. Dependent on the initial value of the parameter set, it is possible to find different local optima. Hence, a local optimization algorithm is not able to determine whether a optimum is also a global optimum. Examples for such algorithms are

- the downhill simplex method which uses only the function value as information,

- gradient-based methods which use also the derivative of the objective, i. e. the Jacobian matrix as information, and

- Newton methods which makes also use of the second derivative of the objective, i. e. the Hessian matrix.

In the case that in the optimization does not occur any equality or inequality constraint, a set of such methods is already provided by MATLAB, e. g. the simplex method is implemented in the `fminsearch` function, or some gradient-based and quasi-Newton methods are part of the the `fminunc` function of MATLABs Optimization Toolbox. In the more general case of a constraint optimization, MATLAB provides some suitable algorithms with the `fmincon` function.

Contrary to the class of local optimization algorithms, a global optimization algorithm incorporates a non-deterministic, random element which increases the probability of finding the global optimum. Examples for such algorithms are genetic algorithms or simulated annealing. MATLAB implementations of such algorithms are provided by the Global Optimization Toolbox.
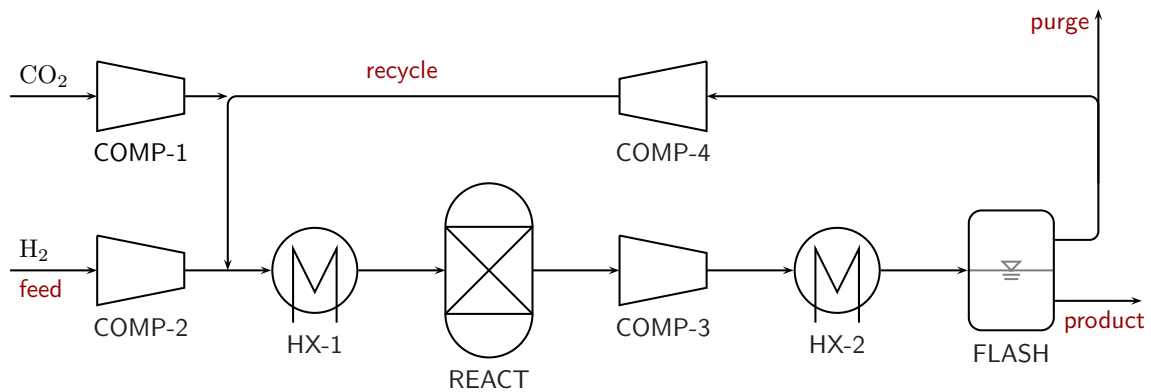
Figure 5.1: Flowsheet of the methanol synthesis process.

5.1   Energetic Optimization of the Methanol Synthesis Process

In section 4.3.1, the methanol synthesis process from carbon dioxide and hydrogen was simulated by use of the Simultaneous Dynamic Method. This process is now used as an example process for demonstrating the Simultaneous Dynamic Method in the context of process optimization. The set of compounds that may occur in the methanol synthesis process is given by

$$\mathscr{S} = \{CO_2, H_2, CH_3OH, H_2O, CO\}\,, \tag{5.2}$$

and the chemical reactions in the reactor unit are the synthesis reaction from carbon dioxide and carbon monoxide, as well as the reverse water-gas shift reaction,

$$CO_2 + 3\,H_2 \rightleftharpoons CH_3OH + H_2O\,, \tag{5.3a}$$

$$CO + 2\,H_2 \rightleftharpoons CH_3OH\,, \tag{5.3b}$$

$$CO_2 +\ \ H_2 \rightleftharpoons CO + H_2O\,. \tag{5.3c}$$

Since the extent of reaction to the desired product methanol is approximately 50% a recycling of the remaining reactants has to be performed after the product removal via a vapour-liquid separation unit. A flowsheet of this process including compression stages and heat exchangers is shown in Fig. 5.1.

From a purely thermodynamic point of view the synthesis reaction yields to the best results for low temperatures and high pressures. However, for low temperatures the feasibility is limited by the kinetics of the reaction while for high pressures the energy demand is a limiting factor. Therefore, in the subsequent process optimization the pressure levels in the reactor and in the vapour-liquid separation unit are optimized with respect to the energy demand of the process, while the temperature levels are kept constant.

In the reactor, a temperature of $T_{\text{react}} = 450\,\text{K}$ was assumed and the flash separation was carried out at a temperature of $T_{\text{sep}} = 300\,\text{K}$. The feed streams of the reactants carbon dioxide and hydrogen was assumed to be delivered at $T_{\text{feed}} = 300\,\text{K}$ and $P_{\text{feed}} = 0.5\,\text{MPa}$.

In a first study, the energy demands of the process in terms of

- electrical energy,

- heating duty, and

- cooling duty

are regarded. After that, the energy demands are combined to an objective function for the utility costs which combines the single energy demands. The objective function in case of the electrical energy demand of the process consists of the four compression stages, i. e.

$$F_{\text{el}} = \sum_{i=1}^{4} \dot{n}_i R T_{\text{in},i} \frac{\kappa}{\kappa - 1} \left[\left(\frac{P_{\text{out},i}}{P_{\text{in},i}} \right)^{\frac{\kappa-1}{\kappa}} - 1 \right] \frac{1}{\eta} . \tag{5.4}$$

Here, the heat capacity ratio was set to $\kappa = 1.4$ and as isentropic efficiency of $\eta = 0.72$ was assumed. In the case of a decrease in the pressure the unit was modelled as a turbine and the generation of electrical energy was considered analogously.

The thermal energy demands of the heat exchangers are given by

$$\dot{Q}_{\text{h}i} = \sum_{\alpha} \dot{n}_\alpha \left[h_\alpha \left(T_{\text{out},i} \right) - h_\alpha \left(T_{\text{in},i} \right) \right] \quad \forall i \in \{1, 2\}, \tag{5.5a}$$

the cooling demand in the isothermal reactor is

$$\dot{Q}_{\text{r}} = \sum_{\alpha} \left[\dot{n}_{\alpha,\text{out}} - \dot{n}_{\alpha,\text{in}} \right] h_\alpha \left(T_{\text{r}} \right) , \tag{5.5b}$$

and the cooling demand for the condensation of the formed methanol and water is given by

$$\dot{Q}_{\text{f}} = \sum_{\substack{\alpha \in \{\text{H}_2\text{O} \\ \text{MeOH}\}}} \dot{n}_\alpha \Delta_{\text{vap}} h_\alpha . \tag{5.5c}$$

The values of positive energy demands are assigned to the heating duty while the negative values are assigned to the cooling duty of the overall process according to

$$F_{\text{heat}} = \sum_{u \in \{\text{h1,h2,r,f}\}} R \left(\dot{Q}_u \right) , \tag{5.6}$$

$$F_{\text{cool}} = \sum_{u \in \{\text{h1,h2,r,f}\}} R \left(-\dot{Q}_u \right) \tag{5.7}$$

where $R(x) \equiv x H(x)$ is the ramp function and $H(x)$ is the Heaviside step function.
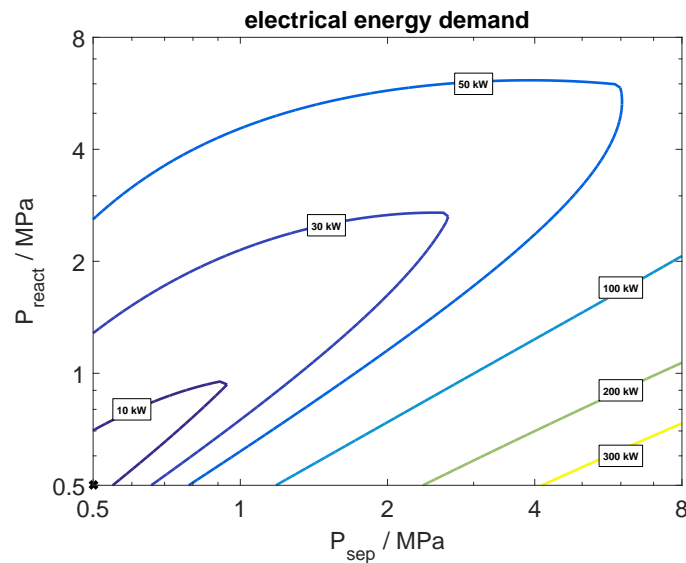
Figure 5.2: Electrical energy demand of the methanol synthesis process as function of the operating pressures.

The behaviour of the gas phase in the reaction unit, as well as in the vapour-liquid separation unit was predicted using the predictive Soave-Redlich-Kwong Equation of State, see also section 2.8.

In order to identify optimal process conditions in terms of the energy demand of the process the pressure in the reactor P_{react} and in the separation unit P_{sep} are varied on the range

$$0.5\,\text{MPa} \leq P_{react} \leq 8\,\text{MPa}, \tag{5.8a}$$

$$0.5\,\text{MPa} \leq P_{sep} \leq 8\,\text{MPa}. \tag{5.8b}$$

Additionally, the optimal process conditions can easily obtained by the simplex method which is implemented in MATLABs `fminsearch` function. In this unconstrained optimization it is ensured that the pressure ranges are not violated by adding quadratic penalty functions to the objective function.

The electrical energy demand of the process as function of the operating pressures is shown in Fig. 5.2. It can be seen that the optimal process condition in terms of the electrical energy demand is at the constant pressure level of the feed streams, i.e. $P_{react} = P_{sep} = P_{feed} = 0.5\,\text{MPa}$ where the energy demand is zero since no compressor work has to be done. However, it should be noted that the extent of reaction at this point is fairly low and large amounts of unreacted gas has to be recycled.

The heating duty as function of the process pressures is given in Fig. 5.3. For reactor pressures $P_{react} > 2\,\text{MPa}$ there is a region where actually no heating power in the overall process is required.

Since the methanol synthesis is a strongly exothermic reaction, large amounts of cooling energy is required which is depicted in Fig. 5.4 as function of the process pressures. The optimal point in
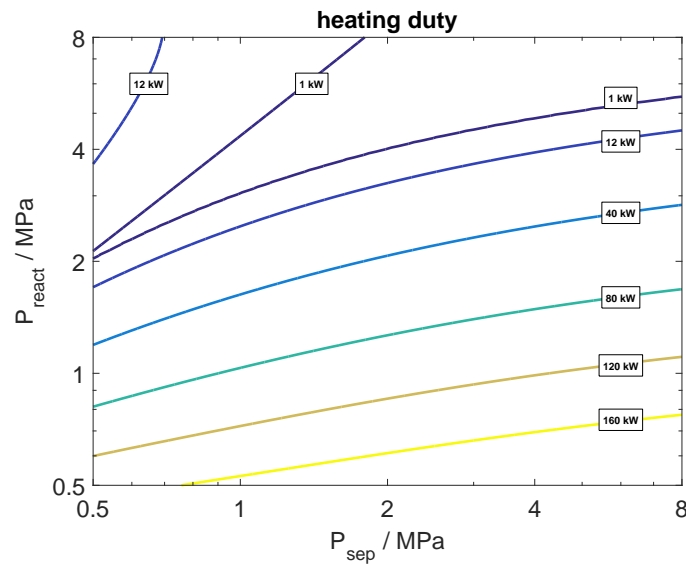
Figure 5.3: Heating duty of the methanol synthesis process as function of the operating pressures.

terms of the cooling duty can be found at $P_{react} = 2.07\,\text{MPa}$ and $P_{sep} = 0.5\,\text{MPa}$ where the required cooling energy is $F_{cool} = 91.3\,\text{kW}$.

These three different types of energy demands of the process can be combined to a cost function

$$F_{costs} = c_{el}F_{el} + c_{heat}F_{heat} + c_{cool}F_{cool}. \tag{5.9}$$

The specific costs for the different energies are chosen according to Peters et al. (2003) as follows. The costs for the electricity are set to $c_{el} = 0.04\,\$/\text{kWh}$. The heating demand is realised using low-pressure steam at 790 kPa with assumed costs of 7.5 $/1000 kg which corresponds to $c_{heat} = 0.0145\,\$/\text{kWh}$. Costs for the cooling water are set to 0.22 $/m^3 which corresponds to specific costs of the cooling duty of $c_{cool} = 0.0069\,\$/\text{kWh}$. Additionally, a yearly runtime of the plant is assumed to be 8200 h/yr. With this information the yearly costs for the utilities can be estimated as function of the process pressures, see also Fig. 5.5. An optimal parameter set in terms of the utility costs can be identified at $P_{react} = 2.02\,\text{MPa}$ and $P_{sep} = 0.85\,\text{MPa}$. The yearly utility costs of the methanol plant at this point are given by $F_{costs} = 18\,700\,\$/\text{yr}$.
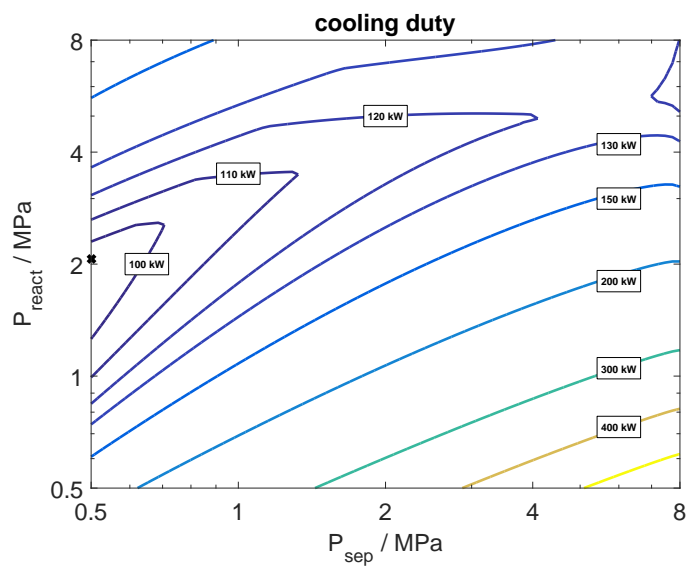
Figure 5.4: Cooling duty of the methanol synthesis process as function of the opertaing pressures.
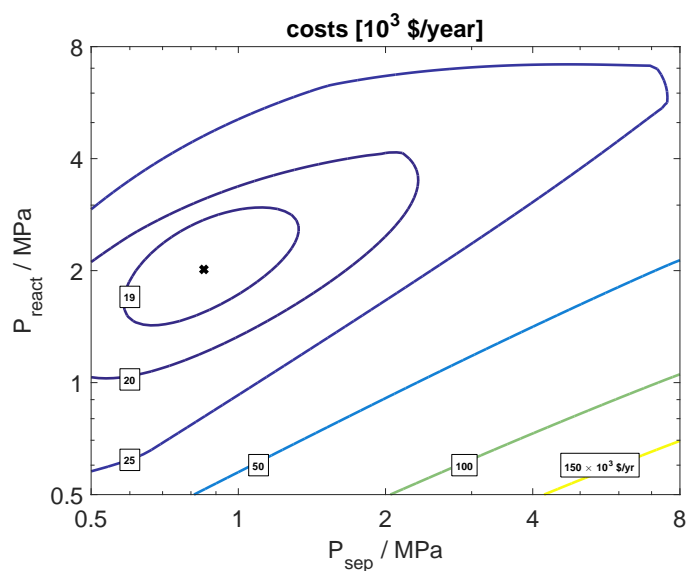
Figure 5.5: Utility costs of the methanol synthesis process as function of the operating pressures.

Summary & Outlook

6.1 Summary

In this work, a methodological framework for thermodynamic equilibrium calculations in process simulation and optimization was derived and applied to several examples. This framework is based on the dynamic evolution of a set of ordinary differential equations from an initial point towards the thermodynamic equilibrium.

The Dynamic Method (DM) was derived in chapter 3 and is able to solve chemical equilibria and phase equilibria as well as simultaneous chemical and phase equilibria. This method is physically motivated by the fluxes between two distinct phases and the fluxes due to chemical reactions. It is based on a set of ODEs which satisfies the equilibrium condition in its steady state. The feasibility of the DM was exemplified at five examples of different type and complexity. For the case of chemical equilibria it was compared with the conventional Gibbs energy minimization technique. It was shown that it can compete with conventional approaches in terms of computational efficiency. Additionally, an eigenvalue analysis of this example is performed and the influence of the solution algorithm of the ODE solver is examined. It is shown that the DM leads to stiff ODE systems and therefore, implicit algorithms for the solution of the ODE system have to be applied. For systems that exhibit equilibrium constants with different orders of magnitude, it is shown how the rate expressions can be normalized for further improvement of the computational complexity. For the example of the vapour-liquid-liquid equilibrium of the Fischer-Tropsch products the applicability of the DM on systems with three different phases is shown. Additionally, this example is employed to derive an approach for the reduction of the complexity of the ODE system of the DM for systems with more than two distinct phases.

Some more example calculations concerning reactive multiphase systems are performed in Zinser and Sundmacher (2016). For the sake of clarity, these examples were not discussed in this thesis. Additionally, there one can find a comparison of the DM with the direct solution of the algebraic equilibrium conditions at the example of phase equilibrium calculations.

Since the DM was only applied to vapour and liquid systems, this method can also be applied on solid phases, such as solid-liquid-equilibrium problems, if a suitable activity coefficient model for the solid phase is available.

The DM was extended to the Simultaneous Dynamic Method (SDM) in chapter 4. Here, the class of tearing methods was introduced as a reference approach. These methods require an expensive iterative procedure and exhibit slow convergence for processes featuring high recycle ratios. The SDM is formulated in a way that solves all equilibria in the distinct process units simultaneously and fulfils the mass balances of the streams implicitly. Therefore, no iterative solution strategy between the process units and the overall process model is required. The proposed methods are applied on the methanol synthesis process. It is shown that the SDM is significantly more efficient than the conventional strategy. Additionally, it is shown that the efficiency of the SDM is nearly invariant regarding the size of the recycle ratio which is another clear advantage compared to tearing methods.

In chapter 5 an energetic analysis and optimization of the methanol synthesis process which was introduced in chapter 4 is performed. Therefore the pressure levels in the process are varied in order to identify an optimal set of process parameters w. r. t. the energy demand and the utility costs.

Some further ideas towards a methodology that combines the process simulation and the process optimization in a single calculation step are presented in Zinser et al. (2017).

An additional strategy for energetic process optimization was proposed by Zinser et al. (2012). This strategy is based on the optimization of the energy demand of a process by the use of additional heat exchangers and compression stages in a process. Since this methodology does not touch the scope of the dynamic methods, it is not discussed within this thesis.

6.2 Outlook

In this thesis, a framework of dynamic methods was developed which is able to solve a bunch of engineering tasks in the area of process simulation and process optimization. Nevertheless, there are still some open points for further development of the presented methods.

The ODE solvers that were used to solve the evolution equations are not able to detect the steady state behaviour of the system. This problem is overcome in this work by the use of "sufficiently long" integration intervals. A routine for automatic steady state detection in the ODE solver could avoid too short or unnecessary long integration intervals.

The DM is not able to simulate distillation columns. The reason is, that the temperatures on each column stage are not known *a priori*. One possibility for overcoming this problem is to compute the temperatures on each stage numerically in each integration step of the DM. Nevertheless, this would lead to an expensive iterative procedure and generates unwanted numerical noise on the r. h. s. of the evolution equations of the DM. A second possibility would be to extend the DM by the introduction of additional evolution equations which describe also the temperatures on each stage besides the composition.

The DM is not a rigorous method. In case of phase equilibrium calculations a bad initial guess could lead to the trivial solution $x_\alpha^\pi = x_\alpha^{\pi'}$ which also fulfils the equilibrium condition $x_\alpha^\pi \gamma_\alpha^\pi = x_\alpha^{\pi'} \gamma_\alpha^{\pi'}$ of a liquid-liquid system but only describes one phase. Hence the results have to be verified, especially when one of the phases disappears, and a good initial set-up of the system should be used.

Since a cubic Equation of State can have one or three real solutions it describes either the vapour phase or the liquid phase or both phases of a mixture. Therefore, when applying the DM one has to make sure that the trajectory from the initial composition towards the equilibrium composition stays completely in the region where the equation of state provides informations for both phases, i. e. the vapour as well as the liquid phase.

When a process cannot attain the thermodynamic equilibrium or when the desired product is thermodynamically not favoured but only an intermediate product in the reactor, this problem can easily be overcome via the formulation of the dynamic method. In this case the thermodynamic model can be extended to a kinetic model by inserting a kinetic prefactor in the rate expressions. In case of the SDM, the mean residence time of the process unit has to be provided additionally.

And finally, a generalized implementation of the dynamic methods, which are completely independent of the considered thermodynamic system or the considered process, could become a powerful tool for process systems engineering.

Thermodynamic Methods, Derivations and Parameters

A.1 Derivation of the Parameters Ω_a and Ω_b for the Peng-Robinson Equation of State

We start with the Peng-Robinson equation of state

$$P = \frac{RT}{v-b} - \frac{a\alpha}{v(v+b)+b(v-b)} \tag{A.1}$$

and apply the two conditions that have to be fulfilled at the critical point (T_c, P_c)

$$\left.\frac{\partial P}{\partial v}\right|_{T_c} = 0 \tag{A.2a}$$

$$\text{and} \quad \left.\frac{\partial^2 P}{\partial v^2}\right|_{T_c} = 0. \tag{A.2b}$$

Note, that the α-function is constructed in a way, that it cancels out at the critical temperature T_c, i. e. $\alpha(T = T_c) = 1$. Additionally, the thermodynamic state in terms of temperature T, pressure P and volume v refers to the corresponding critical properties in the following equations. For a better readability, the subscripts are omitted in this derivation, i. e. $T \equiv T_c$, $P \equiv P_c$ and $v \equiv v_c$. Solving the first condition, Eq. (A.2a), for a yields to

$$a = \frac{RT\left(v^2 + 2bv - b^2\right)^2}{2\left(v-b\right)^2\left(v+b\right)}. \tag{A.3a}$$

Doing the same with the second condition, Eq. (A.2b), yields to

$$a = \frac{RT \left(v^2 + 2bv - b^2\right)^3}{\left(v - b\right)^3 \left(3v^2 + 6bv + 5b^2\right)} \,. \tag{A.3b}$$

Equalising Eq. (A.3a) and Eq. (A.3b) gives

$$\frac{1}{2\left(v + b\right)} = \frac{\left(v^2 + 2bv - b^2\right)}{\left(v - b\right)\left(3v^2 + 6bv + 5b^2\right)} \,, \tag{A.4}$$

which is a cubic polynomial in b and can be solved to

$$b = \frac{1}{3}\left[K - \frac{2}{K} - 1\right] v \tag{A.5}$$

with

$$K = \sqrt[3]{8 + 6\sqrt{2}}. \tag{A.6}$$

Applying the result for b, Eq. (A.5), on Eq. (A.3a) gives an expression for the parameter a

$$a = \frac{1}{96}\left[\left(95 - 60\sqrt{2}\right)K^2 - \left(20 - 45\sqrt{2}\right)K - 34\right] vRT \,. \tag{A.7}$$

With Eq. (A.5) and Eq. (A.7), we have already expressions for the EoS parameter a and b in terms of the critical volume $v \equiv v_{\mathrm{c}}$ and the critical temperature $T \equiv T_{\mathrm{c}}$. Nevertheless, in most practical cases, they are computed from $(T_{\mathrm{c}}, P_{\mathrm{c}})$, see also Gmehling et al. (2012, p. 45). Therefore, we apply the results from Eq. (A.5) and Eq. (A.7) on the original EoS, Eq. (A.1), and solve it for the critical volume v, which leads to

$$v = \frac{1}{64}\left[-\left(5 - 4\sqrt{2}\right)K^2 - \left(4 - \sqrt{2}\right)K + 22\right]\frac{RT}{P} \,. \tag{A.8}$$

This leads to the EoS parameter

$$a = \Omega_a \frac{R^2 T_{\mathrm{c}}^2}{P_{\mathrm{c}}} \,, \qquad\qquad b = \Omega_b \frac{RT_{\mathrm{c}}}{P_{\mathrm{c}}} \,, \tag{A.9}$$

with the coefficients

$$\Omega_a = \frac{1}{1024}\left[\left(405 - 276\sqrt{2}\right)K^2 + \left(36 + 111\sqrt{2}\right)K - 118\right] \,. \tag{A.10}$$

$$\Omega_b = \frac{1}{64}\left[\left(15 - 12\sqrt{2}\right)K^2 + \left(12 - 3\sqrt{2}\right)K - 2\right] \,. \tag{A.11}$$

A.2 Correlations for the Heat Capacity c_p

A very fundamental thermodynamic property of a pure substance is its ideal gas heat capacity

$$c_p := \left(\frac{\partial h}{\partial T} \right)_{P=\text{const.}} \tag{A.12}$$

which depends on the temperature T of the system.

In literature, those temperature-dependent values are mostly given by a set of parameter $\{p_i\}$ and a functional expression f, such that $f : (T, \{p_i\}) \mapsto c_p(T)$. A common representation of the heat capacity is the polynomial

$$c_p(T) = p_1 + p_2 T + p_3 T^2 + p_4 T^3 + p_5 T^4 \tag{A.13}$$

or the Shomate equation which also accounts for a reciprocal term

$$c_p(T) = p_1 + p_2 T + p_3 T^2 + p_4 T^3 + \frac{p_5}{T^2} \tag{A.14}$$

which differs only in the last term from the polynomial representation.

Another correlation, which is derived from statistical mechanics, was proposed by Aly and Lee (1981) and is given by

$$c_p = p_1 + p_2 \left(\frac{p_3/T}{\sinh(p_3/T)} \right)^2 + p_4 \left(\frac{p_5/T}{\sinh(p_5/T)} \right)^2 \tag{A.15}$$
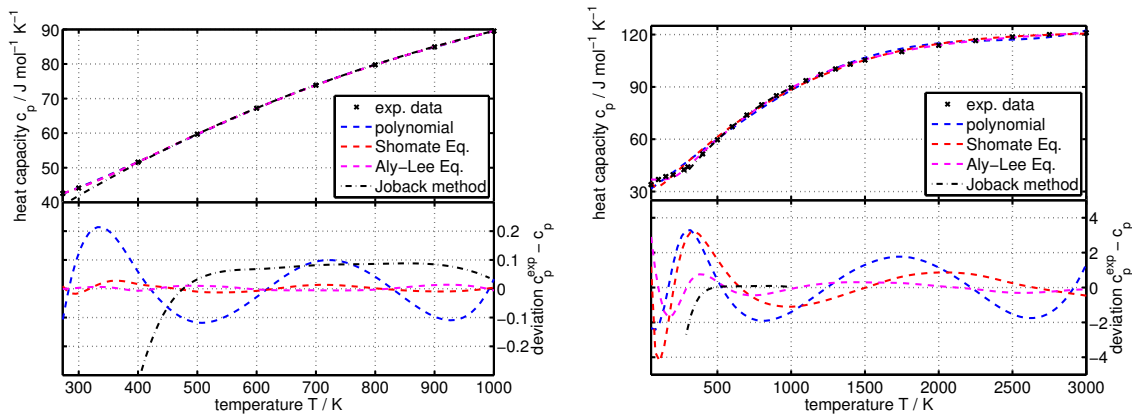
Figure A.1: Heat capacities as a function of the temperature.

A.3   Lee-Kesler Method

The method of Lee and Kesler (1975) is a three-parameter corresponding states correlation for the vapour pressure P^{vap} which is based on critical data $(T_{\mathrm{c}}, P_{\mathrm{c}})$ and the acentric factor ω and can be given by

$$\ln P_{\mathrm{r}}^{\mathrm{vap}} = f_1 + \omega f_2 \tag{A.16}$$

$$f_1 = 5.92714 - \frac{6.09648}{T_{\mathrm{r}}} - 1.28862 \ln T_{\mathrm{r}} + 0.169347 T_{\mathrm{r}}^6 \tag{A.17}$$

$$f_2 = 15.2518 - \frac{15.6875}{T_{\mathrm{r}}} - 13.4721 \ln T_{\mathrm{r}} + 0.43577 T_{\mathrm{r}}^6 \tag{A.18}$$

where T_{r} and $P_{\mathrm{r}}^{\mathrm{vap}}$ refer to their reduced properties

$$T_{\mathrm{r}} = \frac{T}{T_{\mathrm{c}}} \quad \text{and} \qquad P_{\mathrm{r}}^{\mathrm{vap}} = \frac{P^{\mathrm{vap}}}{P_{\mathrm{c}}}, \tag{A.19}$$

respectively.

A.4   PSRK-UNIFAC Parameters

The following tables summarize all PSRK-UNIFAC parameter used in this thesis. Tab. A.1 shows the pure group contribution parameters, namely the van-der-Waals volume R_k and the van-der-Waals surface Q_k. Tab. A.2 provides the binary interaction parameters a_{ij}, b_{ij}, and c_{ij}.

Table A.1: Pure group parameters, i. e. the van-der-Waals volume R_k and the van-der-Waals surface Q_k, for the groups that are used in this work according to Horstmann et al. (2005).

main group		sub group		R_k	Q_k	component
1	C	1	CH_3	0.9011	0.848	n-heptane (2 CH_3, 5 CH_2)
		2	CH_2	0.6744	0.54	
3	AC	9	ACH	0.5313	0.4	aniline (5 ACH, 1 $ACNH_2$)
17	ACN	36	$ACNH_2$	1.06	0.816	
6	MeO	15	CH_3OH	1.4311	1.432	methanol
7	H_2O	16	H_2O	0.92	1.4	water
56	CO_2	117	CO_2	1.3	0.982	carbon dioxide
57	CH_4	118	CH_4	1.1292	1.124	methane
62	H_2	113	H_2	0.416	0.517	hydrogen
63	CO	112	CO	0.711	0.828	carbon monoxide

Table A.2: Binary interaction coefficients a_{ij}, $10 \times b_{ij}$, and $10^3 \times c_{ij}$ of the PSRK-UNIFAC group contribution method according to Horstmann et al. (2005). This table shows only the coefficients that are used in this thesis. The symbol "//" refers to binary pairs that do not occur in this work but there are values available in the cited work, and "//*" refers to binary pairs for which no interaction parameters are available.

a_{ij}	1 C	3 AC	17 ACN	6 MeO	7 H_2O	56 CO_2	57 CH_4	62 H_2	63 CO
C	—	61.13	920.7	//	1318	//	-39.101	//	//
AC	-11.12	—	648.2	//	903.8	//	//	//	//
ACN	1139	247.5	—	//	243.2	//*	//*	//*	//*
MeO	//	//	//	—	-181	-72.04	//	250.05	261.54
H_2O	300	362.3	-341.6	289.6	—	-1163.5	-1573.2	-1531.6	-1665.5
CO_2	//	//	//*	414.57	1720.6	—	73.563	838.06	161.54
CH_4	68.141	//	//*	//	-1149.1	196.16	—	253.92	62.419
H_2	//	//	//*	2136.6	5564.1	3048.9	128.55	—	863.18
CO	//	//	//*	231.32	-6058.1	4.2038	1.6233	494.67	—

$10 \times b_{ij}$	C	ACH	ACN	MeO	H_2O	CO_2	CH_4	H_2	CO
C	—	0	0	//	0	//	0.8459	//	//
AC	0	—	0	//	0	//	//	//	//
ACN	0	0	—	//	0	//*	//*	//*	//*
MeO	//	//	//	—	0	0	//	0	3.35
H_2O	0	0	0	0	—	54.765	11.993	121.74	137.72
CO_2	//	//	//*	0	-43.437	—	0	-10.158	0
CH_4	-7.386	//	//*	//	58.604	0	—	0	0
H_2	//	//	//*	0	-274.1	-102.47	0	—	-123.09
CO	//	//	//*	-0.476	312.81	0	0	-81.869	—

$10^3 \times c_{ij}$	C	AC	ACN	MeO	H_2O	CO_2	CH_4	H_2	CO
C	—	0	0	//	0	//	0	//	//
AC	0	—	0	//	0	//	//	//	//
ACN	0	0	—	//	0	//*	//*	//*	//*
MeO	//	//	//	—	0	0	//	0	0
H_2O	0	0	0	0	—	-2.603	-12.25	-6.931	-14.05
CO_2	//	//	//*	0	1.31	—	0	0	0
CH_4	0	//	//*	//	-5.122	0	—	0	0
H_2	//	//	//*	0	71.15	0	0	—	46.32
CO	//	//	//*	0	-33.08	0	0	47.18	—

A.5 Critical Data and Mathias-Copeman Parameters

All critical data, acentric factors, as well as Mathias-Copeman parameters that are used in this work are summarized in Tab. A.3. If there are no Mathias-Copeman parameters given in this table they are computed instead from the acentric factor according to

$$c_1 = 0.48 + 1.574\omega - 0.176\omega^2, \tag{A.20a}$$

$$c_2 = c_3 = 0. \tag{A.20b}$$

Table A.3: Critical data (T_c, P_c), acentric factor ω, and Mathias-Copeman parameters. Critical data and acentric factors according to Yaws (1999), and Mathias-Copeman parameters according to Horstmann et al. (2005).

component	critical data and acentric factor			Mathias-Copeman parameters		
	T_c/K	$P_c/10^5\,\mathrm{Pa}$	ω	c_1	c_2	c_3
H_2	33.18	13.13	-0.22	0.1252	0	0
H_2O	647.13	220.55	0.345	1.0783	-0.58321	0.54619
CO	132.92	34.99	0.066	0.5567	0	0
CO_2	304.19	73.82	0.228	0.8255	0.16755	-1.7039
CH_4	190.58	46.04	0.011	0.49258	0	0
CH_3OH	512.58	80.96	0.566	1.4297	-0.66558	-0.12578
C_2H_6	305.42	48.80	0.099			
C_3H_8	369.82	42.49	0.152			
C_4H_{10}	425.18	37.97	0.199			
C_5H_{12}	469.65	33.69	0.249			
C_6H_{14}	507.43	30.12	0.305			
C_7H_{16}	540.26	27.36	0.351			
C_8H_{18}	568.83	24.86	0.396			
C_9H_{20}	595.65	23.06	0.438			
$C_{10}H_{22}$	618.45	21.23	0.484			
$C_{11}H_{24}$	638.76	19.66	0.536			
$C_{12}H_{26}$	658.20	18.24	0.573			
$C_{13}H_{28}$	675.80	17.23	0.619			
$C_{14}H_{30}$	692.40	16.21	0.662			
$C_{15}H_{32}$	706.80	15.20	0.705			
$C_{16}H_{34}$	720.60	14.19	0.747			

A.6 Caloric Data

The values of the ideal gas standard enthalpy of formation $\Delta_f h°$ as well as the ideal gas standard Gibbs energy of formation $\Delta_f g°$ that are used in this thesis are summarized in Tab. A.4. Additionally, parameters for the polynomial

$$\frac{c_p}{\mathrm{J\,mol^{-1}\,K^{-1}}} = p_1 + p_2 \frac{T}{K} + p_3 \left(\frac{T}{K}\right)^2 + p_4 \left(\frac{T}{K}\right)^3 + p_5 \left(\frac{T}{K}\right)^4 \tag{A.21}$$

describing the ideal gas heat capacities of the considered species are given in this table.

Table A.4: Ideal gas standard enthalpy of formation and Gibbs energy of formation in $\mathrm{kJ\,mol^{-1}}$, as well as the parameters for the polynomial of the heat capacity according to Yaws (1999).

component	$\Delta_f h°$	$\Delta_f g°$	p_1	$10^3 p_2$	$10^6 p_3$	$10^9 p_4$	$10^{12} p_5$
H_2	0	0	22.399	20.178	-38.549	31.880	-8.7585
H_2O	-241.8	-228.6	33.933	-8.4186	29.906	-17.825	3.6934
CO	-110.54	-137.28	29.556	-6.5807	20.13	-12.227	2.2617
CO_2	-393.51	-394.38	27.437	42.315	-19.555	3.9968	-0.29872
CH_4	-74.85	-50.84	34.942	-39.957	191.84	-153.03	39.321
CH_3OH	-201.17	-162.51	40.046	-38.287	245.29	-216.79	59.909

Mathematical Theorems

B.1 Cardano's formula

Cardano's formula, see also Weisstein (1999a), is an analytical solution for the cubic polynomial

$$0 = x^3 + ax^2 + bx + c. \tag{B.1}$$

The original equation (B.1) is reduced via the substitution

$$x = y - \frac{a}{3}, \tag{B.2}$$

which leads to

$$0 = y^3 - 3Py - 2Q \tag{B.3}$$

with the coefficients

$$P = \frac{a^2}{9} - \frac{b}{3}, \qquad\qquad Q = -\frac{a^3}{27} + \frac{ab}{6} - \frac{c}{2}. \tag{B.4}$$

Then, the number and type of solutions is defined by the sign of the discriminant

$$\Delta = Q^2 - P^3. \tag{B.5}$$

- $\Delta > 0$ leads to one real and two conjungate-complex solutions

$$y_1 = u + v \quad y_{2,3} = \frac{-(u+v) \pm \mathrm{i}\sqrt{3}(u-v)}{2} \quad u = \sqrt[3]{Q + \sqrt{\Delta}} \quad v = \sqrt[3]{Q - \sqrt{\Delta}} \tag{B.6}$$

where the conjungate-complex solutions $y_{2,3}$ also may be ignored in the context of Cubic Equations of State, because they do not describe any physical solution.

- $\Delta < 0$, the so-called "Casus Irreduciblis", leads to three different real solutions

$$y_k = 2\sqrt{P}\cos\left(\frac{\phi + 2(k-1)\pi}{3}\right) \qquad \cos\phi = \frac{Q}{\sqrt{P^3}} \qquad k \in \{1,2,3\}. \qquad (\text{B.7})$$

- $\Delta = 0$ leads to the special case of three real solutions, where two of them are identical:

$$y_1 = 2\sqrt[3]{Q} \qquad\qquad y_2 = y_3 = -\sqrt[3]{Q}. \qquad (\text{B.8})$$

It can be shown that this is a special case of both formulas given above ($\Delta > 0$ and $\Delta < 0$).

Now, we have solved the reduced cubic equation (B.3) and get the solutions of the original equation (B.1) from

$$x_k = y_k - \frac{a}{3}. \qquad (\text{B.9})$$

B.2 Jacobian Matrix

The Jacobian matrix, see also Weisstein (1999b), of a function $\mathbf{F}: \mathbb{R}^n \to \mathbb{R}^n$ is the matrix containing all partial derivatives of the vector-valued function $\mathbf{F} = [F_1 \dots F_n]^{\mathrm{T}}$ and is defined by

$$\mathbf{J} = \begin{bmatrix} \dfrac{\partial \mathbf{F}}{\partial x_1} & \cdots & \dfrac{\partial \mathbf{F}}{\partial x_n} \end{bmatrix} = \begin{bmatrix} \dfrac{\partial F_1}{\partial x_1} & \cdots & \dfrac{\partial F_1}{\partial x_n} \\ \vdots & \ddots & \vdots \\ \dfrac{\partial F_n}{\partial x_1} & \cdots & \dfrac{\partial F_n}{\partial x_n} \end{bmatrix}. \qquad (\text{B.10})$$

In MATLAB, the Jacobian of an ODE system `ode(t,x)` can be evaluated numerically by the MATLAB script given in Listing B.1. The approximation of the Jacobian matrix of a n-dimensional function $\mathbf{F}$ requires $n+1$ function evaluations. In the case of sparse matrices, e. g. band matrices, there are specialized algorithms to compute the Jacobian with lower computational costs in terms of function evaluations. See for example Coleman et al. (1984).

Listing B.1: Small Matlab function that computes the Jacobian numerically.

```matlab
function J = jacobian(fun,t,x)
n = numel(x);            % number of dynamic states
J = zeros(n);            % initialize dimension of the Jacobian
H = diag(sqrt(eps(x)));  % deflection for approximation of the derivative
f = feval(fun,t,x);      % function value f(t,x)
for k = 1:n              % approximation of the derivatives
  J(:,k) = (feval(fun, t, x + H(:,k)) - f) / H(k,k);
end
```

B.3 Iterative Solution of Systems of Linear Equations

Assuming the system of linear equations

$$\mathbf{A}\mathbf{x} = \mathbf{b} \tag{B.11}$$

with $\mathbf{A} \in \mathbb{R}^{n \times n}$, $\mathbf{b} \in \mathbb{R}^n$, and the unknown variables $\mathbf{x} \in \mathbb{R}^n$. Furthermore, it is assumed that the diagonal elements of the matrix $\mathbf{A} = [a_{ij}]$ are different from zero, $a_{ii} \neq 0$. Alternatively, the matrix equation (B.11) can also be written in its scalar form:

$$\sum_{j=1}^{n} a_{ij}x_j = b_i, \qquad \forall i = 1, 2. \ldots, n. \tag{B.12}$$

For this type of problems, there exists some iterative methods, namely

- Jacobi method,

- Gauss-Seidel method, and

- method of successive over-relaxation (SOR)

which are described below. These methods are based on the Banach fixed-point theorem (Walter, 2002) and iterate an initial state $\mathbf{x}^0$ into the solution of the problem. For more detailed descriptions of these algorithms, see also Dahmen and Reusken (2006).

B.3.1 Jacobi Method

In order to construct the Jacobi method, the scalar equation (B.12) is solved for the i-th unknown x_i

$$x_i^{k+1} = \frac{1}{a_{ii}} \left[b_i - \sum_{j=1}^{i-1} a_{ij} x_j^k - \sum_{j=i+1}^{n} a_{ij} x_j^k \right] \tag{B.13}$$

where on the r. h. s. the information of the last iteration step x_i^k is used and on the l. h. s. the information of the new iteration step x_i^{k+1} is obtained.

By splitting the matrix $\mathbf{A}$ into a lower triangular matrix $\mathbf{L}$, a diagonal matrix $\mathbf{D}$, and an upper triangular matrix $\mathbf{U}$,

$$\mathbf{L} = \begin{bmatrix} 0 & & & 0 \\ a_{21} & 0 & & \\ \vdots & \ddots & 0 & \\ a_{n1} & \cdots & a_{n,n-1} & 0 \end{bmatrix}, \tag{B.14a}$$

$$\mathbf{D} = \begin{bmatrix} a_{11} & & & 0 \\ & a_{22} & & \\ & & \ddots & \\ 0 & & & a_{nn} \end{bmatrix}, \tag{B.14b}$$

$$\mathbf{U} = \begin{bmatrix} 0 & a_{12} & & a_{1n} \\ & 0 & \ddots & \\ & & 0 & a_{n-1,n} \\ 0 & & & 0 \end{bmatrix}, \tag{B.14c}$$

such that

$$\mathbf{A} = \mathbf{L} + \mathbf{D} + \mathbf{U}, \tag{B.14d}$$

the Jacobi method can also be written as a matrix equation:

$$\mathbf{x}^{k+1} = \mathbf{D}^{-1} \left[\mathbf{b} - (\mathbf{L} + \mathbf{U}) \mathbf{x}^k \right]. \tag{B.15}$$

B.3.2 Gauss-Seidel Method

While the Jacobi method uses always the old values x_j^k in order to compute the new values x_i^{k+1}, the Gauss-Seidel method uses also those values which are already updated within the current iteration step:

$$x_i^{k+1} = \frac{1}{a_{ii}} \left[b_i - \sum_{j=1}^{i-1} a_{ij} x_j^{k+1} - \sum_{j=i+1}^{n} a_{ij} x_j^k \right]. \tag{B.16}$$

With the definition if the matrix splitting, Eq. (B.14), the Gauss-Seidel method can also be written in matrix notation as follows:

$$\mathbf{x}^{k+1} = (\mathbf{D} + \mathbf{L})^{-1} \left[\mathbf{b} - \mathbf{U}\mathbf{x}^k \right]. \tag{B.17}$$

B.3.3 Method of Successive Over-Relaxation

The Gauss-Seidel method, Eq. (B.16), can be reformulated as

$$x_i^{k+1} = x_i^k + \frac{1}{a_{ii}} \left[b_i - \sum_{j=1}^{i-1} a_{ij} x_j^{k+1} - \sum_{j=i}^{n} a_{ij} x_j^k \right], \tag{B.18}$$

which has the form "new value" is equal to "old value" plus "correction". In order to construct the method of successive over-relaxation, the correction term is multiplied by the parameter $\lambda \in (0, 2)$:

$$x_i^{k+1} = x_i^k + \frac{\lambda}{a_{ii}} \left[b_i - \sum_{j=1}^{i-1} a_{ij} x_j^{k+1} - \sum_{j=i}^{n} a_{ij} x_j^k \right] \tag{B.19}$$

$$= (1-\lambda) x_i^k + \frac{\lambda}{a_{ii}} \left[b_i - \sum_{j=1}^{i-1} a_{ij} x_j^{k+1} - \sum_{j=i+1}^{n} a_{ij} x_j^k \right]. \tag{B.20}$$

Therefore, the method of successive over-relaxation can also be seen as a weighted average between "doing nothing" $\left(x_i^{k+1} = x_i^k \right)$, and doing a Gauss-Seidel iteration step. Note, that the "Gauss-Seidel weight" λ is allowed to be larger than one.

By applying the matrix notation, the method can be written as

$$\mathbf{x}^{k+1} = (\mathbf{D} + \lambda \mathbf{L})^{-1} \left[\lambda \mathbf{b} - \left[(\lambda - 1) \mathbf{D} + \lambda \mathbf{U} \right] \mathbf{x}^k \right]. \tag{B.21}$$

Additionally, it can be shown (Dahmen and Reusken, 2006) that for every problem $(\mathbf{A}, \mathbf{b})$, there exists an optimal relaxation parameter λ_{opt} that leads to the highest speed of convergence.

B.3.4 Implementation

For all of these algorithms the *a posteriori* error estimation

$$\sum_{j=1}^{n} \left| x_j^{k+1} - x_j^k \right| \overset{!}{<} M \tag{B.22}$$

can be used as a stop criterion with a small threshold, e. g. $M = 10^{-6}$. MATLAB implementations of the three introduced methods are given in the following listings. These MATLAB functions take the matrix $\mathbf{A}$, the vector $\mathbf{b}$, and the threshold M as input arguments and return the computed vector $\mathbf{x}$. In the case of the method of successive over-relaxation, the relaxation parameter λ is

required as a fourth input argument. The only difference between these implementations is the construction of the method matrices and the update step, while the general procedure and the stop criterion are identical for each method. See Listing B.2 for the Jacobi method, Listing B.3 for the Gauss-Seidel method, and Listing B.4 for the method of successive over-relaxation.

Listing B.2: MATLAB implementation of the Jacobi method.

```matlab
1  function x = lineqJacobi(A,b,thresh)
2  D  = diag(A);         % init method matrices: diagonal matrix
3  LU = A - D;           % and lower + upper triangular matrix
4  maxIter = 100;        % maximum number of iterations
5  nIter   = 1;          % init iteration counter
6  x = zeros(size(b));   % initial guess
7  while nIter < maxIter % main loop
8    xold = x;
9    x    = D \ (b - LU * xold);             % update x vector
10   if sum(abs(x - xold)) < thresh, break; end % check error
11   nIter = nIter + 1;                       % counter increment
12 end
```

Listing B.3: MATLAB implementation of the Gauss-Seidel method.

```matlab
1  function x = lineqGausSeidel(A,b,thresh)
2  DL = tril(A,0);       % init method matrices: lower + diagonal matrix
3  U  = triu(A,1);       % and upper triangular matrix
4  maxIter = 100;        % maximum number of iterations
5  nIter   = 1;          % init iteration counter
6  x = zeros(size(b));   % initial guess
7  while nIter < maxIter % main loop
8    xold = x;
9    x    = DL \ (b - U * xold);             % update x vector
10   if sum(abs(x - xold)) < thresh, break; end % check error
11   nIter = nIter + 1;                       % counter increment
12 end
```

Listing B.4: MATLAB implementation of the method of successive over-relaxation (SOR).

```matlab
function x = lineqSOR(A,b,thresh,lambda)
D  = diag(A);          % init method matrices..
A1 = D + lambda * tril(A,-1);
A2 = (lambda-1) * D + lambda * triu(A,1);
b1 = lambda * b;
maxIter = 100;         % maximum number of iterations
nIter   = 1;           % init iteration counter
x = zeros(size(b));    % initial guess
while nIter < maxIter % main loop
  xold = x;
  x    = A1 \ (b1 - A2 * xold);            % update x vector
  if sum(abs(x - xold)) < thresh, break; end % check error
  nIter = nIter + 1;                       % counter increment
end
```

Bibliography

Abrams, D. S. and Prausnitz, J. M. Statistical Thermodynamics of Liquid Mixtures: A New Expression for the Excess Gibbs Energy of Partly or Completely Miscible Systems. *AIChE Journal*, 21(1):116–128, 1975. doi:10.1002/aic.690210115.

Ahlers, J. and Gmehling, J. Development of an Universal Group Contribution Equation of State: I. Prediction of Liquid Densities for Pure Compounds with a Volume Translated Peng-Robinson Equation of State. *Fluid Phase Equilibria*, 191(1–2):177–188, 2001. doi:10.1016/S0378-3812(01)00626-4.

Aly, F. A. and Lee, L. L. Self-Consistent Equations for Calculating the Ideal Gas Heat Capacity, Enthalpy, and Entropy. *Fluid Phase Equilibria*, 6(3–4):169–179, 1981. doi:10.1016/0378-3812(81)85002-9.

Byrd, R. H., Hribar, M. E., and Nocedal, J. An Interior Point Algorithm for Large-Scale Nonlinear Programming. *SIAM Journal on Optimization*, 9(4):877–900, 1999. doi:10.1137/S1052623497325107.

Byrd, R. H., Gilbert, J., and Nocedal, J. A Trust Region Method Based on Interior Point Techniques for Nonlinear Programming. *Mathematical Programming*, 89(1):149–185, 2000. doi:10.1007/PL00011391.

Coleman, T. F., Garbow, B. S., and More, J. J. Software for Estimating Sparse Jacobian Matrices. *ACM Transactions on Mathematical Software*, 10(3):329–345, 1984. doi:10.1145/1271.1610.

Dahmen, W. and Reusken, A. *Numerik für Ingenieure und Naturwissenschaftler*. Springer, 2006.

El-Sibai, A., Rihko-Struckmann, L., and Sundmacher, K. Synthetic Methane from CO_2: Dynamic Optimization of the Sabatier Process for Power-to-Gas Applications. *Computer Aided Chemical Engineering*, 37:1157–1162, 2015. doi:10.1016/B978-0-444-63577-8.50038-3.

Fischer, F. and Tropsch, H. Über die direkte Synthese von Erdöl-Kohlenwasserstoffen bei gewöhnlichem Druck. (Erste Mitteilung). *Berichte der deutschen chemischen Gesellschaft (A and B Series)*, 59(4):830–831, 1926. doi:10.1002/cber.19260590442.

Flory, P. J. Molecular Size Distribution in Linear Condensation Polymers. *Journal of the American Chemical Society*, 58(10):1877–1885, 1936. doi:10.1021/ja01301a016.

Fredenslund, A., Jones, R. L., and Prausnitz, J. M. Group-Contribution Estimation of Activity Coefficients in Nonideal Liquid Mixtures. *AIChE Journal*, 21(6):1086–1099, 1975. doi:10.1002/aic.690210607.

Fredenslund, A., Gmehling, J., and Rasmussen, P. *Vapor-Liquid Equilibria Using UNIFAC - A Group Contribution Method*. Elsevier, Amsterdam, 1977.

Gasem, K. A. M., Gao, W., Pan, Z., and Robinson Jr., R. L. A modified Temperature Dependence for the Peng-Robinson Equation of State. *Fluid Phase Equilibria*, 181:113–125, 2001. doi:10.1016/S0378-3812(01)00488-5.

Gmehling, J., Kolbe, B., Kleiber, M., and Rarey, J. *Chemical Thermodynamics for Process Simulation*. Wiley, 2012.

Guldberg, C. M. and Waage, P. Concerning Chemical Affinity. *Erdmann's Journal für Practische Chemie*, 127:69–114, 1879.

Haynes, W. M. and Lide, D. R. *CRC Handbook of Chemistry and Physics*. CRC Press, 2010.

Hermann, M. *Numerik gewöhnlicher Differentialgleichungen*. Oldenbourg Verlag, 2004.

Holderbaum, T. *Die Vorausberechnung von Dampf-Flüssig-Gleichgewichten mit einer Gruppenbeitragszustandsgleichung*. PhD thesis, University Dortmund, 1991.

Holderbaum, T. and Gmehling, J. PSRK: A Group Contribution Equation of State Based on UNIFAC. *Fluid Phase Equilibria*, 70(2–3):251–265, 1991. doi:10.1016/0378-3812(91)85038-V.

Horstmann, S., Jabłoniec, A., Krafczyk, J., Fischer, K., and Gmehling, J. PSRK Group Contribution Equation of State: Comprehensive Revision and Extension IV, including Critical Constants and α-function Parameters for 1000 Components. *Fluid Phase Equilibria*, 227(2):157–164, 2005. doi:10.1016/j.fluid.2004.11.002.

Huron, M.-J. and Vidal, J. New Mixing Rules in Simple Equations of State for Representing Vapour-Liquid Equilibria of Strongly Non-Ideal Mixtures. *Fluid Phase Equilibria*, 3(4):255–271, 1979. doi:10.1016/0378-3812(79)80001-1.

International Union of Pure and Applied Chemistry. Notation for States and Processes, Significance of the Word Standard in Chemical Thermodynamics, and Remarks on Commonly Tabulated Forms of Thermodynamic Functions. *Pure and Applied Chemistry*, 54(6):1239–1250, 1982. doi:10.1351/pac198254061239.

Joback, K. G. and Reid, R. C. Estimation of Pure-Component Properties from Group-Contributions. *Chemical Engineering Communications*, 57:233–243, 1987. doi:10.1080/00986448708960487.

Ketchum, R. G. A Combined Relaxation-Newton Method as a New Global Approach to the Computation of Thermal Separation Processes. *Chemical Engineering Science*, 34(3):387–395, 1979. doi:10.1016/0009-2509(79)85072-1.

Klamt, A. Conductor-like Screening Model for Real Solvents: A New Approach to the Quantitative Calculation of Solvation Phenomena. *The Journal of Physical Chemistry*, 99(7):2224–2235, 1995. doi:10.1021/j100007a062.

Kurihara, K., Nakamichi, M., and Kojima, K. Isobaric Vapor-Liquid Equilibria for Methanol + Ethanol + Water and the Three Constituent Binary Systems. *Journal of Chemical & Engineering Data*, 38:446–449, 1993. doi:10.1021/je00011a031.

Lagarias, J. C., Reeds, J. A., Wright, M. H., and Wright, P. E. Convergence Properties of the Nelder-Mead Simplex Method in Low Dimensions. *SIAM Journal on Optimization*, 9(1):112–147, 1998. doi:10.1137/S1052623496303470.

Le Guennec, Y., Lasala, S., Privat, R., and J.-N-Jaubert. A Consistency Test for α-functions of Cubic Equations of State. *Fluid Phase Equilibria*, 427:513–538, 2016. doi:10.1016/j.fluid.2016.07.026.

Lee, B. I. and Kesler, M. G. A Generalized Thermodynamic Correlation Based on Three-Parameter Corresponding States. *AIChE Journal*, 21(3):510–527, 1975. doi:10.1002/aic.690210313.

Linstrom, P. J. and Mallard, W. G., Editors. *NIST Chemistry WebBook, NIST Standard Reference Database Number 69*. National Institute of Standards and Technology, 2015. URL `http://webbook.nist.gov`.

Lucia, A., Padmanabhan, L., and Venkataraman, S. Multiphase Equilibrium Flash Calculations. *Computers & Chemical Engineering*, 24(12):2557–2569, 2000. doi:10.1016/S0098-1354(00)00563-9.

Luckas, M. and Krissmann, J. *Thermodynamik der Elektrolytlösungen*. Springer, 2001.

Lwin, Y. Chemical Equilibrium by Gibbs Energy Minimization on Spreadsheets. *International Journal of Engineering Education*, 16(4):335–339, 2000.

Mathias, P. M. and Copeman, T. W. Extension of the Peng-Robinson Equation of State to Complex Mixtures: Evaluation of the Various Forms of the Local Composition Concept. *Fluid Phase Equilibria*, 13:91–108, 1983. doi:10.1016/0378-3812(83)80084-3.

Mohr, P. J., Taylor, B. N., and Newell, D. B. CODATA Recommended Values of the Fundamental Physical Constants: 2010. *Reviews of Modern Physics*, 84(4):1527–1605, 2012. doi:10.1103/RevModPhys.84.1527.

Nelder, J. A. and Mead, R. A Simplex Method for Function Minimization. *The Computer Journal*, 7(4):308–313, 1965. doi:10.1093/comjnl/7.4.308.

Peng, D.-Y. and Robinson, D. B. A New Two-Constant Equation of State. *Industrial and Engineering Chemistry: Fundamentals*, 15(1):59–64, 1976. doi:10.1021/i160057a011.

Peters, M. S., Timmerhaus, K. D., and West, R. E. *Plant Design and Economics for Chemical Engineers*. McGraw-Hill, 5th edition, 2003.

Poling, B. E., Prausnitz, J. M., and O'Connell, J. P. *The Properties of Gases and Liquids*. McGraw-Hill, 5th edition, 2001.

Ramirez, W. F. *Computational Methods for Process Simulation*. Butterworth-Heinemann, 1997.

Redlich, O. and Kwong, J. N. S. On the Thermodynamics of Solutions. V. An Equation of State. Fugacities of Gaseous Solutions. *Chemical Reviews*, 44(1):233–244, 1949. doi:10.1021/cr60137a013.

Reutemann, W. and Kieczka, H. Formic Acid. In *Ullmann's Encyclopedia of Industrial Chemistry*. Wiley-VCH, 2000. doi:10.1002/14356007.a12_013.pub2.

Rihko-Struckmann, L., Peschel, A., Hanke-Rauschenbach, R., and Sundmacher, K. Assessment of Methanol Synthesis Utilizing Exhaust CO_2 for Chemical Storage of Electrical Energy. *Industrial & Engineering Chemistry Research*, 49(21):11073–11078, 2010. doi:10.1021/ie100508w.

Rönsch, S. *Anlagenbilanzierung in der Energietechnik: Grundlagen, Gleichungen und Modelle für die Ingenieurpraxis*. Springer Vieweg, 2015.

Seidel, A. Calculating Chemical Reaction Equilibrium for a Homogeneous Phase from the Material Balance of a Batch Reactor. *Chemical Engineering Science*, 45(9):2970–2973, 1990. doi:10.1016/0009-2509(90)80190-P.

Shampine, L. F. and Hosea, M. E. Analysis and Implementation of TR-BDF2. *Applied Numerical Mathematics*, 20(1-2):21–37, 1996. doi:10.1016/0168-9274(95)00115-8.

Shampine, L. F. and Reichelt, M. W. The MATLAB ODE Suite. *SIAM Journal on Scientific Computing*, 18:1–22, 1997. doi:10.1137/S1064827594276424.

Shampine, L. F., Reichelt, M. W., and Kierzenka, J. A. Solving Index-1 DAEs in MATLAB and Simulink. *SIAM Review*, 41(3):538–552, 1999. doi:10.1137/S003614459933425X.

Soave, G. Equilibrium Constants from a modified Redlich-Kwong Equation of State. *Chemical Engineering Science*, 27(6):1197–1203, 1972. doi:10.1016/0009-2509(72)80096-4.

Sørensen, J. M., Magnussen, T., Rasmussen, P., and Fredenslund, A. Liquid-Liquid-Equilibrium Data: Their Retrieval, Correlation and Prediction Part I: Retrieval. *Fluid Phase Equilibria*, 2 (4):297–309, 1979. doi:10.1016/0378-3812(79)80015-1.

Steyer, F., Flockerzi, D., and Sundmacher, K. Equilibrium and Rate-based Approaches to Liquid–Liquid Phase Splitting Calculations. *Computers & Chemical Engineering*, 30(2):277–284, 2005. doi:10.1016/j.compchemeng.2005.09.005.

van der Waals, J. D. *Over de Continuiteit van den Gas en Vloeistoftoestand*. PhD thesis, Leiden University, 1873.

Walas, S. M. *Phase Equilibria in Chemical Engineering*. Butterworth-Heinemann, 1985.

Walter, W. *Analysis 2*. Springer, 5 edition, 2002.

Waltz, R. A., Morales, J. L., Nocedal, J., and Orban, D. An Interior Algorithm for Nonlinear Optimization that Combines Line Search and Trust Region Steps. *Mathematical Programming*, 107(3):391–408, 2006. doi:10.1007/s10107-004-0560-5.

Wegstein, J. H. Accelerating Convergence of Iterative Processes. *Communications of the ACM*, 1 (6):9–13, 1958. doi:10.1145/368861.368871.

Weisstein, E. W. *CRC Concise Encyclopedia of Mathematics*, chapter Cubic Equation, pages 362–365. CRC Press, 1999a.

Weisstein, E. W. *CRC Concise Encyclopedia of Mathematics*, chapter Jacobian. CRC Press, 1999b.

Yaws, C. L. *Chemical Properties Handbook*. McGraw-Hill, 1999.

Yaws, C. L. *Thermophysical Properties of Chemicals and Hydrocarbons*. Andrew, 2008.

Ye, K. *Process Design Based on CO_2-Expanded Liquids as Solvents*. PhD thesis, Otto-von-Guericke University, 2014.

Zinser, A. and Sundmacher, K. Dynamische Methode zur Berechnung thermodynamischer Gleichgewichte in reaktiven Mehrphasensystemen. *Chemie Ingenieur Technik*, 88(11):1617–1627, 2016. doi:10.1002/cite.201600070.

Zinser, A., Rihko-Struckmann, L., and Sundmacher, K. Storage of Renewable Energies via Chemical Conversion using CO_2: Energy Systems Analysis. *Computer Aided Chemical Engineering*, 31:995–999, 2012. doi:10.1016/B978-0-444-59506-5.50030-4.

Zinser, A., Ye, K., Rihko-Struckmann, L., and Sundmacher, K. A Dynamic Method for Computing Thermodynamic Equilibria in Process Simulation. *Computer Aided Chemical Engineering*, 37: 299–304, 2015. doi:10.1016/B978-0-444-63578-5.50045-1.

Zinser, A., Rihko-Struckmann, L., and Sundmacher, K. Dynamic Method for Computation of Chemical and Phase Equilibria. *Computers & Chemical Engineering*, 89:1–10, 2016a. doi:10.1016/j.compchemeng.2016.02.014.

Zinser, A., Rihko-Struckmann, L., and Sundmacher, K. Computationally Efficient Steady-State Process Simulation by Applying a Simultaneous Dynamic Method. *Computer Aided Chemical Engineering*, 38:517–522, 2016b. doi:10.1016/B978-0-444-63428-3.50091-6.

Zinser, A., Rihko-Struckmann, L., and Sundmacher, K. Process Optimization by Applying a Simultaneous Dynamic Method. *Computer Aided Chemical Engineering*, 40:2047–2053, 2017. doi:10.1016/B978-0-444-63965-3.50343-3.